Geology of the Alexander City 7.5' Quadrangle, Alabama and U-Pb Zircon Dating of the Elkahatchee Quartz Diorite, southernmost Appalachian orogen

by

Benjamin R. Weinmann

A thesis submitted to the Graduate Faculty of
Auburn University
in partial fulfillment of
requirements for the Degree of
Master of Science

Auburn University
May, 5, 2019

Keywords: Alexander City Blue Ridge, Elkahatchee Quartz Diorite, Wedowee Group, Emuckfaw Group, southernmost Appalachians

Approved by

Mark G. Steltenpohl, Chair, Professor of Geology
Willis E. Hames, Professor of Geology
Haibo Zou, Professor of Geology
Chong Ma, Researcher

ABSTRACT

Geological mapping of the Alexander City Quadrangle in the eastern Blue Ridge of the Southern Appalachian orogen in Alabama reveals newly recognized units and supports multi-phase magmatism within the 880 km^2 Elkahatchee Quartz Diorite batholith. Major findings from mapping include: (1) the Alexander City shear zone variably deformed rocks within the quadrangle during the Alleghenian orogeny through oblique-dextral and normal shear; (2) the earliest intrusive phase within the Elkahatchee batholith is a medium-grained biotite-rich quartz diorite, whereas later, more felsic phases are medium- to coarse-grained K-feldspar-rich granites and leucocratic plagioclase- and muscovite-rich trondhjemites and tonalites, appearing as small, lens-shaped, elongate bodies; (3) a newly recognized granitic body, referred to as Oaktasasi granite, conforms to the regional structural grain yet is undeformed to weakly deformed and corresponds to several areas previously mapped as Hackneyville Schist; (4) the ~335 Ma Sugar Creek trondhjemite intrudes the Elkahatchee Quartz Diorite and contains low angle right-lateral strike-slip shear zones with tops-southwest displacements; and (5) high-angle normal faults are documented in the northwest parts of the quadrangle.

Whole rock geochemistry for the Elkahatchee Quartz Diorite suggests that it was derived from slab melt due to subduction during the Neoacadian orogeny. Rb-Hf-Ta and Rb-(Y+Nb) diagrams indicate the magmatic origin in a volcanic arc setting. Sr/Y values of ≥ 40, $Al_2O_3 > 15$, and $Yb < 1.9$ ppm, and enrichment in light REE and depletion in heavy REE, conform to an "adakitic" signature. Magmatic

zircons from three samples of Elkahatchee Quartz Diorite were dated using U-Pb geochronology laser-ablation-sector field-inductively coupled plasma-mass spectrometry. A sample representative of the earliest, most mafic phase (SiO_2 62.5%) gave a weight mean age of 378.3 ± 5.5 Ma (2σ). A younger population was found in the more felsic samples (SiO_2 65.3% and 67.2%, respectively) that gave weighted mean ages of 328.6 ± 5.1 and 329.8 ± 5.3 Ma (2σ). These age data support a multi-phase magmatic history for the Elkahatchee Quartz Diorite that spanned the late Acadian-Neoacadian and early Alleghenian orogenies.

The magmatic crystallization ages reported herein for felsic plutons combine with previously reported ages to support that the Wedowee-Emuckfaw boundary, on a regional scale, separates eastern Blue Ridge units intruded by granites of Devonian to Carboniferous age to the northwest from those intruded by Middle Ordovician plutons to the southeast. Such age-specific plutons could preferentially intrude different structural levels within an intact stratigraphic package or else a fault is responsible for the age disparity. The author favors that a cryptic fault may best explain this relationship.

ACKNOWLEDGEMENTS

I would like to thank Dr. Mark G. Steltenpohl for expanding my geologic knowledge of the southern Appalachians and his aid in both field mapping and unraveling the structure and kinematics of complexly deformed rocks in the Alabama Blue Ridge.

Dr. Chong Ma has been a great help in interpreting the U-Pb results, petrology, petrography, and geochemistry, and for that I express my gratitude.

I also thank Drs. Willis Hames and Haibo Zou for helpful discussions and thoughtful reviews of this report.

I would like to also thank the faculty and professors of the Department of Geosciences at Auburn University for their continuous aid and support.

Funding for portions of this project was provided by the National Cooperative Geologic Mapping Program and the USGS for EdMap No. G17AAC00303 to Dr. Mark Steltenpohl, Auburn University. I am very appreciative of this support.

Style manual used:

Bulletin of the Geological Society of America

Computer software used:

Microsoft Office Suite 2010/2013®

ArcGIS 10.6®

ESRI ArcGIS®

Adobe Illustrator CS®

Adobe Photoshop CS®

Stereonet 10®

Python

sliplineCalc_0.5.py

SCslip.xlsm

TABLE OF CONTENTS

LIST OF FIGURES

LIST OF TABLES

PLATE

LIST OF ABBREVIATIONS

CIPW	Cross, Iddings, Pirsson, and Washington
EBR	Eastern Blue Ridge
EQD	Elkahatchee Quartz Diorite
GIS	Geographic Information System
GPS	Global Positioning System
LOI	Loss on Ignition
Ma	Million Years
S-C	schistoste and cisaillement
REE	Rare Earth Elements
USGS	United States Geological Survey

Mineral Abbreviations

amp	amphibole
bt	biotite
chl	chlorite
gt	garnet
ksp	potassium feldspar
mus	muscovite
myr	myrmekite
plg	plagioclase
ser	sericite
qtz	quartz

Lithologic Units

Hcpq - Hatchet Creek Group, Pinchoulee Gneiss Quartzite
Ewe – Wedowee Group
Eweh – Wedowee Group, Hackneyville Schist member
Eem – Emuckfaw Group
Eeqd – Elkahatchee Quartz Diorite
Ekg – Kowaliga Gneiss
Ezg - Zana Granite
Esct – Sugar Creek trondhjemite
Eog – Oaktasasi granite

INTRODUCTION

The Alexander City, Alabama 7.5 Minute Quadrangle is located in northeastern Tallapoosa County in the eastern Blue Ridge province of the southernmost Appalachian orogen (Fig. 1). There are no reports of the geology of the quadrangle having ever been mapped at the 1:24,000 scale. The quadrangle's boundaries are 33° 00' on the north, 32° 52' 30" on the south, 86° 00' on the west, and 85° 52' 30" on the east with Alexander City itself generally in the center of the quadrangle (Plate 1). The Alexander City shear zone trends northeast through the middle of the quadrangle corresponding to the boundary between the Wedowee and Emuckfaw Groups. According to the 1988 Geological Map of Alabama (1:250K-scale), four main lithologies, two metasedimentary and two meta-igneous, are present in the Alexander City Quadrangle (Osborne et al., 1988).

The Alexander City shear zone has been interpreted as a dextral strike-slip fault (Neathery and Reynolds, 1975; Steltenpohl et al., 2013b) that had reactivated an earlier-formed thrust fault (e.g., Bentley and Neathery, 1970). Recent workers have argued for an upright stratigraphic boundary between the Wedowee and Emuckfaw Groups, questioning the presence of the fault (Barineau and Tull, 2012; Harstad and Barineau et al., 2014). An age disparity appears, however, in the intrusive igneous rocks across the Alexander City shear zone in Alabama. To the northwest are Devonian-Carboniferous granites and trondhjemites, with no Middle Ordovician intrusive rocks (Fig. 2). To the southeast, the granitic bodies are of a

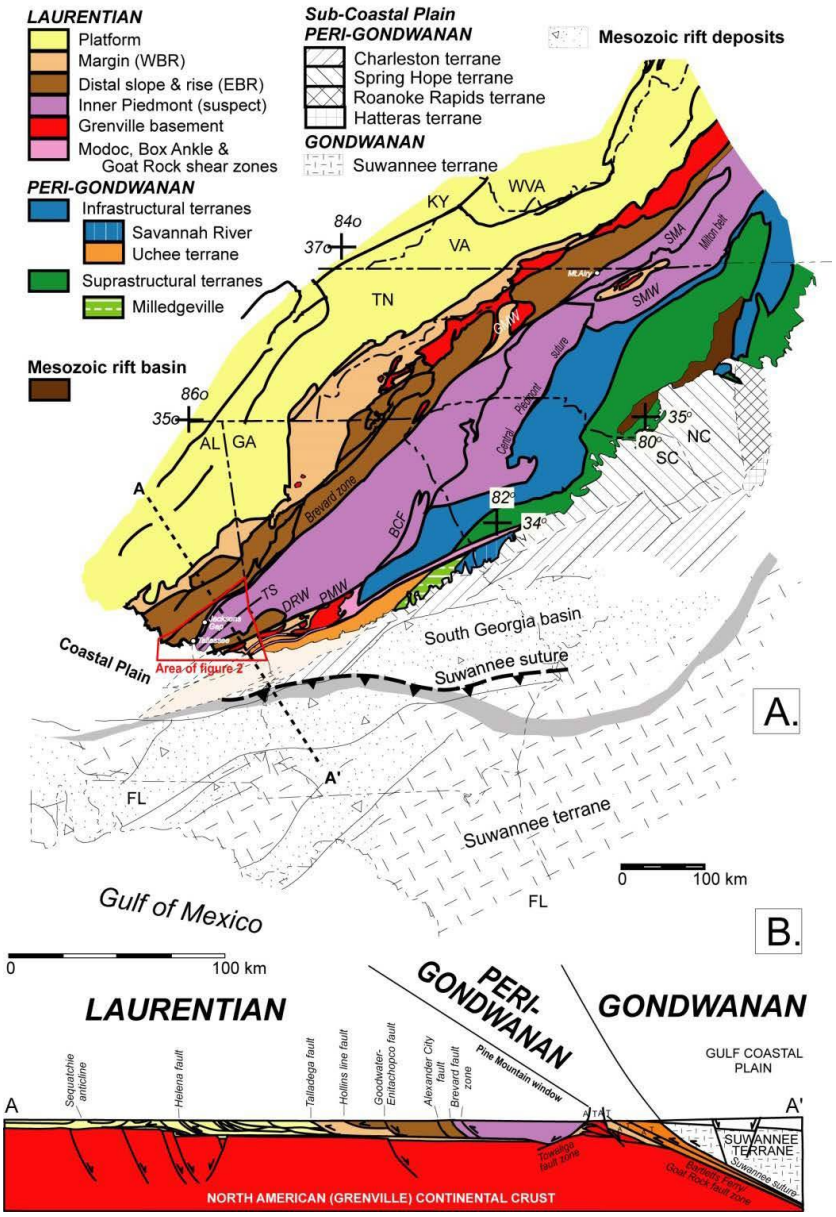

Figure 1 - **A**. Tectonic map illustrating Alabama's position within the southern Appalachians with section line A-A' (from Steltenpohl et al., 2013b, McClellan et al., 2007; as modified from Hatcher, 2004, Horton et al., 1984; Hibbard et al., 2002; Steltenpohl, 2005). Red Polygon illustrates the area of Fig. 2. **B.** Simplified cross section A-A' (modified from W.A. Thomas and coworkers as depicted in Thomas et al. [1989], Hatcher et al. [1990], and Steltenpohl [2005]). Map abbreviations: BCF–Brindle Creek fault; CR–Cartersville reentrant; CST–Cat Square terrane; DRW–Dog River window; EBR–eastern Blue Ridge; GMW–Grandfather Mountain Window; HLF–Hollins Line fault; PMW–Pine Mountain window; SMW–Sauratown Mountain Window; SRA–Smith River allochthon; TS–Tallassee synform; WBR–western Blue Ridge. Cross-Section: A–away; T–toward; no vertical exaggeration.

general Middle Ordovician age with no known Devonian to Mississippian intrusions. A possible exception, however, is the Elkahatchee Quartz Diorite, the origin and age of which are not well defined. Age dates for the Elkahatchee range from as old as 515 Ma (Russell, 1978) to as young as ~370 Ma (Tull et al., 2009), and Steltenpohl et al. (2013a) report a trondhjemite dike that cross-cuts the metamorphic and mylonitic fabric of the quartz diorite is dated at 369 Ma.

The geology of the Alexander City Quadrangle is well positioned to examine the age and magmatic setting of the Elkahatchee Quartz Diorite as well as the debate surrounding the Alexander City shear zone. Hence, the rocks and structures of the quadrangle have been mapped and analyzed and geochemistry and U-Pb geochronology on zircons from select intrusive rocks are presented. The results have significance for the tectonic evolution of the southernmost part of the Appalachian Blue Ridge.

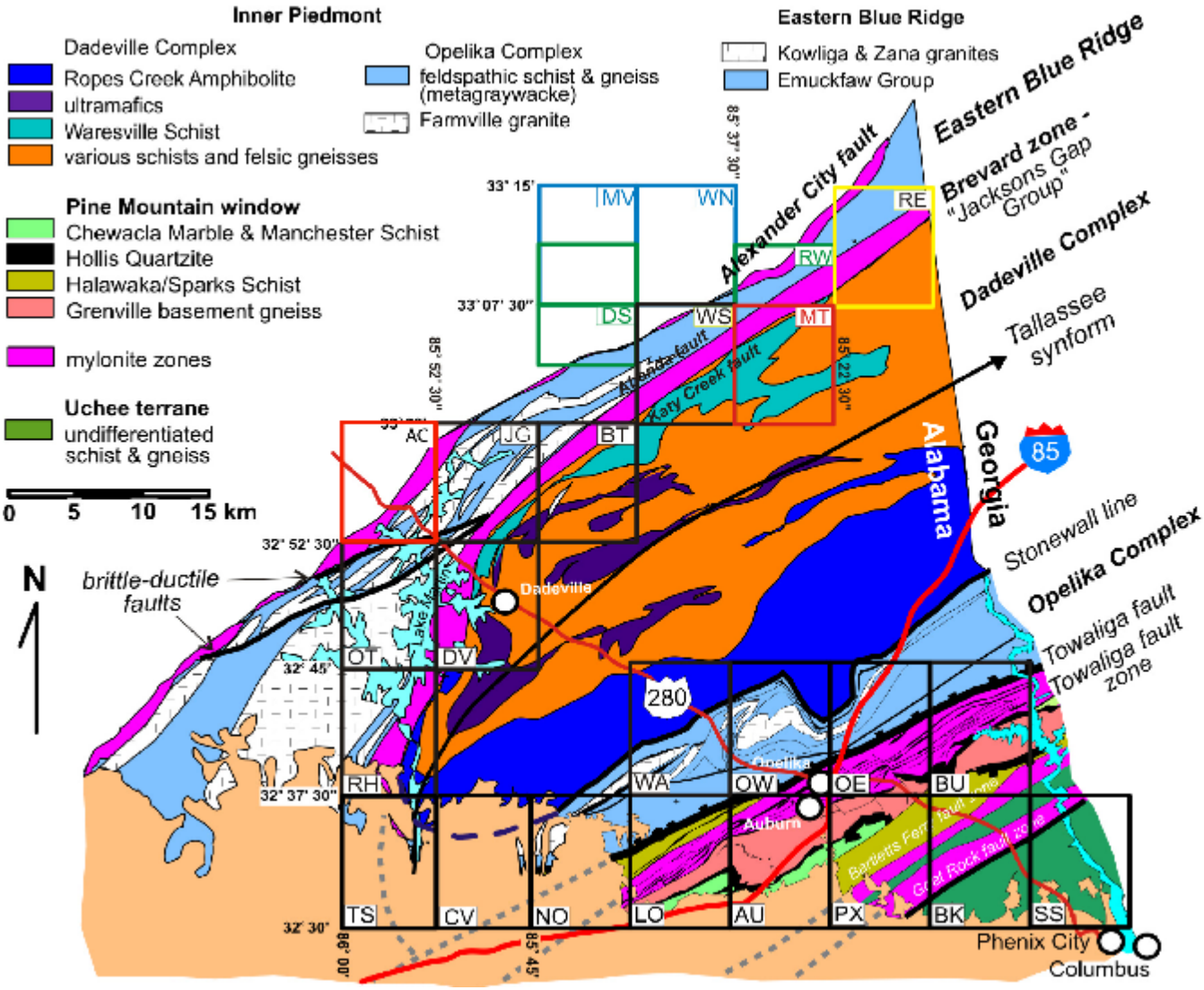

Figure 2 - Geologic map of the Alabama Piedmont (from Osborne et al., 1988, Steltenpohl, 2005, and Steltenpohl et al., 2013a) noting the location of the Alexander City (AC) Quadrangle (outlined in red). Dashed gray lines are geophysical lineaments beneath the Coastal Plain onlap from Horton et al. (1989); dashed blue line represents the base of the Dadeville Complex from White (2007). Rectangles are 1:24,000 quadrangle maps completed in this part of Alabama.

GEOLOGIC BACKGROUND

The Alexander City Quadrangle (Fig. 1 and Plate 1) is located in the eastern Blue Ridge geologic province and contains metasedimentary country rocks playing host to the intrusive metaigneous rocks. The eastern Blue Ridge of Alabama lies to the northwest of the Brevard zone and southeast of the Hollis Line fault (Figs. 1 and 2) and is predominately composed of rocks of the ancient rifted margin and slope/rise of Laurentia and their deformed and metamorphosed components of the Appalachian orogeny (Hatcher, 1972, 1978; Hatcher et al., 1987; Merschat et al., 2005; Steltenpohl, 2005). Generally, three metamorphic events are recorded in rocks throughout the eastern Blue Ridge - the Ordovician Taconian, the Devonian Neo-Acadian, and the Mississippian to Permian Alleghenian orogenic phases – although Taconian metamorphic assemblages have not yet been confirmed in the Alabama segment (Bentley and Neathery, 1970; Hatcher, 1972, 1978, 2005, 2010, Bream et al., 2004; Barineau and Tull, 2012). Two principal lithotectonic units underlying the area of the Alexander City quadrangle are the Wedowee and Emuckfaw groups, occurring, respectively, in the northwest and southeast parts of the quad (Plate 1).

Early geologic investigations of the Alabama Blue Ridge focused primarily on gold occurrences and included mine locations, descriptions, mineralogy and a brief account of the regional geology (e.g. Tuomey, 1858; Phillips 1892; Adams, 1930; Park, 1935; Pardee and Park, 1948; Saunders et al., 2013). The Wedowee Group was originally termed the Talladega Series by Prouty (1923). Adams (1926, 1933), describing the crystalline rocks of Alabama, defined the Wedowee Formation and

interpreted rocks of the Brevard zone as being correlative with altered Wedowee Formation. Significant regional work by Bentley and Neathery (1970) described the geology of the Brevard fault zone and Inner Piedmont, which set the foundation for subsequent geological studies in the area. In their report, the authors designated the Wedowee Formation as the Wedowee Group. Lithologies of the Wedowee include graphitic and sericitic phyllites, and muscovite and quartz-rich schists, with some interbedded mafic volcanic rocks (Bentley and Neathery, 1970; Neathery and Reynolds, 1973). Units of the Wedowee Group have been intruded by a host of Paleozoic felsic intrusions, the largest of these bodies is the Elkahatchee Quartz Diorite, a pre-metamorphic batholith that underlies 60% of the northwestern part of the Alexander City quadrangle (Plate 1: Bentley and Neathery, 1970; Russell, 1978; Stowell et al., 1996; Steltenpohl et al., 2005; Ingram et al., 2011; Schwartz et al., 2011). Neathery (1975) further broke out the Hatchet Creek Group, a group of dense, fine- to coarse-grained schists and gneisses that lies to the west of the Wedowee and the Elkahatchee Quartz Diorite.

Rocks between the Wedowee Group and the Brevard fault zone were originally designated as the Heard Group (Bentley and Neathery, 1970), but Neathery and Reynolds (1975) later redesignated them as the Emuckfaw Formation for exposures along Emuckfaw Creek, Tallapoosa County. Later, Raymond et al. (1988) renamed the unit as the Emuckfaw Group. This metasedimentary package was divided into three formations comprising metapelites, metagraywackes, metaturbidites, graphite-bearing schists, and occasional thin bands of amphibolite.

Barineau et al. (2014) suggested further subdividing the Emuckfaw Group into a lower Josie Leg formation, comprising non-graphitic garnet mica schist and subordinate metagraywacke and amphibolite, and an upper Timbergut formation with slightly graphitic garnet mica schist, subordinate metagraywacke, metaconglomerate and rare kyanite schist. The Emuckfaw Group is intruded by Middle Ordovician plutons, the Zana Granite and the Kowaliga Gneiss.

The nature of the contact between the Emuckfaw and Wedowee groups is the source of debate and one of the objectives of the current report is to better characterize its nature. The contact has traditionally been interpreted as a fault - the Alexander City fault (Neathery and Reynolds, 1975; Osborne et al., 1988; Steltenpohl et al., 2013a). On the other hand, Muangnoicharoen, (1975) and later Tull et al. (2007) and Barineau et al. (2014) argued that the contact is stratigraphic and that the entire Wedowee and Emuckfaw Groups are one continuous, upright stratigraphic succession. The latter authors argue that the Alexander City fault dies out directly to the southwest of the Alexander City quadrangle, with shear strains having been concentrated mainly along the southeastern margin of the Elkahatchee Quartz Diorite, which presented a strong competency contrast to the softer Wedowee Group schists. Most all earlier maps depict the trace of the Alexander City fault trending nearly diagonally, southwest-to-northeast, across the Alexander City quadrangle (Bentley and Neathery, 1970; Neathery and Reynolds, 1973; Osborne et al., 1988; Guthrie, 1995; Steltenpohl et al., 2013b), making it a good place to directly map the boundary to help clarify its origin.

The Brevard fault zone (Fig. 1) is a fundamental Appalachian structure generally separating the eastern Blue Ridge from the Inner Piedmont terrane and it occurs less than two miles southeast of the southeast corner of the Alexander City quadrangle (Figs. 1 and 2). The Brevard zone is an extensive, retrograde, polyphase fault zone that formed in response to Acadian-Neoacadian crystal-plastic thrusting and Alleghenian brittle-plastic dextral strike-slip shearing (Hatcher, 1972, 1987, 2005; Bobyarchick et al., 1988; Sterling, 2006; Steltenpohl et al., 1990, 2013a; VanDervoort, 2016). In Alabama, the Brevard zone is defined by a <3.2 km wide zone of weakly to strongly mylonitized metasiliciclastic and metapelitic rocks lithologically identified as the Jackson Gap Group (Fig. 2) (Bentley and Neathery, 1970). Bentley and Neathery (1970) suggested that the entire southern Appalachian Piedmont is allochthonous along a massive, west-directed thrust comprising the Brevard fault zone and major faults framing the Pine Mountain basement-cover window (i.e., Towaliga, Bartletts Ferry, and Goat Rock fault zones), an interpretation that was further substantiated by COCORP (COnsortium for COntinental Reflection Profiling) seismic-reflection profiling that identified the southern Appalachian master décollement (Cook et al., 1979; Cook et al., 1983).

Generally, rocks of the eastern Blue Ridge and Inner Piedmont of Alabama and adjacent Georgia experienced metamorphism during two separate events, one at ~350 Ma (Neoacadian) and another at ~330 Ma (early Alleghanian), with localized shearing between ~300 and ~285 Ma (late Alleghanian) (Steltenpohl and Kunk, 1993; Dennis and Wright, 1997; Carrigan et al., 2001; Kohn, 2001; Bream,

2002, 2003; Cyphers and Hatcher 2006; Stahr et al., 2006; Hames et al., 2007; McClellan et al., 2007; McDonald et al., 2007; Poole, 2015; Whitmore, 2018). This is compatible with studies in the immediate vicinity of the Alexander City Quadrangle, where rocks of the eastern Blue Ridge are documented as having experienced one period of middle amphibolite-facies Barrovian-style prograde M_1 metamorphism, followed later by a retrogressive middle to upper greenschist-facies M_2 event that was concentrated along shear zones and faults (Muangnoicharoen, 1975; Wielchowsky, 1983; Johnson, 1988; Steltenpohl et al., 1990; Reed, 1994; Sterling, 2006; Hawkins, 2013; Abrahams, 2014; Singleton and Steltenpohl, 2014; Poole, 2015).

Within the Emuckfaw Group of the New Site quadrangle directly to the north of the study area, Guthrie and Dean (1989) documented prograde M_1 mineral assemblages of kyanite ± staurolite ± muscovite ± biotite ± garnet ± plagioclase ± quartz, indicating lower to middle amphibolite-faces peak M_1 metamorphism (Holdaway, 1971; Ernst, 1973). Hawkins (2013), working in the Our Town quadrangle directly south of the current study area (Fig. 2), documented deformational microstructures in quartz and feldspar grains of the Kowaliga Gneiss that demonstrate subgrain rotation, bulging recrystallization, and grain-boundary migration recrystallization compatible with lower amphibolite-facies conditions. Replacement of hornblende by actinolite and chlorite in the Emuckfaw Group has been interpreted as having occurred during middle to upper greenschist-facies retrograde metamorphism (Guthrie and Dean, 1989; Hawkins, 2013).

Steltenpohl (2005) first reported similar rheologies, geometries, and right-slip kinematics of mylonites and phyllonites in both the Brevard and the Alexander City fault zones. Crystal-plastic and crystal-brittle shears with mainly dextral and/or oblique normal movement indicators predominate mylonites and phyllonites of the Alexander City fault zone (Steltenpohl et al., 2013b) and they also appear to characterize the deformation plan in eastern Blue Ridge rocks in the areas between these two fault zones; see reports based on detailed 7.5'-scale geologic mapping and structural analysis in Auburn University theses between 1988 and 2018 (Johnson, 1988; Keefer, 1992; Grimes, 1993; Reed, 1994; McCullars, 2001; Sterling, 2006; White, 2007; Hawkins, 2013; Poole, 2015; VanDervoort, 2016; Harstad, 2017; Whitmore, 2018). Steltenpohl (2005) and Steltenpohl et al. (2013b) also reported that several brittle-on-ductile splays obliquely connecting the two fault zones (Fig. 2) effected partitioning of dextral motion between them, and that extension along them has locally excised the Alexander City fault zone (see also Hawkins et al., 2012, and Steltenpohl et al., 2013b). On the other hand, Barineau and Tull (2012) suggest that both the Brevard zone and the Alexander City shear zones die out along these splays and that both faults are Carboniferous rotational normal faults hinged along fault-tip lines that are separated by transfer zones (or relay ramps). The timing of movement along these oblique shears is not well constrained. A ~315 Ma $^{40}Ar/^{39}Ar$ isotopic age date on fabric-forming muscovite collected from one of them (Hawkins, 2013) only provides a maximum on the age of movement. The timing and significance of normal movement in the southernmost Appalachians

remains a topic of debate (see Steltenpohl et al., 2013b). Given the current uncertainty surrounding the precise nature of the origin of the Alexander City shear zone, be it a fault or a zone of concentrated ductile shearing, the current author prefers the term Alexander City shear zone.

There appears to be a disparity in the ages of Paleozoic granitic intrusions within rocks of the Wedowee Group and those of the Emuckfaw Group, which is difficult to reconcile with the interpretation for their shared boundary being an upright stratigraphic contact (Muangnoicharoen, 1975; Tull et al., 2007; Barineau et al., 2014). In the Wedowee Group, the most voluminous intrusion is the Elkahatchee Quartz Diorite (Fig. 2: Bentley and Neathery, 1970; Drummond and Guthrie, 1986; Osborne et al., 1988; Allison, 1992; Drummond et al., 1994, 1997). Russell et al. (1987) reported a late Cambrian age of 490 Ma based on an Rb/Sr whole-rock isochron, and 516 Ma based on upper-intercept multi-grain U-Pb analyses of zircons. Subsequent reconnaissance SHRIMP RG U-Pb dating of zircons from two samples assigned to the Elkahatchee, however, suggest igneous crystallization ages between ~388 and 370 Ma (Barineau, 2009; Tull et al., 2009). Steltenpohl et al. (2013b) report a 369.4 ± 4.8 Ma U-Pb Thermal Ionization Mass Spectrometry (TIMS) date for a trondhjemite dyke that cuts across the set of intensely developed metamorphic and retrograde mylonitic fabrics within the Elkahatchee, and this sample was collected from one of the same outcrops where Barineau (2009) and Tull et al. (2009) collected their sample. Other Neoacadian intrusions in the Wedowee and Hatchet Creek groups are lumped broadly into the

Rockford and Bluff Springs granites (Deininger et al., 1973; Deininger, 1975; Russell, 1978; Dean, 1979; Defant, 1980; Defant and Ragland, 1981; Drummond, 1986; Defant et al., 1987; Osborne et al., 1988; Drummond et al., 1997), from which Schwartz et al. (2011) recently reported U-Pb LA-ICPMS zircon dates of 376.6 ± 2.8 Ma and 363.8 ± 3.6 Ma, respectively. In contrast to the Neoacadian granites, which are K-felspar rich true granites and granodiorites, a suite of younger, early-Alleghanian trondhjemites are grouped within the Almond Trondhjemite (Bentley and Neathery, 1970; Neathery and Reynolds, 1975; Russell, 1978; Osborne et al., 1988; Drummond et al., 1997). Schwartz et al. (2011) dated zircons from two of these plutons (i.e., the Wedowee pluton and Almond pluton) that yielded ages of 334.3 ± 3.0 Ma and 340.5 ± 2.7 Ma, respectively. Another sample, from the Blakes Ferry pluton, yielded complex results with rim ages ranging from ca 350 to 330 Ma (peak ages at 345.8 ± 2.1 Ma and 336.6 ± 2.4 Ma). Recent U-Pb zircon dating of one of these phases - a large trondhjemite body below named the Sugar Creek trondhjemite that intrudes the Elkahatchee Quartz Diorite – reveals a range of ages from 350 - 335 Ma (a concordant grain as 335.9 ± 6 Ma), documenting it as belonging to the suite of early-Alleghanian trondhjemites (i.e., Almond Trondhjemite: Schwartz et al., 2011). In summary, felsic plutons within the Wedowee Group appear to have intruded and crystallized during the Middle Devonian and middle Mississippian Periods.

Only two suites of granites are known, however, to have intruded the Emuckfaw Group in Alabama - the Zana Granite and the Kowaliga Gneiss. Bentley

and Neathery (1970) described the Zana Granite as a number of quartz monzonite plutons that are characterized by microcline, oligoclase, quartz, muscovite, and biotite. The Kowaliga is a granitic to granodioritic gneiss, characterized by plagioclase or K-feldspar megcrysts up to 8 mm in diameter. Muangonoicharoen (1975) and Stoddard (1983) report that the Zana and the Kowaliga are temporally related, with the Zana representing apophyses off a larger Kowaliga intrusion. Additionally, Hawkins (2013) reported whole-rock major and trace element analyses of the Kowaliga Gneiss compared with previously reported geochemical data for the Zana Granite (Stoddard, 1983) demonstrating strong similarities in geochemical signatures, crystallization ages, and field and textural occurrences further supporting that the (meta)granites are the same unit formed during one intrusive event. Sinha et al. (1981) interpreted that the strongly lineated and foliated Zana was emplaced as a sheet and later experienced compressional stress and dated it at 460 Ma using U-Pb isotopes. Russell et al. (1987), using multi-grain U-Pb zircon analytical techniques, constrained an age of 461 ± 12 Ma for the Zana Granite and related Kowaliga Gneiss; additionally, the same author reported an Rb-Sr whole-rock age of 437 Ma and 395 Ma for the Kowaliga Gneiss and Zana Granite, respectively, with analytical uncertainties on the order of ± 100 Ma. More recently, U-Pb SHRIMP data obtained for the Kowaliga Gneiss and Zana Granite suggest a crystallization age of 430 Ma and 439 Ma, respectively (Barineau and Tull, 2012). Based on U/Pb Secondary Ion Mass Spectrometry (SIMS) age dating of zircons, Hawkins (2013) confirmed an Ordovician-Silurian age (441 ± 6.6 Ma) for intrusion

and crystallization for the Kowaliga and Zana granites. The much older and relatively narrow age range of intrusions within the Emuckfaw, coupled with the distinct absence of younger plutons is in sharp contrast to that documented for the Wedowee Group.

Several lines of evidence suggest the possibility, however, that the Elkahatchee batholith contains intrusive phases that predated the emplacement of the other Middle Devonian plutons into the Wedowee Group protoliths, which draws into question the suggested age disparity corresponding to the Wedowee-Emuckfaw boundary. Firstly, several workers reported that the Elkahatchee is a complex, diachronous batholith comprised of multiple intrusive phases (Drummond, 1986; Drummond et al., 1994; Tull et al., 2009). Tull et al. (2009) reported that the Elkahatchee has components as young as 370 Ma, but the age of earliest intrusive phase has yet to be confirmed. Russell's (1978) U-Pb isotopic dating of multi-grain aliquots of Elkahatchee zircons pointed toward a Cambrian age, which could reflect the presence of an older xenocrystic component that has yet to be identified. It would seem unlikely that this particular phase of the Elkahatchee could be any younger than 370 Ma given only one million years in which to crystallize from a magma, recrystallize under amphibolite-facies metamorphic conditions, undergo retrograde mylonitization, and then be cross-cut by a 369 Ma dyke. For these reasons, the Elkahatchee is a focus of the current report, particularly with the aim of finding the oldest intrusive phase of batholith evolution.

The Elkahatchee Quartz Diorite is a ~880 km^2 batholith-scale intrusive body, one of the largest igneous bodies in the entire southern Blue Ridge (Drummond et al., 1994; 1997). The batholith is covered by coastal plain sedimentary rocks to the south and magnetic surveys have traced it below the coastal plain that nonconformably overlaps it (Gault, 1945; Hatcher, 1978; Horton et al., 1984; Drummond et al., 1994, 1997, Steltenpohl et al., 2013a). Drummond et al. (1994) described it as a peraluminous to metaluminous, I-type tonalite to granodiorite with pockets of gabbro, metadacite, felsic granitoids, and schists. The granitoids consist of granite, trondhjemite, and quartz monzonite. The more mafic components are found on the outer edges, and the more felsic components are found more toward the core as seen in Figure 3. Drummond et al. (1994) proposed a model of a laccolith with convective currents crystallizing more mafic rocks on the outside and becoming progressively more felsic toward the core. Unpublished geologic mapping of the southern margin of the Elkahatchee Quartz Diorite batholith within and adjacent to the Alexander City quadrangle (M.G. Steltenpohl, personal communication, 2018) supports that there are multiple intrusive phases within it that need to be more systematically investigated. The geologic mapping, petrography, geochemistry, and U-Pb geochronology presented below are aimed at addressing the age and origin of the early-phase history of the Elkahatchee batholith, which has significance for tectonic evolution of the southernmost Appalachian Blue Ridge.

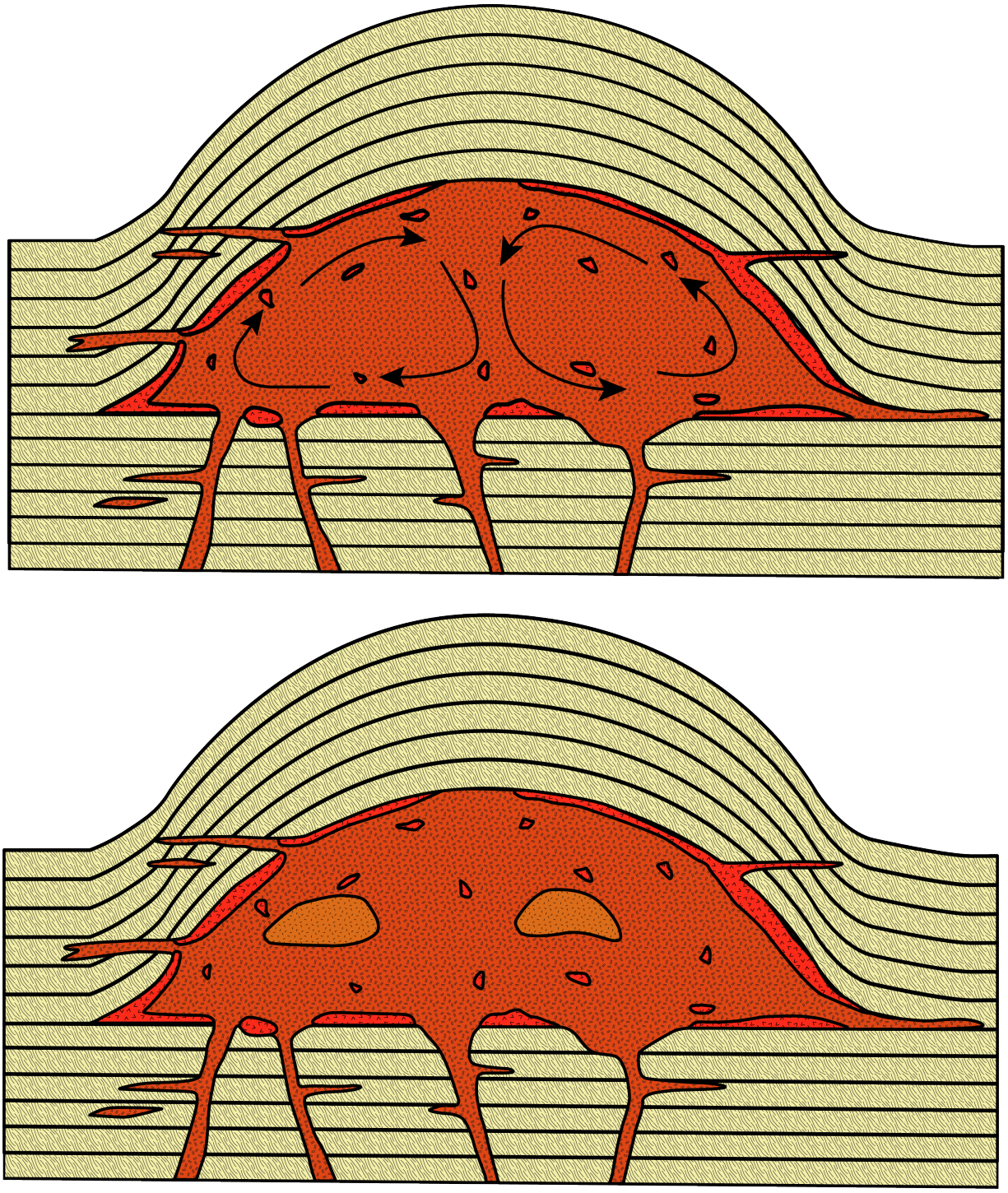

Figure 3 - A proposed mechanism of emplacement of the Elkahatchee Quartz Diorite, adapted from Drummond et al. (1994). **Top**: As the intruding magma of intermediate composition convects, fractional crystallization occurs and the first to crystallize is more mafic, shown in red along the outer margins of, and as enclaves within, the laccolith. **Bottom**: As fractional crystallization continues, and the mafic magma crystallizes, the composition becomes more felsic toward the core, leaving granitic cores.

METHODS

Field Mapping

Field mapping at the 1:24,000 scale was completed by employing standard techniques. As many roads as possible were walked to find and map outcrops. Transects were chosen where the best outcrops can be found, mainly along streams, ridge crests and gaps, and under bridges. Locations of stations and outcrops were recorded with GPS and all observations recorded in a Rite-in-the-Rain® notebook and transferred into a spreadsheet. A standard Brunton Pocket Transit® was utilized to measure tectonic structures and fabrics. Structural measurements were then imported into Stereonet 10® to create lower hemisphere stereograms. Oriented samples were collected from outcrops that contain appropriate foliation and kinematic indicators. Samples were cut for slab analysis and to make thin sections. Sixteen samples were selected for thin section. Rock fabrics, mineralogy, and microstructures were examined using petrographic microscopes in the Department of Geosciences at Auburn University. Field data were transferred from the notebook into the attribute table of ESRI ArcGIS® including location of observation stations and structural data and any other relevant data. The final geologic map of the Alexander City 7.5' Quadrangle was created in ArcGIS® 10.6 and delivered to the Geologic Survey of Alabama and the USGS.

Zircon Geochronology

Three samples of Elkahatchee Quartz Diorite were collected for zircon U-Pb geochronology. Field mapping had shown that the Elkahatchee is strongly mylonitized in the areas near its contact between the Elkahatchee Quartz Diorite and schists of the Wedowee Group. Therefore, samples were preferentially gathered away from the contact. To extract zircons, standard USGS methods were followed (Strong and Driscoll, 2016). First, the samples were crushed using a jaw crusher, then further in a disk mill. The samples were then sieved to between 0.425- and 1-mm diameter, and the rest was saved. After washing and drying, the sieved material was then run through a Frantz magnetic separator at three different current levels (0.4 amps, 0.8 amps, and 1.5 amps) to preferentially remove different heavy and magnetic minerals. Heavy liquid, MEI (methylene iodide; density = 3.325 g/cm^3) was used to separate heavy minerals, including zircons. The concentrated heavy minerals were then placed in a petri dish in ethanol under a stereoscope to be wet picked.

The three Elkahatchee Quartz Diorite samples, 17BRW154, 17BRW168, and 17BRW177 were collected in an attempt to find the oldest phase, under the assumption that the more mafic phases should have crystallized first, following the model from Drummond (1994). Sample 17BRW168 was the most mafic, having the lowest SiO_2 content (62.5% SiO_2) and containing the highest volume of biotite. It was collected from an exposure along Elkahatchee Creek where Elkahatchee Road crosses it (0595431E 3639670N). Sample 17BRW154 (65.3% SiO_2) was collected in

the Charles E. Bailey Sportplex close to the equestrian area (0595576E 3642967N). Sample 17BRW177 (67.2% SiO_2) was collected at the Alexander City Quarry (0589872E 3636913N), which is located approximately 3.5 kilometers southwest of the Alexander City Quadrangle. The last sample was chosen because Russell (1978) cited collecting a sample in a very similar location (sample FSU 106-110).

Over one hundred zircons were extracted from each sample and between twenty and forty per sample were dated in the LA-ICP-MS lab at California State University – Northridge. Data was reduced by Dr. Schwartz, and further refined with the help of Dr. Chong Ma, Auburn University.

Petrography

Thin sections were made for representative samples of each lithology in the quadrangle and others with notable textural characteristics related to metamorphism or mylonitization, as well as the samples that were sent off for age dating. Thin-section billets were cut at Auburn University and sent off to Wagner Petrographic to be prepared. Thin sections were examined under a petrographic microscope for mineralogy and for fabric and microstructural analysis.

Geochemistry

Six samples, four of Elkahatchee Quartz Diorite, one of Oaktasasi granite, and one of Sugar Creek trondhjemite, were sent to ALS Geochemistry in Reno, Nevada for whole rock geochemical analysis. Samples 17BRW154, 17BRW168P / 168NP, and 17BRW177 were the Elkahatchee Quartz Diorite samples from which the zircons were to be dated. Samples 17BRW202 and 17BRW217 were collected from Oaktasasi granite and Sugar Creek trondhjemite, respectively. 168P and 168NP were sampled from the same location, however, 168P was pulverized at Auburn, while 168NP was sent whole (not pulverized) to be crushed by ALS Geochemistry at their lab. All other samples were sent whole and pulverized at ALS. Samples 17BRW202 and 17BRW217 were analyzed as they were only recently recognized and previously unmapped. Sampling locations are shown in Figure 4.

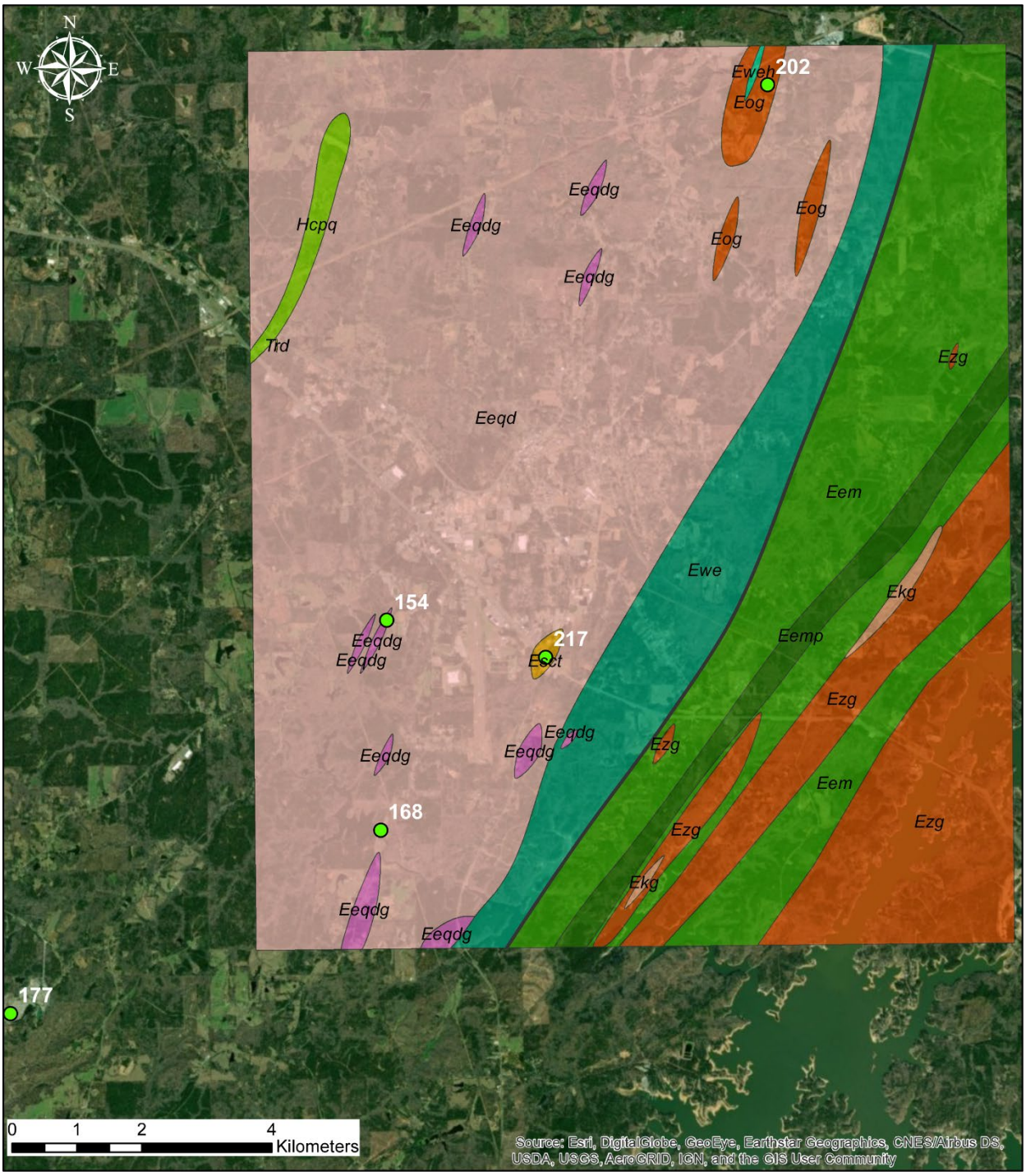

Figure 4 – Location map of all samples collected for geochemistry and geochronology. Lithology abbreviations are the same as those used in Plate 1, and they can be found in the List of Abbreviations in the forward section of this report.

LITHOSTRATIGRAPHIC UNITS

Plate 1 is the geologic map of the Alexander City quadrangle which was completed as part of this investigation. Abbreviations used in Plate 1, and in Figure 4, can be found in the List of Abbreviations in the forward section of this report. Previous workers reported finer sub-units within the Emuckfaw and Wedowee Groups (e.g. Guthrie and Dean, 1989; Hawkins, 2013; Barineau et al., 2014). The current author, however, treated the two groups as generally undifferentiated with the exception of the prominent ridge forming Perryville Member of the Emuckfaw Group as it could be traced along strike with a high degree of confidence. Focus was given to delineating the trace of the Alexander City shear zone and unraveling the complex and multi-phase nature of the Elkahatchee Quartz Diorite. A single xenolith of Pinchoulee Schist (Hatchet Creek Group) is exposed within the Elkahatchee Quartz Diorite in the northwest part of the quadrangle.

Hatchet Creek Group

Pinchoulee Gneiss

The Pinchoulee Gneiss is a thin package of fine- to medium-grained, medium to dark gray, biotite quartzite and fine- to medium-grained, dark brown-gray, quartz-rich, biotite-muscovite schist assigned to the Hatchet Creek Group in the study area; it occurs as a xenolith infolded within the Elkhatchee Quartz Diorite. The quartzite forms a prominent north to northeast striking ridge in the northwest corner of the quadrangle. The southern exposure of the Pinchoulee Gneiss crops out

along the railroad behind West End Baptist Church (Fig. 5) where a northeast-striking, down-to-the-southeast normal fault (Figs. 6A and B) (0593748E 3647296N) is expressed in the same exposure. Mineral stretching lineations in the quartzite plunge shallowly to the south-southwest.

Figure 5 - Pinchoulee Gneiss quartzite. **A**: Lineated, brown-orange, fine to medium grained quartzite (0594640E 3649584N). **B**: Contact between Pinchoulee quartzite and associated granite; dashed red line is the approximate contact with quartzite above to the right and granite in the bottom left of the photograph.

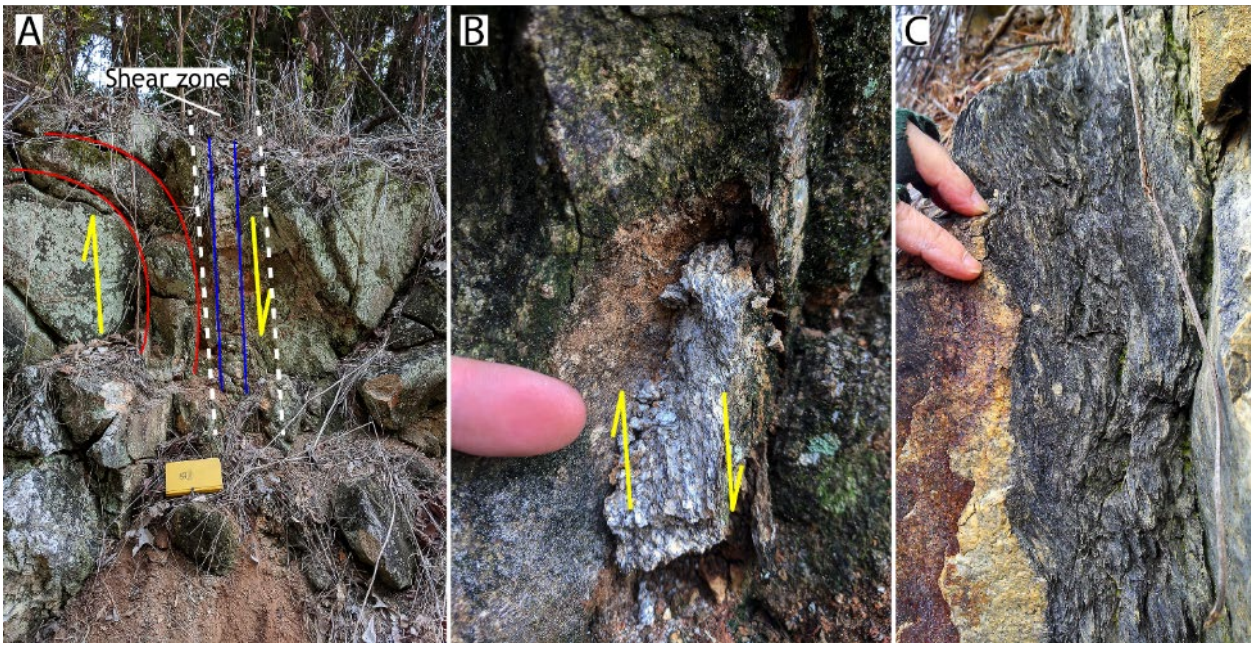

Figure 6 – High-angle normal faults within Elkhatchee Quartz Diorite directly adjacent to its contact with Pinchoulee Gneiss quartzite (0593748E 3647296N) and within Sugar Creek trondhjemite (0598028E 3642394N). **A**: Outlined in blue a subvertical quartz vein, in red drag folded Elkahatchee with yellow arrows indicating fault movement, and the shear zone boundaries outlined in white dashes. **B**: Sheared and mylonitized quartzo-feldspathic material between blue and red lines in A showing dextral rotation with right-most (southeast) side down normal-slip movement. **C**: Subvertical brittle-ductile normal fault cutting the Sugar Creek trondhjemite (0598066E 3642529N); looking northeast along strike.

Wedowee Group

Wedowee Undifferentiated

The Wedowee Group in the Alexander City Quadrangle is located to the west and structurally below the southeast-dipping Alexander City shear zone. The Wedowee Group comprises multiply foliated and interlayered medium- to coarse-grained, locally graphitic, garnetiferous muscovite-biotite-quartz-feldspar phyllite and schist (Fig. 7), and thin garnetiferous muscovite-biotite schist. Quartz veins and stringers are common and coplanar with the principal metamorphic foliation, S_1, (Fig. 7), which also is generally parallel to the axial surfaces to F_2 and F_3 folds. Garnets are rusty-red in color and usually < 5mm in diameter. The schists commonly have a golden-tan sheen and weather to a reddish-brown color; more quartz- and biotite-rich layers are dark gray. The schists and phyllites are strongly sheared with distinct S-C fabrics and phacoidal-shaped lithons that indicate right-slip movement (Fig. 7). Small, rootless, oblique-downdip plunging asymmetrical z-folds folds are common (Fig. 8). Weathering is nearly complete such that natural outcrops of the phyllite are rare and typically the only indication that Wedowee schists are present in a given area are mica fish or buttons found in tree throw and along talus slopes.

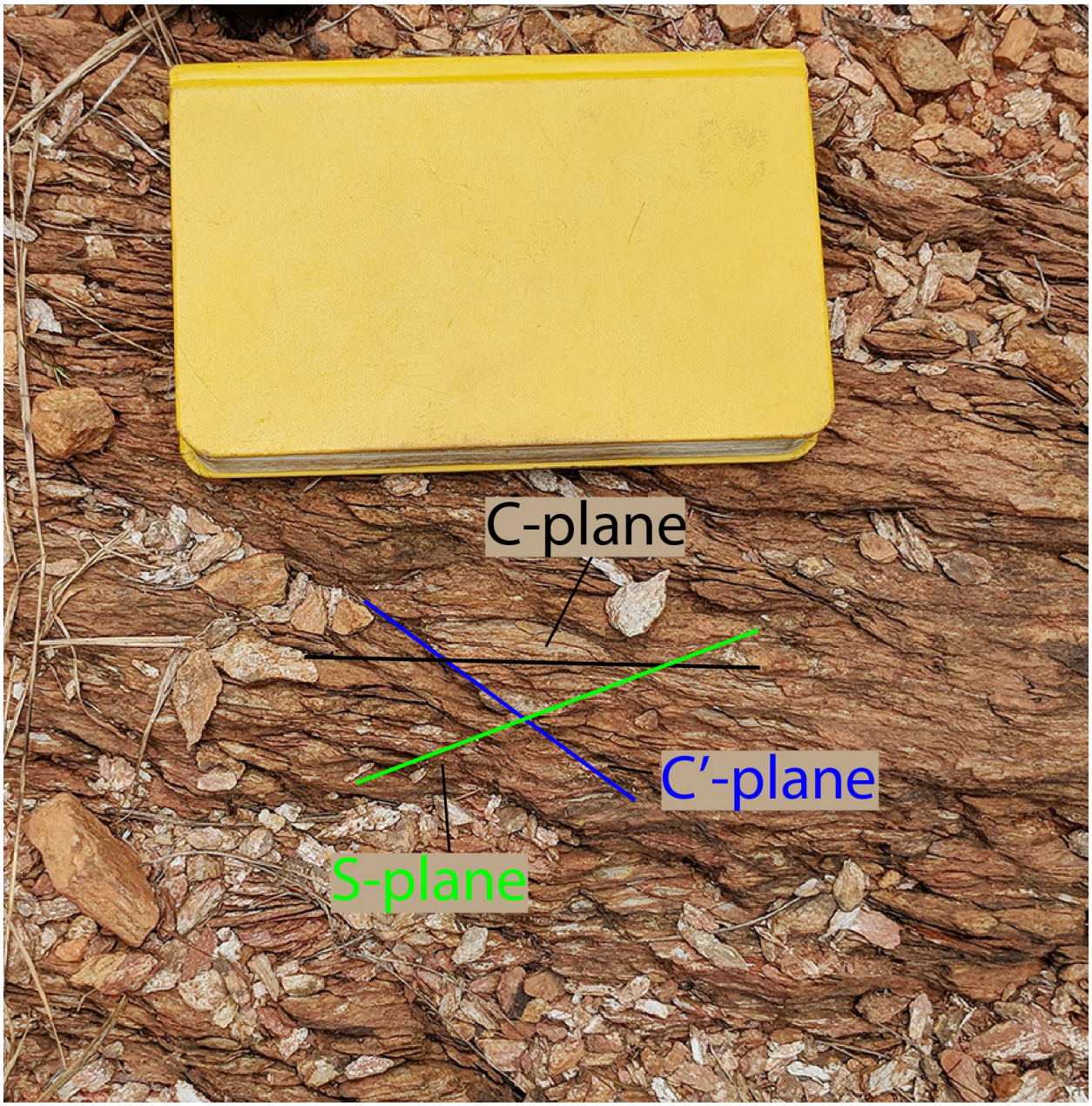

Figure 7 - Wedowee schist in the northeast section of the Alexander City Quadrangle showing S-C fabrics looking down plunge of the moderately southeast plunging S-C intersection. Outcrop is of a fine to medium grained schist with muscovite, sericite, quartz, and very small garnets. (Location: 0603522E 3651413N)

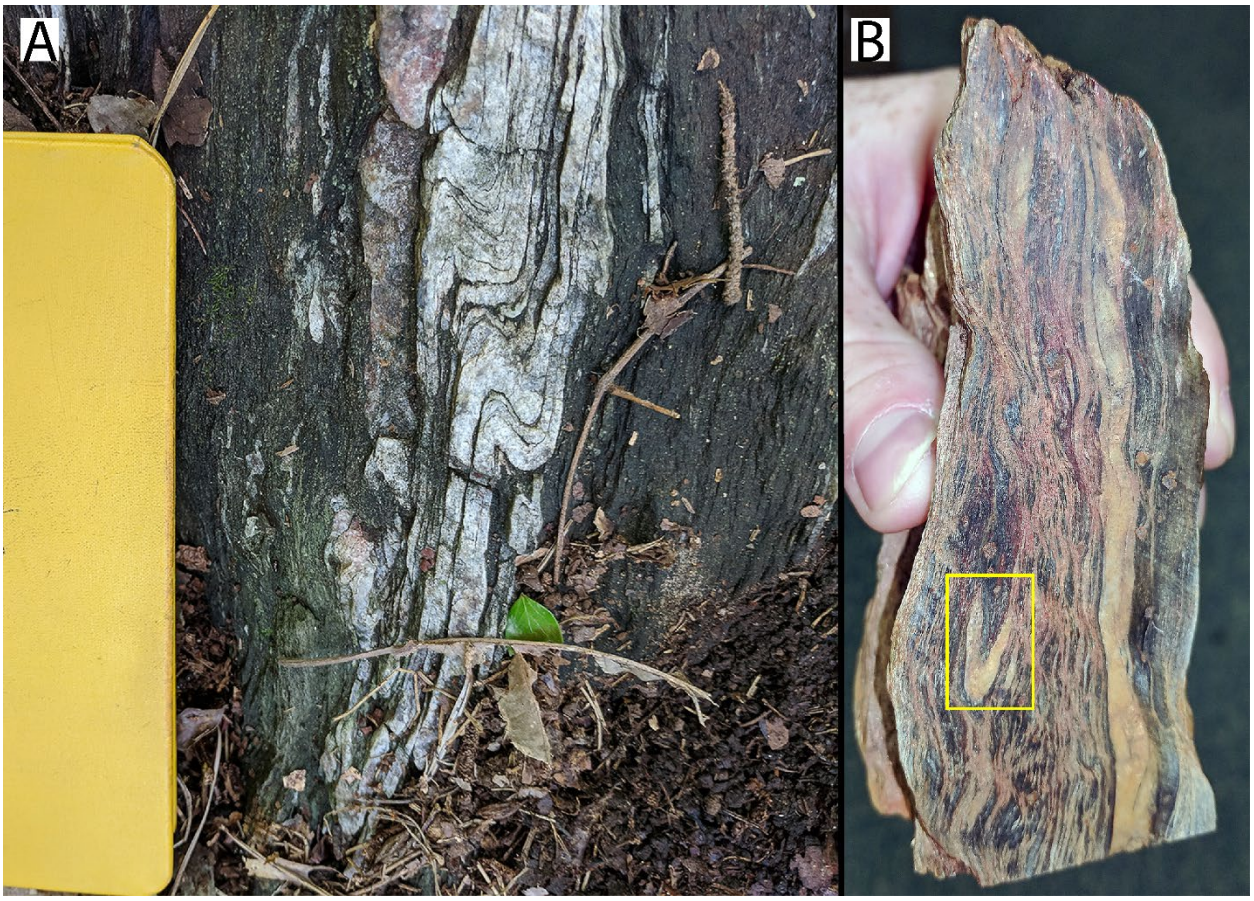

Figure 8 - Wedowee Group schist. **A**: Outcrop of a schist within the Wedowee Group showing rootless, asymmetric Z folds in a quartz vein indicating a dextral shear sense. View looking northeast down-plunge of fold axis. (Location: 0597251E 3638697N); **B**: Slabbed hand sample of Wedowee garnetiferous graphitic schist showing dextral shear and flattening with a rootless, isolated tight-to-isoclinal F_2 fold hinge within a quartz sand layer. The fold within the yellow rectangle is shown under thin section in Figure 8.

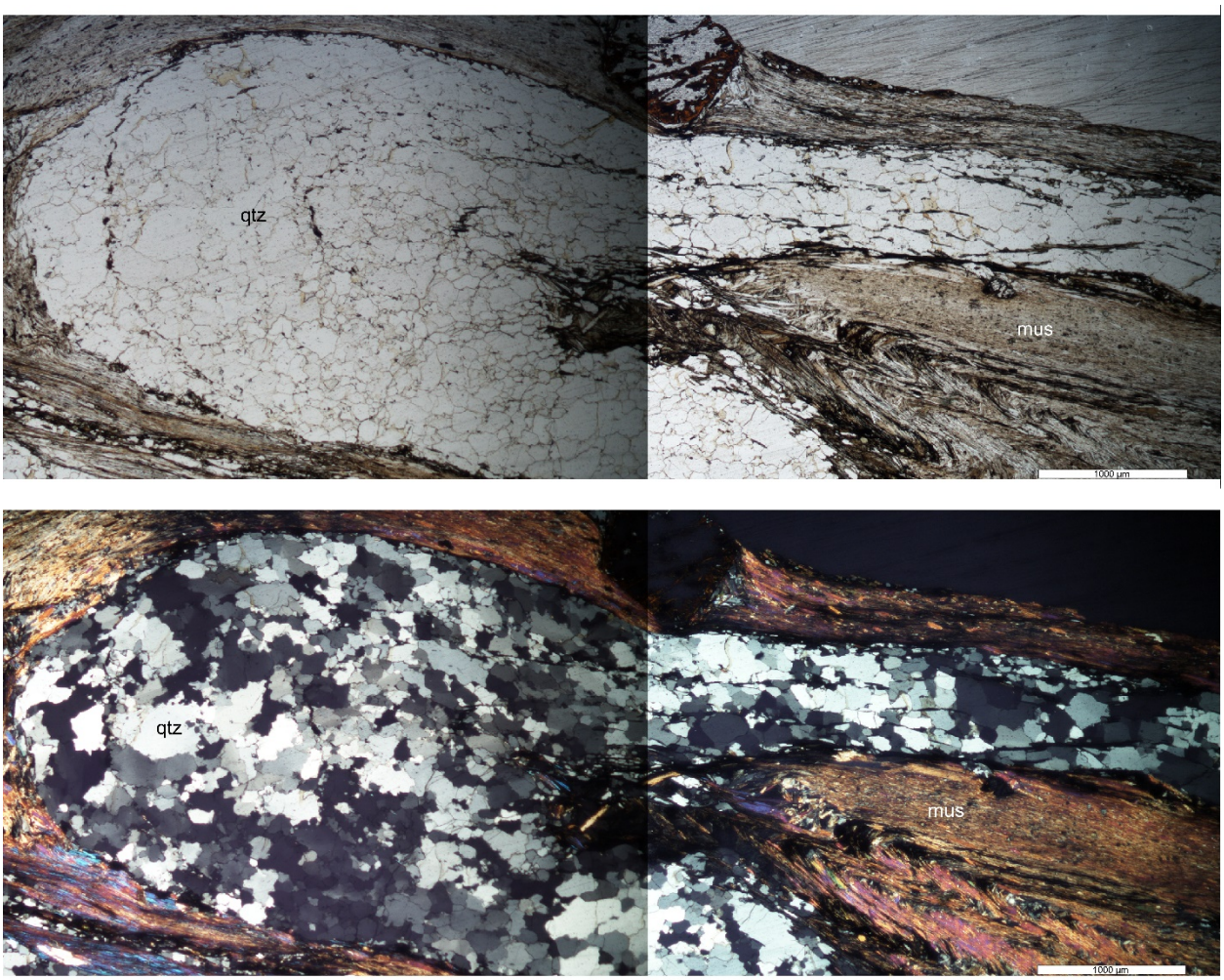

Figure 9 - Photomicrograph of Wedowee schist, zoomed into yellow rectangle in Figure 7 (top: plain light; bottom: crossed polarized light). The quartz is interpreted to be a folded sand layer or, and quartz in the fold nose shows predominantly lobate grain boundaries indicating grain-boundary migration recrystallization. Note the multiple folds in the micas within the larger quartz fold. These are interpreted to be F_3 folds, in which the principle metamorphic foliation, S_0/S_1, is folded but the axial planar S_3 foliation is not.

Hackneyville Schist

The Hackneyville Schist occurs within the Oaktasasi granite which is itself surrounded by the Elkahatchee Quartz Diorite. It is a fine- to medium-grained, medium to dark gray, banded paragneiss consisting of mainly biotite, quartz, and feldspars and assigned to the Wedowee Group. Outcrop quality is poor and saprolite and soils are orange-brown; saprolite commonly retains the foliation, which is coplanar to the regional foliation measured in the encapsulating Oaktasasi granite and Elkahatchee Quartz Diorite. Float of the Hackneyville is common in areas where the Oaktasasi granite has intruded it, and the generally hard, equigranular appearance likely reflects contact metamorphism that converted the schist to paragneiss.

Emuckfaw Group

The Emuckfaw Group lies east of the main Alexander City shear zone, structurally above the Wedowee Group. In the study area, the Emuckfaw is mainly quartz-muscovite and sericite schist that is variably garnetiferous and interlayered with metagraywacke (Fig. 10). Garnet typically ranges from a few millimeters to nearly a centimeter in diameter, is dark-red almandine, and usually euhedral (Fig. 11). Inclusion trails are common in the garnets, many of which are discontinuous with the orientation of the external foliation which suggests they were rolled during deformation (Fig 12). The schists of the Emuckfaw Group show a silvery-gray sheen and usually crop out as fins.

Emuckfaw phyllonites have prominent S-C fabrics indicating a dextral sense of shear, which is also expressed by asymmetrical rootless folds of the primary foliation (Fig. 10). Quartz ribbons have high aspect ratios of around 20:1. The Perryville Schist (Eemp) is a distinctive, low-amplitude, moderate wavelength ridge former that is traceable at least as far north as New Site, Alabama (Guthrie and Dean, 1989), over approximately 30 km. The Perryville Schist has been referred to as the Perryville quartzite (Guthrie and Dean, 1989), but in the area of the Alexander City quad, it is a medium-gray, quartz-rich, garnetiferous, muscovite schist. The Perryville typically crops out as fins, due to the high quartz content, which also gives it a distinct clink when tapped with a hammer or finger.

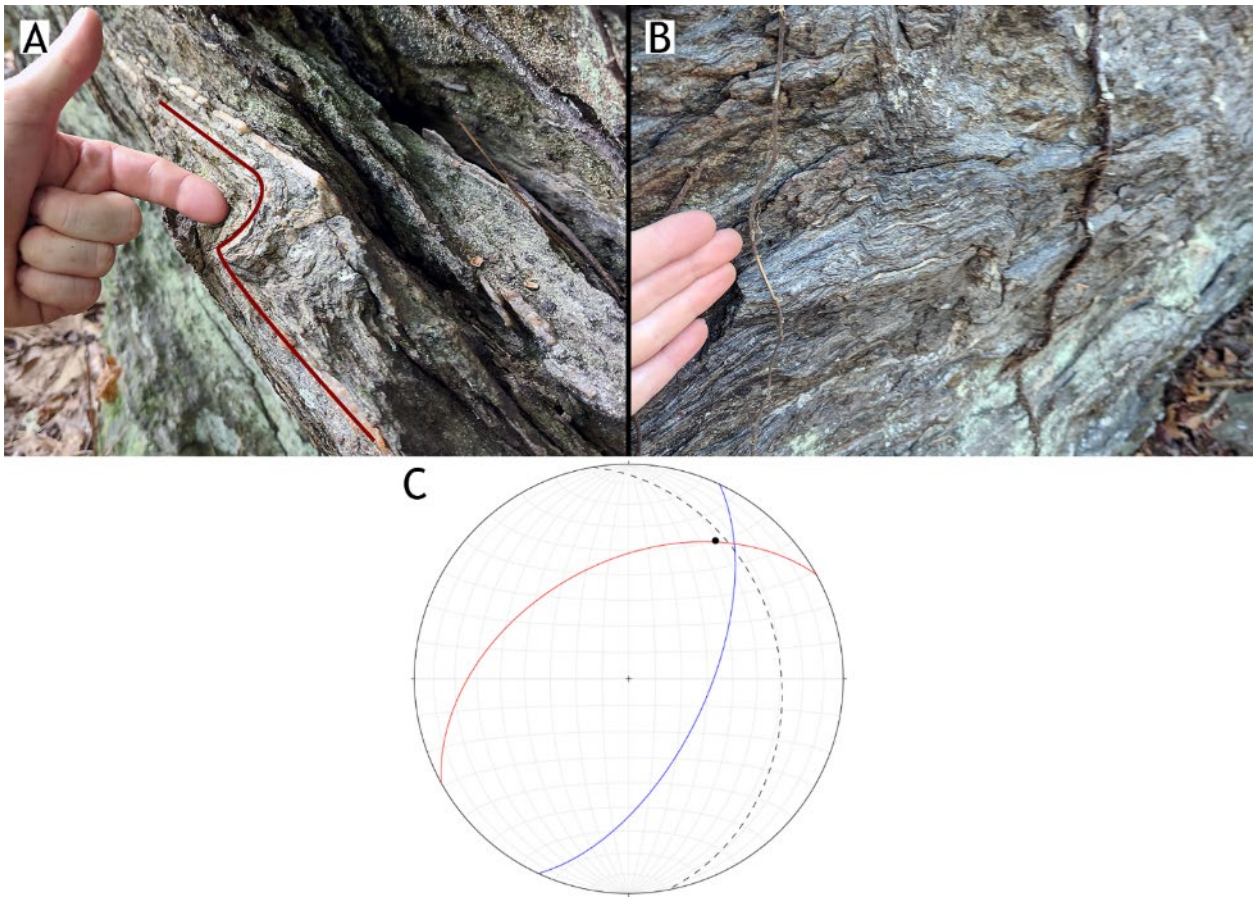

Figure 10 - Lithology and structure of the Emuckfaw Group. **A**: Rootless asymmetric z-fold in Perryville Schist member. The Z-fold indicates a dextral sense of shear associated with D_3. View is looking northeast down-plunge of the axis. **B**: Outcrop view of schist within the Emuckfaw Group. The schist is characteristically medium gray, fine to medium grained, with quartz, muscovite, biotite, and garnet. Note interlayering with salt-and-pepper metagraywacke (e.g. near tips of the ring and pinky finger). **C**: Lower hemisphere equal-area stereoplot of the z-fold in A. The blue line is the long limb, red line is the short limb, dashed line is the axial surface, and the black dot is the measured fold hinge, which is in good agreement with the intersection of the measured planar elements. (Location: 0605157E 3646639N)

Figure 11 - Perryville Schist member of the Emuckfaw Group looking on the plane of compositional layering, S_0, which is generally coplanar with the schistosity, S_1 (i.e., composite S_0/S_1). Note abundant large (~5 mm) almandine garnets. (Location: 0603507E 3644142N).

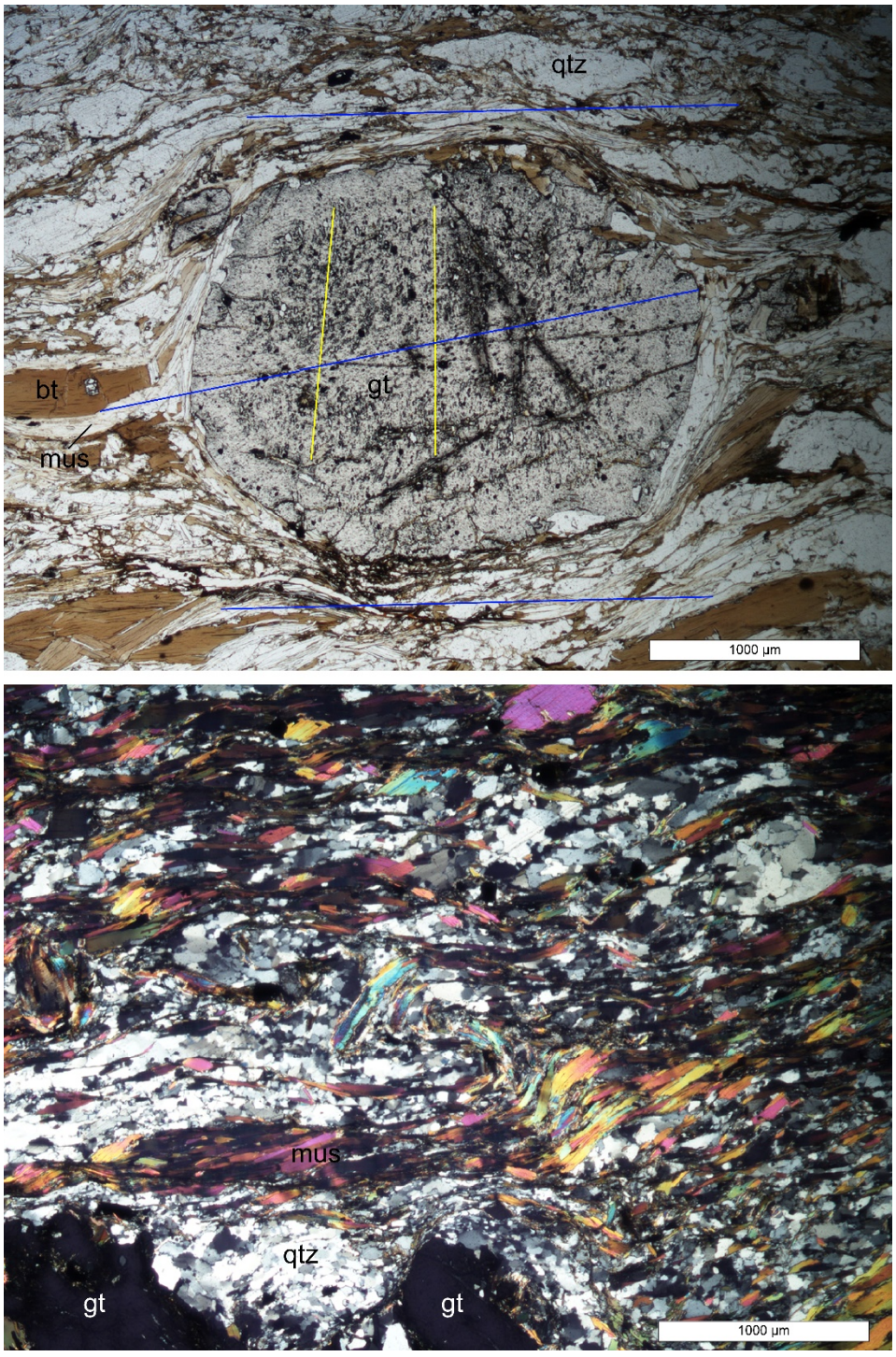

Figure 12 - Photomicrographs of garnet-mica schists of the Emuckfaw Group. **Top**: Sample 17BRW98B under plain light shows a 2.5 mm garnet with numerous aligned inclusions. Blue lines denote the general orientation of the metamorphic foliation, S_1, whereas the yellow lines show the alignment of inclusion trails, S_0, which are discontinuous, suggesting that the garnet has been rolled after crystallization. **Bottom**: Sample 17BRW111 shows warped and folded undulatory micas and mica fish within the main foliation that indicate dextral shear (cross polarized light).

INTRUSIVE UNITS

The northwestern portion of the Alexander City quadrangle is dominated by Elkahatchee Quartz Diorite and associated xenoliths and intrusive phases, whereas the southeastern portion contains schists of the Wedowee and Emuckfaw Groups and intrusive bodies of the Zana Granite and Kowaliga Gneiss (Plate 1). The Alexander City shear zone trends southwest-northeast through quadrangle southeast of Alexander City. Most exposures in the quadrangle show at least some degree of retrograde mylonitic/phyllonitic overprint, but shearing is most prominent in the weaker pelitic units of the Wedowee and Emuckfaw Groups, especially proximal to the contact with the Elkahatchee.

Elkahatchee Quartz Diorite

The Elkahatchee Quartz Diorite (Fig. 13) is an 880 km^2 tonalitic-granodioritic batholith (Drummond et al., 1994). It is primarily composed of feldspar (mainly plagioclase), quartz, biotite, and muscovite, with minor zircon, garnet, sphene, pyrite, magnetite, and apatite (Gault, 1945). In outcrop, it is commonly medium to dark gray. Along the contact with Wedowee schists, the Elkahatchee is strongly sheared with well-developed mylonites displaying S-C fabrics and sigma-porphyroclasts indicating dextral shear (Figs. 13C and D; see also Steltenpohl et al., 2013b). Toward the northwest part of the quadrangle the degree of shearing and penetrative fabric development diminishes, with the rocks becoming generally more massive (Figs. 13A and B). Granitic pods were discovered within the

Elkahatchee and these generally are tan-orange or tan-white in color with more feldspar and/or muscovite and less biotite than the typical tonalite (Fig. 13C). These granitic units are generally less well foliated than the more mafic phases of the Elkahatchee, but their foliation planes generally have the same strike and dips.

Exposures of the Elkahatchee Quartz Diorite are commonly found throughout the northwest part of the Alexander City Quadrangle. Mapping in this area has shown the Elkahatchee to be more complex than was previously recognized. The author documented granodiorite, quartz diorite, granite, and trondhjemite all within what areas that has been mapped as Elkahatchee Quartz Diorite (Osborne et al., 1988). Prominent exposures of Elkahatchee Quartz Diorite include the following: those along U.S. 280 at the intersection with County Road 63 (0598028E 3642394N), where it is in contact with the Sugar Creek trondhjemite; along Elkahatchee Creek both on Fish Pond Road and Elkahatchee Road (0594050E 3640788N and 0595477E 3639662N, respectively); in multiple road cuts along State Road 22 (0598418E 3645566N and 0599464E 3646379); along Elkahatchee Creek where it flows into Lake Martin (0596819E 3638881N); as well as along the contact with schists of the Wedowee Group; good exposures of both the mafic and felsic phases can be found within the Charles E. Bailey Sportplex (0595184E 3642606N).

In thin section, 17BRW154 is medium-grained with a hypidiomorphic texture formed with plagioclase, biotite, muscovite, quartz, and minor myrmekite. It has a weak foliation defined by undulose biotite, muscovite, and quartz, some of which appear to have been weakly dynamically recrystallized (Fig. 14).

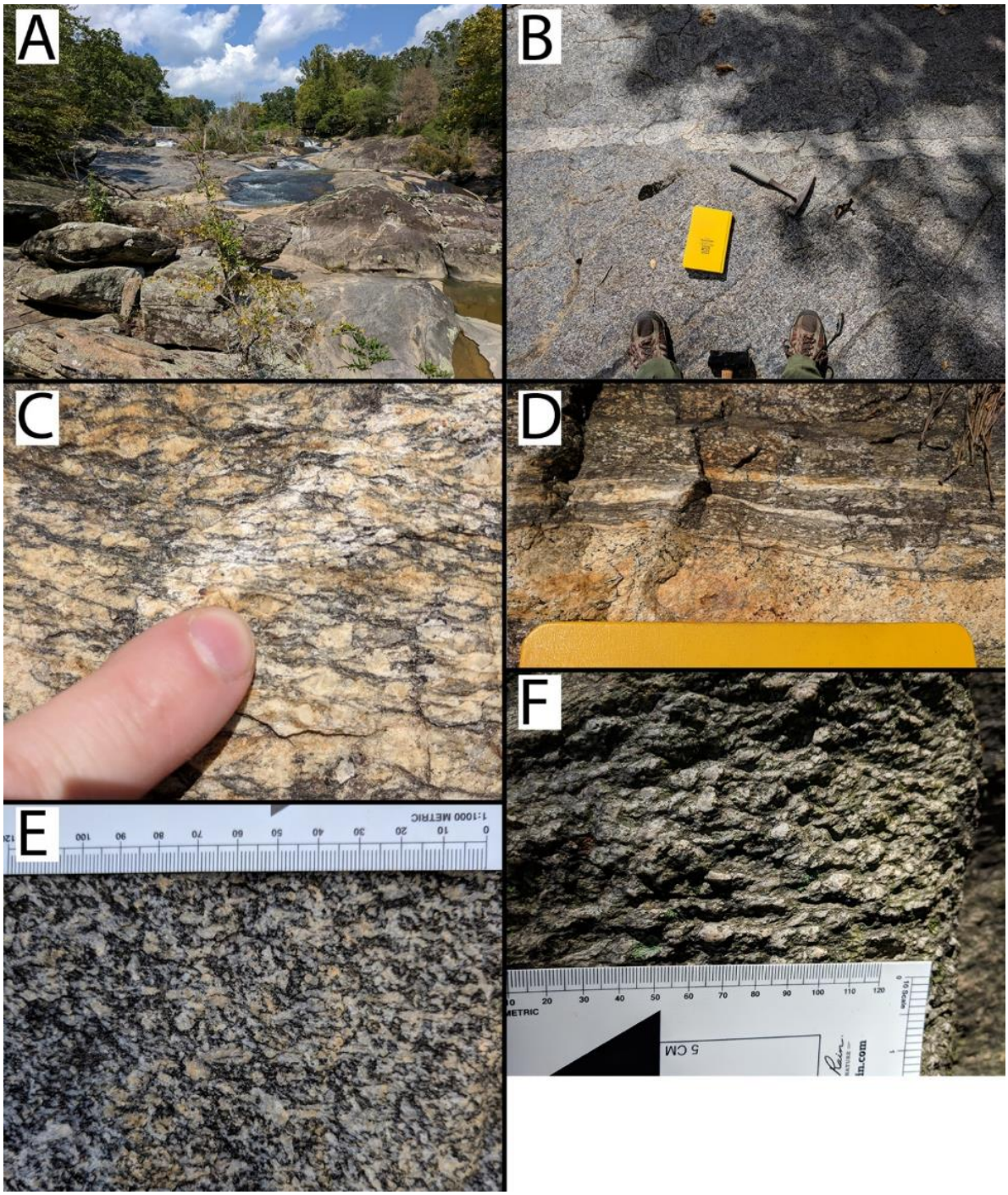

Figure 13 - Elkahatchee Quartz Diorite. **A**: Exposures of tonalite within the Elkahatchee Quartz Diorite along Elkahatchee Creek off Fish Pond Road (0594050E 3640788N); **B**: Trondhjemite dike cutting across foliation, same location as **A**; **C**: Close up of a more felsic phase of the Elkahatchee Quartz Diorite at the Charles E. Bailey Sportplex. Generally the more felsic phases are less strongly foliated than the more mafic phases (see below) but this photo illustrates a well-mylonitized example; S-C fabrics and σ-type indicate a dextral sense of shear viewed down the moderately southeast-plunging S-C intersection lineation (0595880E 3642807N); **D**: Intense ultramylonitic fabrics present in more mafic phase striking northeast, same location as C; **E**: Exposure of Elkahatchee along Highway 22 with abundant biotite and plagioclase. (0599464E 3646379N); **F**: Exposure of well-foliated mylonitized Elkahatchee with large σ-type porphyroclasts of plagioclase on Sugar Creek indicate dextral shear (0598481E 3642214N).

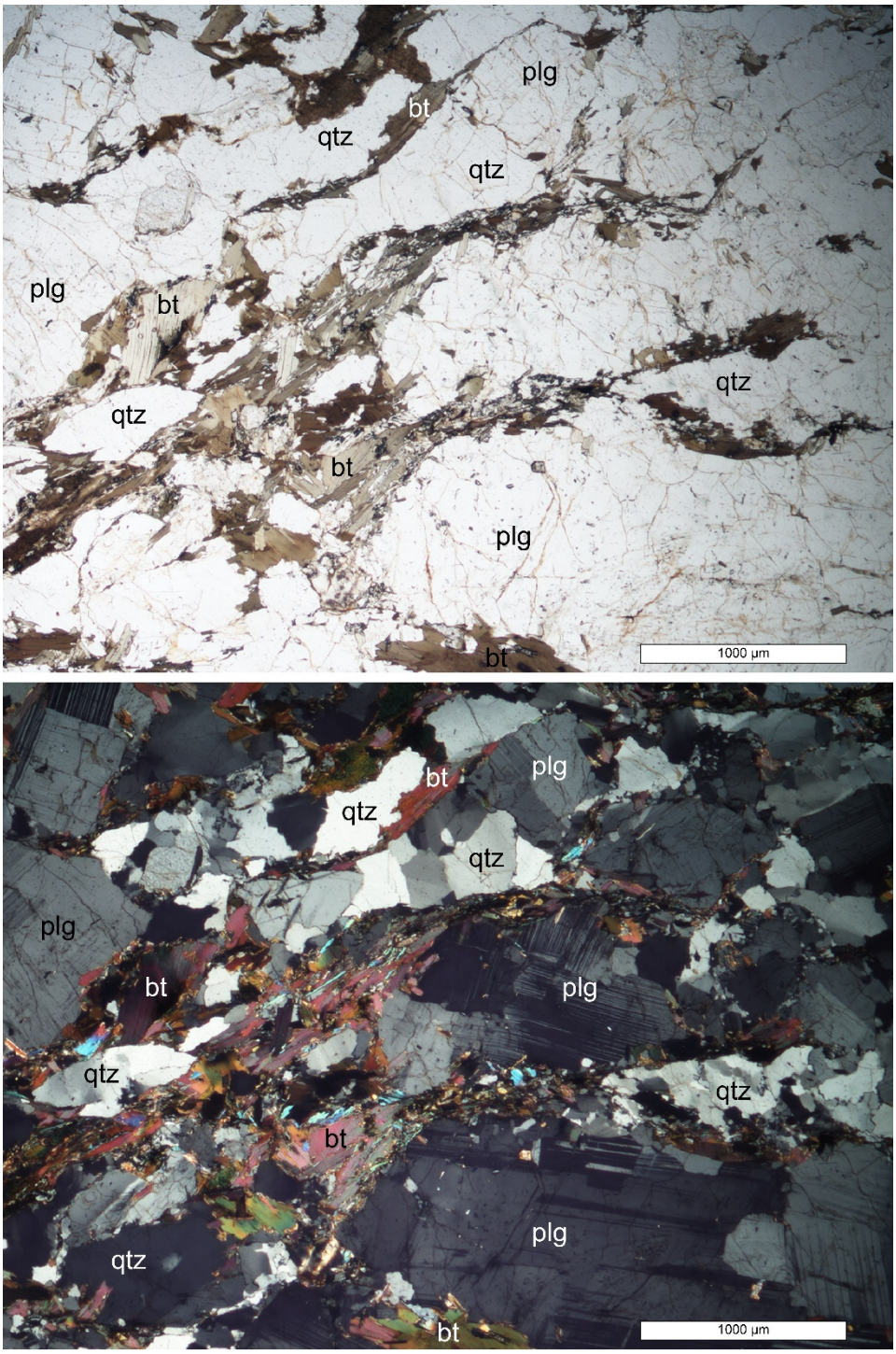

Figure 14 - Photomicrographs of Elkahatchee Quartz Diorite sample 17BRW154 show hypidiomorphic grains of plagioclase and quartz, with foliation defined by undulose biotite and mild dynamic recrystallization of quartz. Upper photomicrograph is under plain light and the lower one is the same area under cross-polarized light.

Zana granite & Kowaliga Gneiss

The Zana Granite and Kowaliga Gneiss occur as interleaved plutonic intrusives within the Emuckfaw Group of the Alexander City quadrangle. Bentley and Neathery (1970) and Hawkins (2013) concluded that the Zana Granite and Kowaliga Gneiss are geochemically similar and share very similar crystallization ages (e.g. 441 ± 6.6 Ma for the Kowaliga; Hawkins, 2013) with the only differences being their shear fabrics and geographical occurrence, which is consistent with observations from the current report. Sagul (2016) reported U-Pb zircons ages of 457 ± 9 Ma to 473 ± 12 Ma for the Zana and 455 ± 8 Ma to 467 ± 9 Ma for the Kowaliga, which further supports a relation between the Zana and Kowaliga. In exposures of the current study area, the Zana Granite is a medium- to coarse-grained granitic gneiss containing quartz, plagioclase, muscovite, and biotite (Fig. 15). The Zana has a well-developed foliation defined by the alignment of biotite and muscovite grains and stretched feldspar and quartz grains, with mineral stretching lineations trending northeast and plunging gently (<10°). Good exposure can be found along Coley Creek (0604159E 3644138N) (Fig. 15). Sagul (2016) reported εHf values -6.1 to -23.4 and -9.5 to -10.0 for the Zana and Kowaliga, respectively, and proposed that these values are suggestive of petrogenesis derived from melting of continental crust.

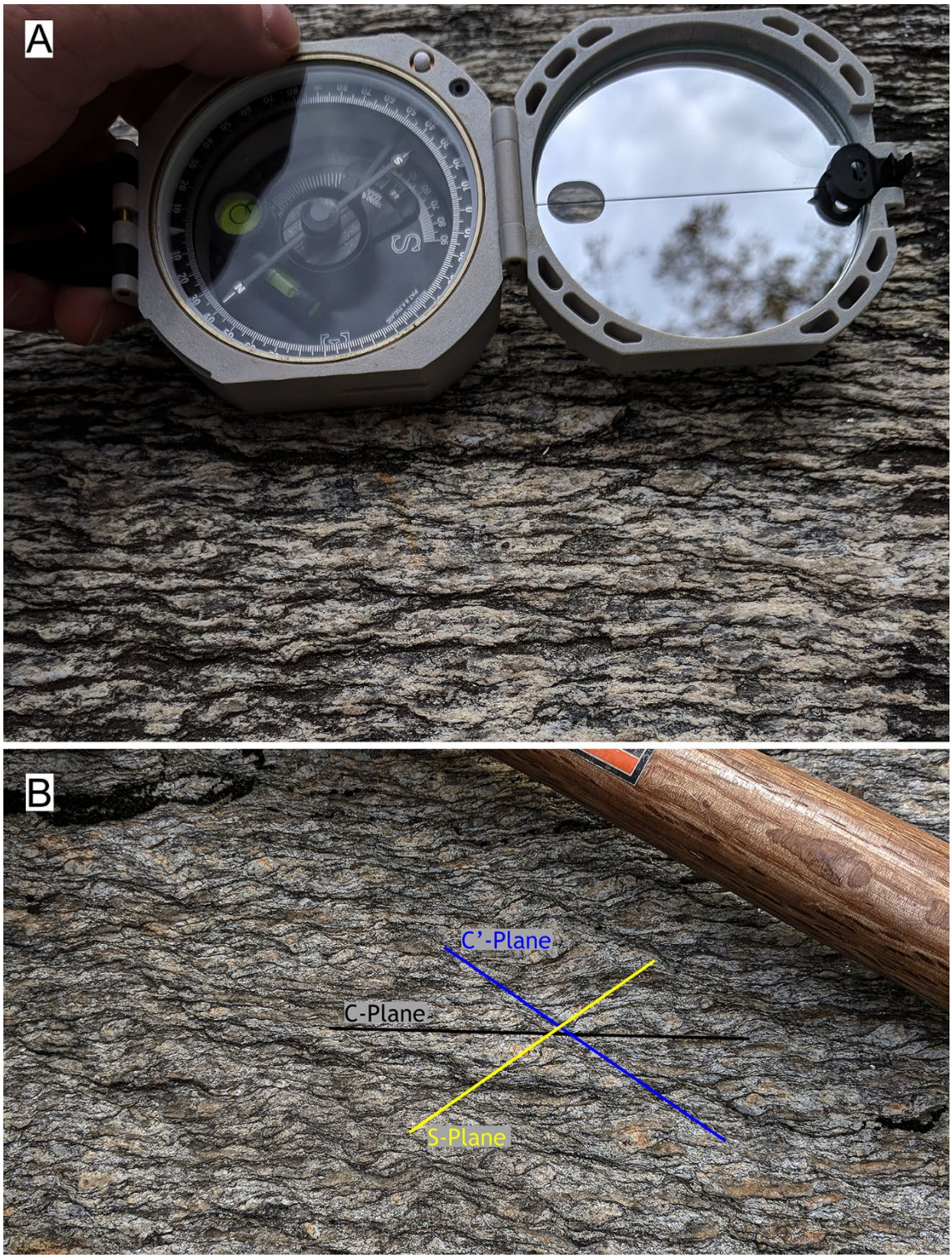

Figure 15 - Zana Granite exposed along Coley Creek (0604152E 3644138N). **A**: Close up of the N40°E striking, moderate southeast-dipping principle foliation (parallel to the long dimension of the photo) that characterizes the Zana. This foliation is considered a highly sheared S-C fabric where both planes (i.e., S_1/S_2) approach parallelism. **B**: Distinct S-C and C'-Plane fabrics in the Zana indicating dextral shear. View looking down dip of moderately southeast-plunging S-C intersection.

In thin section, the Zana Granite is a medium-grained, strongly foliated granitic gneiss. Predominant mineralogy is plagioclase and quartz with quartz and muscovite defining the foliation. Muscovite fish, undulose micas, and micro-boudinage is commonplace in the muscovite sheets indicating post crystallization shearing (Fig. 16).

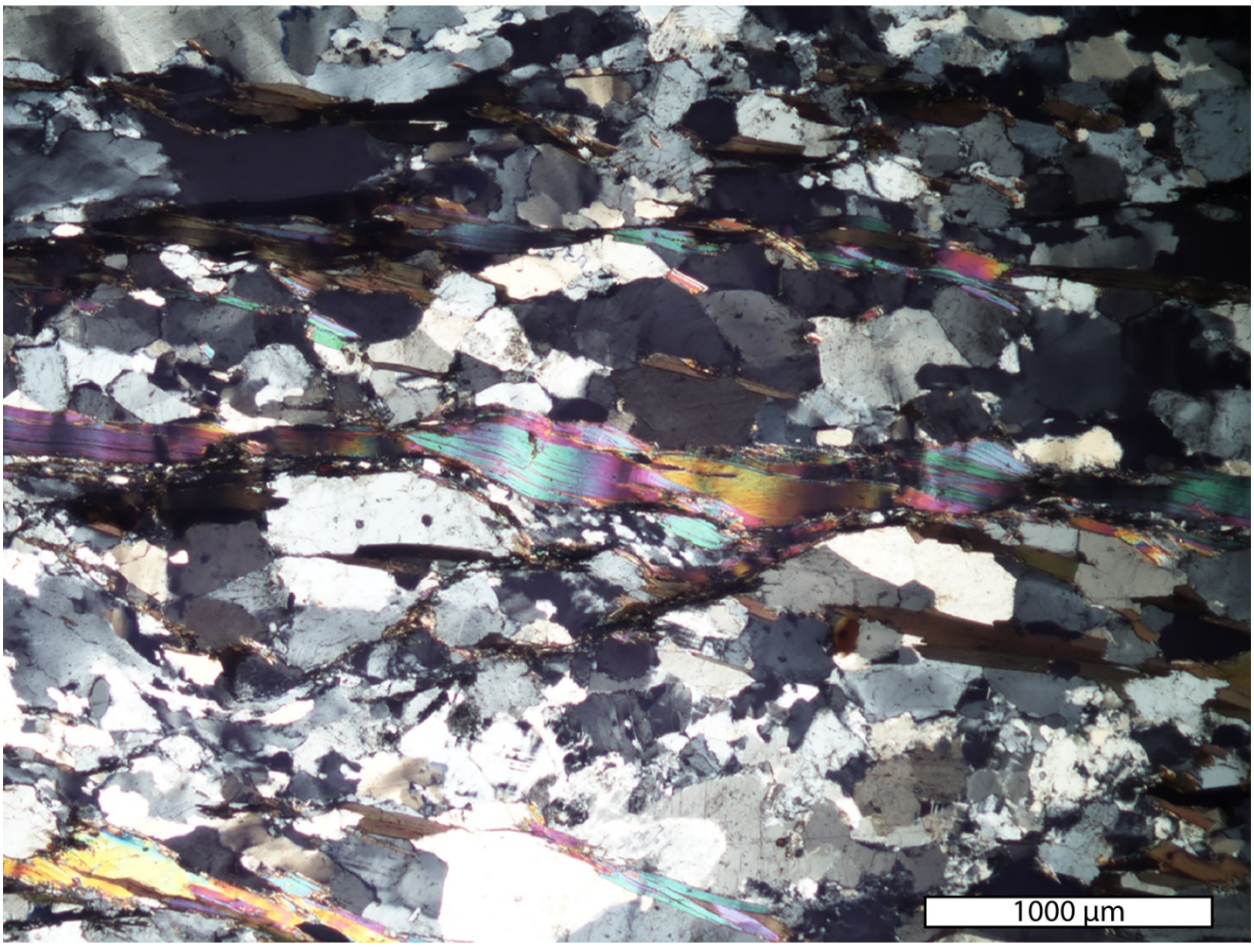

Figure 16 - Photomicrograph of Zana Granite (sample 17BRW08) under crossed polarized light,showing crystal-plastic deformation of quartz and muscovite. Note undulose and boudinaged muscovite in the center of the photomicrograph.

Within the study area, the Kowaliga Gneiss, is a medium- to very coarse-grained megacrystic augen gneiss composed of plagioclase, quartz, potassium feldspar, biotite, muscovite, and retrograde chlorite and epidote (Fig. 17). The dominant foliation is defined by aligned biotite and muscovite grains that drape larger, more competent subhedral K-feldspar megacrysts and augens. The Zana Granite and Kowaliga Gneiss commonly have composite S-C fabrics and asymmetric porphyroclasts indicative of oblique dextral- and a slight normal-slip component of movement. Mineral lineations are characteristic of the Zana Granite, and to a lesser extent, the Kowaliga Gneiss and they comprise stretched feldspar and biotite grains and elongate ribbons of quartz. In fresh outcrops of either unit, the color varies from white-tan to light gray, and saprolitized outcrops are light orange to buff; saprolite commonly retains the primary metamorphic foliation. Small exposures of Kowaliga Gneiss can be found along the railroad tracks under Coley Creek Road (0603083E 3642844N) and along Raintree Drive (0599501E 3638401N) (Fig. 17).

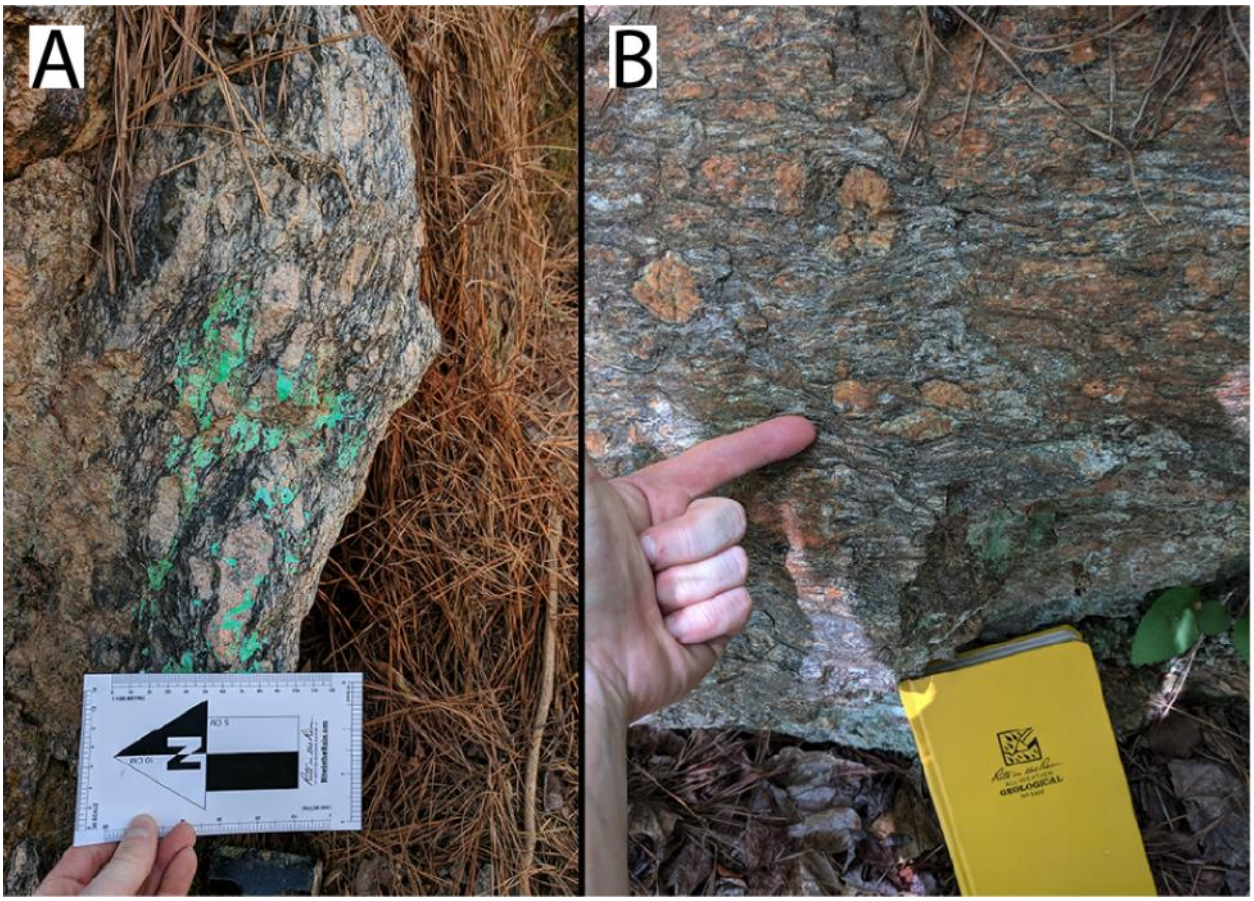

Figure 17 - Kowaliga Gneiss. **A**: Outcrop in railroad cut looking down dip of the southeast dipping foliation oriented N53°E 65° SE. Note the large (8 cm) megacrysts of potassium feldspar with finer matrix of sheared feldspar, biotite, and quartz (0603083E 3642844N). **B**: Another outcrop view of megacrystic Kowaliga Gneiss (0599501E 3638901N).

Sugar Creek trondhjemite

The Sugar Creek trondhjemite is herein informally named for its proximity to Sugar Creek near to its prominent exposure at the intersection of highway U.S. 280 and AL 63 (Cherokee Road) in Alexander City (Fig 18; 0598028E 3642394N). The Sugar Creek trondhjemite is a light-gray, medium- to coarse-grained trondhjemite composed of plagioclase, quartz, minor potassium feldspar, muscovite, and biotite. The main body of the trondhjemite is massive to weakly foliated and generally has an average strike of N24°E and dip of 34° SE, coplanar with the regional metamorphic foliation of the Elkahatchee Quartz Diorite that it intrudes. Locally the trondhjemite is cut by mylonitic shears (Fig. 18 and 19) that appear to be more pronounced along its margins. Along the west-margin of the Sugar Creek trondhjemite (0598066E 3642529N), clear intrusive relations with the older Elkahatchee Quartz Diorite are exposed (Fig 18A). The Sugar Creek trondhjemite has U-Pb zircon ages that suggest a ~335 Ma age of igneous crystallization (Schwartz, personal comm., 2017). Quartz-feldspar elongation lineations are parallel to the strike of shear planes and S-C composite fabrics and σ-type porphyroclasts document right-lateral strike-slip motion (Fig. 20).

In thin section the Sugar Creek trondhjemite is a moderately foliated trondhjemite with plagioclase, quartz, biotite, and muscovite (Fig 21). Plagioclase grains are generally hypidiomorphic whereas quartz grains mostly show undulose extinction. Folia are defined by biotite, muscovite, and quartz. Many of the plagioclase grains have inclusions which

are likely sericite related to the breakdown of the feldspars.

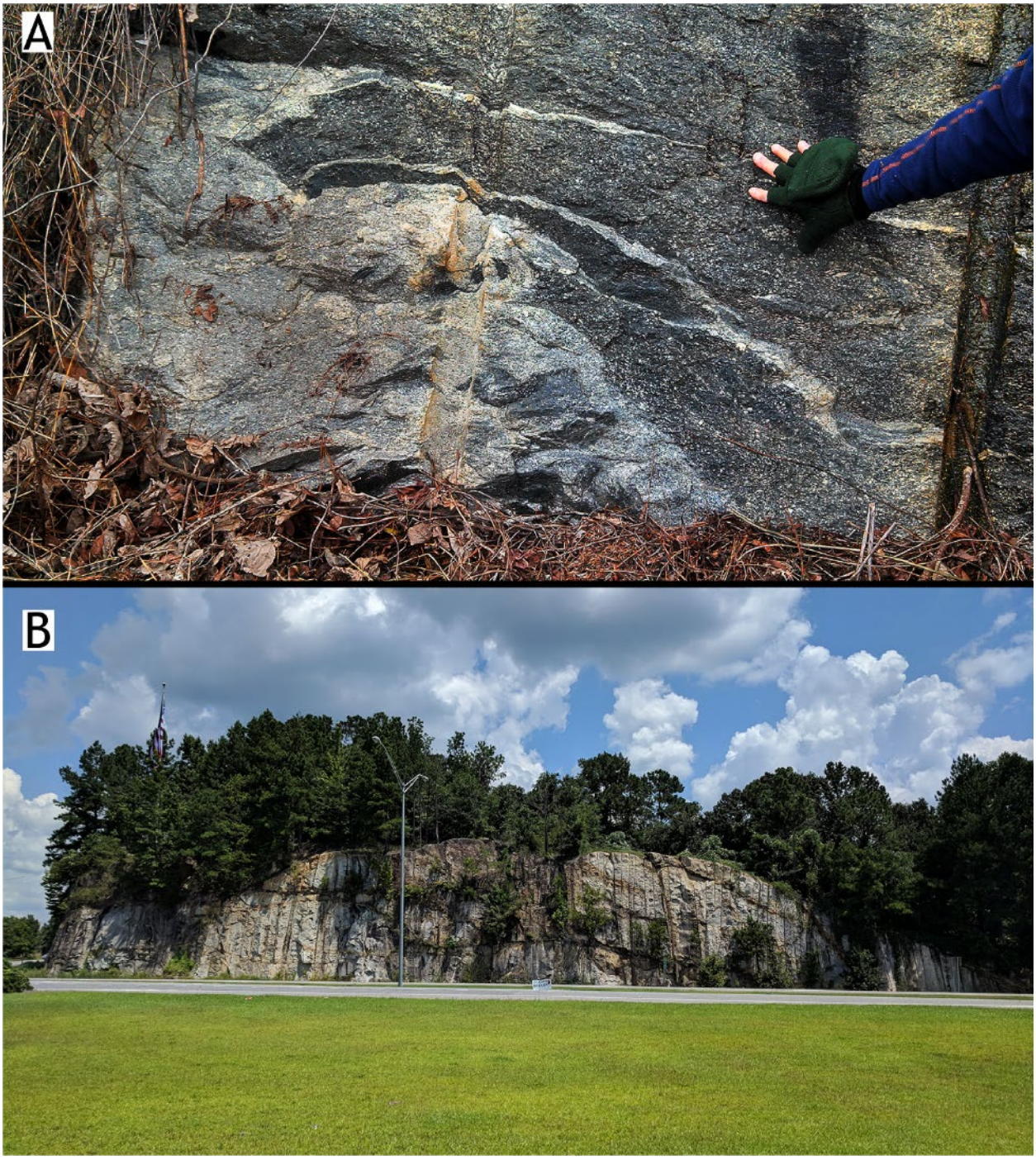

Figure 18 - Sugar Creek trondhjemite. **A**: Intrusive contact between the Sugar Creek trondhjemite (left, light gray) with the Elkahatchee Quartz Diorite (right, dark gray to black). Note the veining and interleaving along the boundary. **B**: Exposure of Sugar Creek trondhjemite along U.S. 280 looking northeast along strike. Dark curved bands are mylonitic shears.

Figure 19 – Shallow to moderately southeast-dipping, tops-southwest, right-lateral strike-slip fault in the Sugar Creek trondhjemite. Arrow tail (circle with cross) indicating movement into the plane of the photo and arrow tip (circle with dot) indicating movement coming out of the plane of the photo; fault plane attitude is N64°E 38° SE.

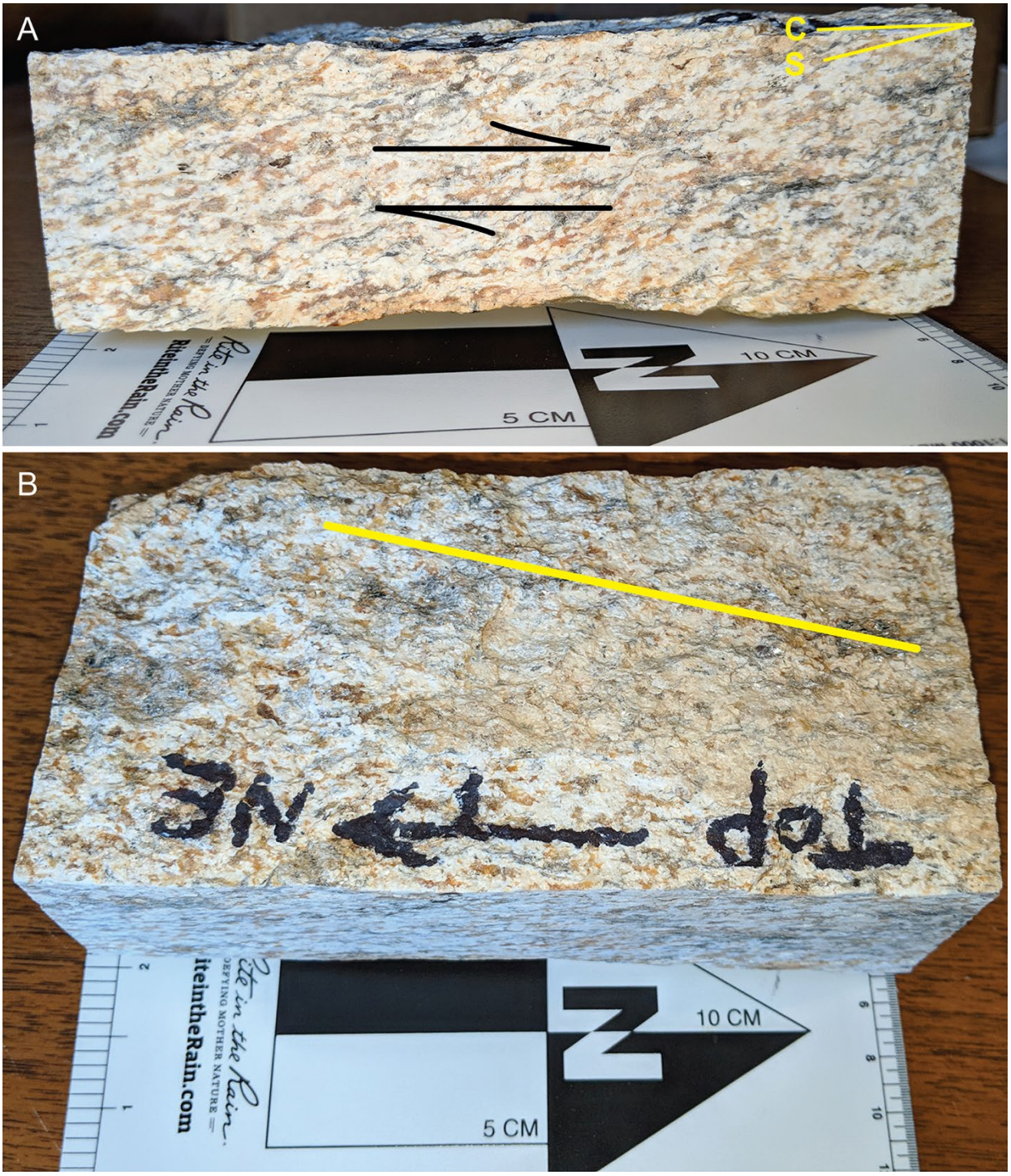

Figure 20 – Slabbed oriented sample of Sugar Creek trondhjemite from the low-angle strike-slip fault illustrated in Figure 19. **A**: View perpendicular to foliation and parallel to the elongation lineation with S-C fabrics indicating dextral, top-to-the-southwest movement. **B:** Looking down upon the foliation plane. The yellow line is the nearly strike-parallel mineral elongation lineation.

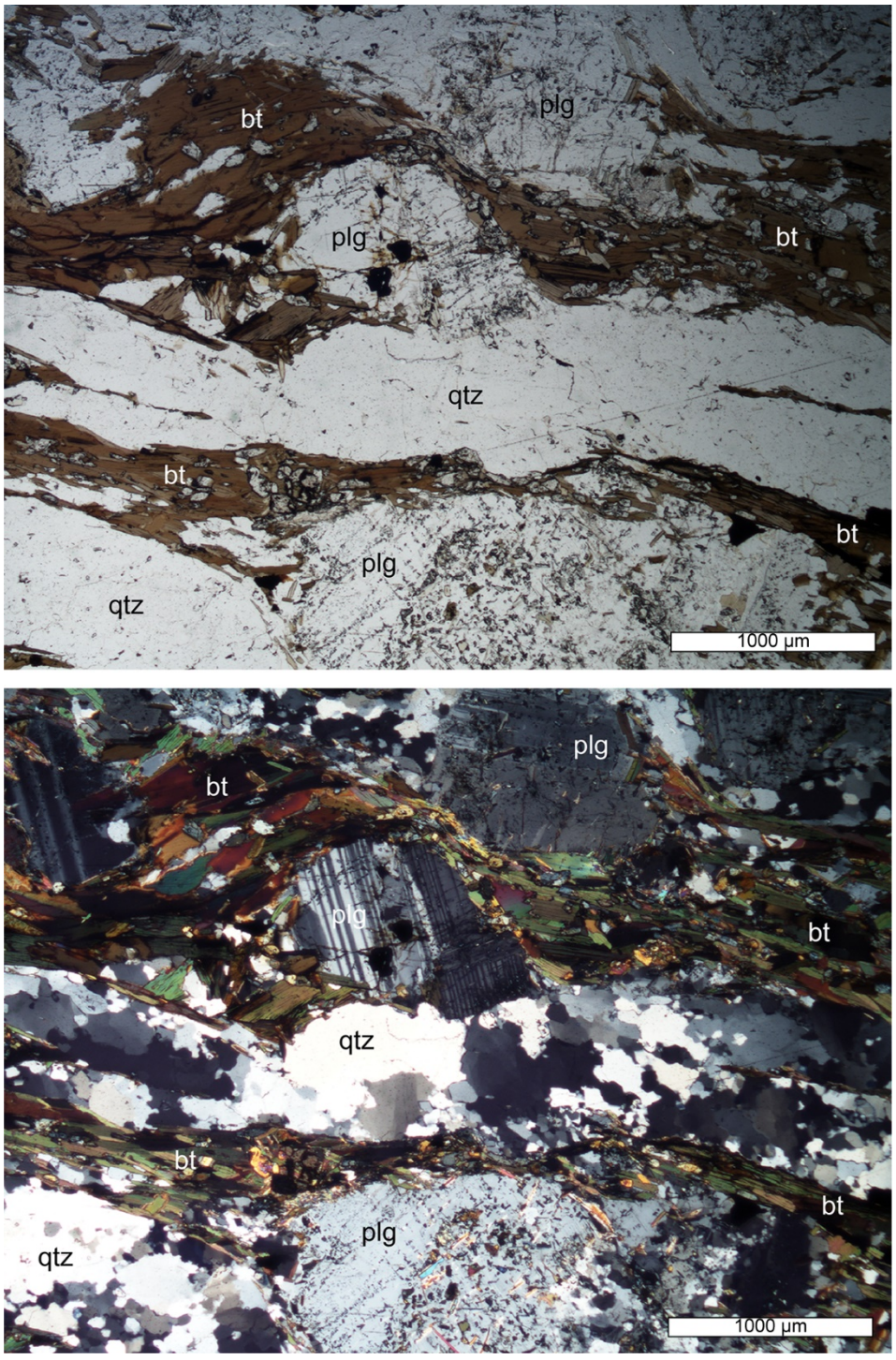

Figure 21 - Photomicrographs of Sugar Creek trondhjemite sample 17BRW211. **Top**: Foliation is defined by biotite and quartz layers. The large plagioclase grain (bottom center) shows numerous inclusions. (Plain light) **Bottom**: Quartz shows undulose extinction and interlobate boundaries within quartz ribbons indicating grain boundary migration recrystallization; biotite is undulose and some fish-like grains are present. (Same view as top photo but under crossed polarized light.)

Oaktasasi granite

Multiple lenticular bodies of granite are also identified in the Elkahatchee Quartz Diorite and are herein informally called the Oaktasasi granite for exposures near Oaktasasi Creek (601515E 3651793N). Several of these granites appear to correspond to areas that were originally mapped as the Hackneyville Schist of the Wedowee Group (Plate 1). The Oaktasasi granite is a pinkish-tan, medium to coarse-grained, massive to weakly foliated granite, with plagioclase, quartz, potassium feldspar, muscovite, and biotite (Fig. 22). The micas appear as <0.5 cm books, with little to no preferred orientation. Where foliated, strike is coplanar to the regional foliation (~N34°E, ~60°SE). Some of the more prominent exposures crop out as large whalebacks, having weathered in a spheroidal fashion (Fig. 23). The general lack of foliation suggests that this unit is younger than the well-foliated Elkahatchee into which it intrudes.

In thin section, the Oaktasasi granite is a medium-grained, massive granite with hypidiomorphic to subhedral plagioclase, quartz, muscovite, and minor potassium feldspar and biotite (Fig 24). Euhedral mica books are unconnected and spaced regularly from one another. Sericite is found at the boundary between muscovite and feldspar having grown in a needle-like habit. The weak foliation is suggestive of flow while the magma intruded the surrounding schist, essentially contact metamorphosing the schist to a somewhat massive and dense paragneiss.

The Oaktasasi granite shares some similarity in composition and texture to the Rockford Granite (compared to Ingram, 2012), though it may represent a completely separate suite of granites altogether. No radiometric age dates exist on samples of the Oaktasasi granite. Based on texture (i.e. a lack of (strong) foliation), however, it is likely younger than the last peak metamorphic (Neoacadian) event.

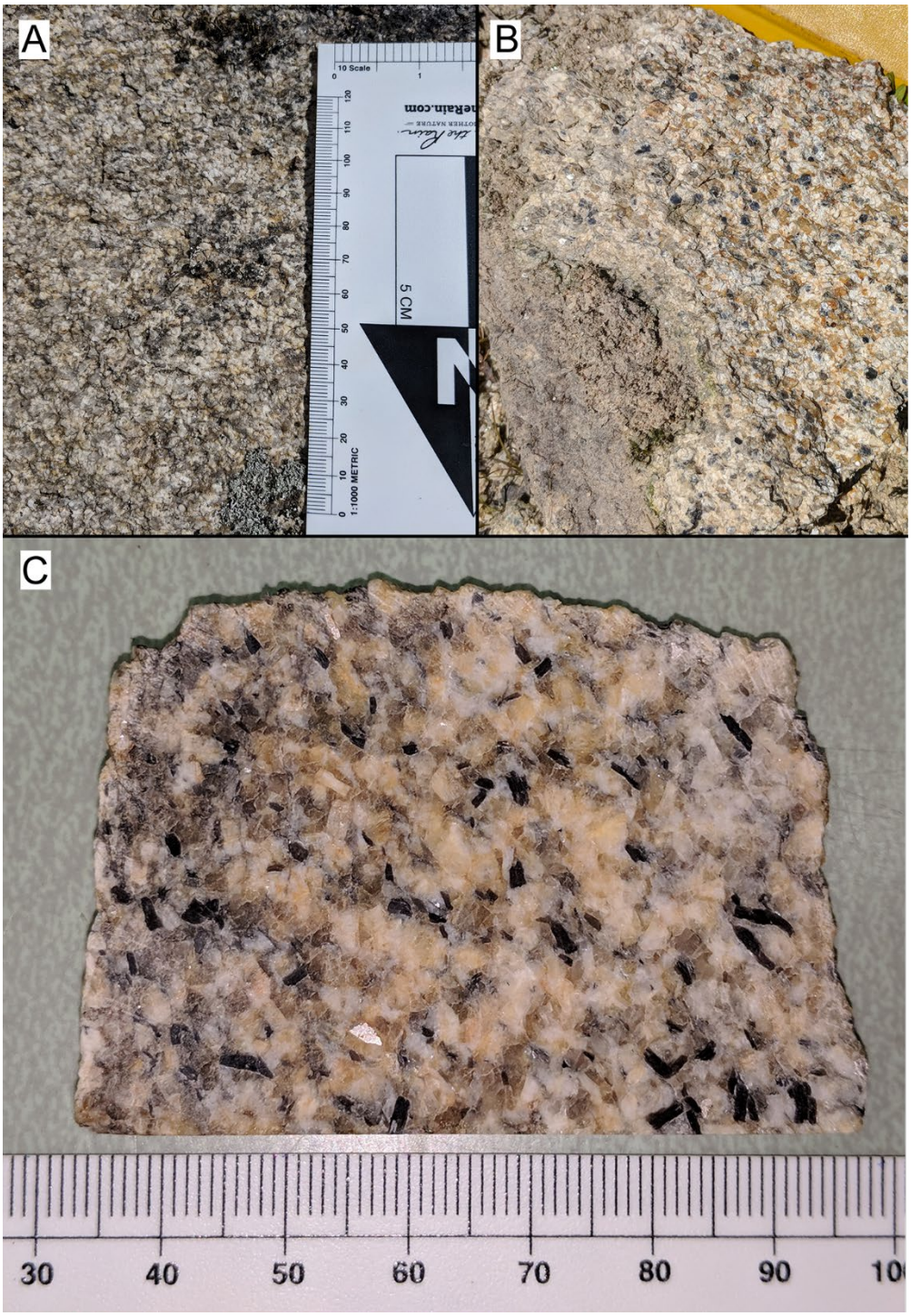

Figure 22 - Oaktasasi granite. **A**: Outcrop of Oaktasasi granite showing a tan-pink, massive, medium grained texture, with plagioclase, quartz, potassium feldspar, muscovite, and biotite. **B**: In this image the individual books/grains of muscovite and biotite can be seen in no preferred orientation and no other foliation is recognized. **C**: Polished slab of Okatasasi granite. Note the distinct books of biotite do not form a foliation and are only weakly aligned. (Location: 0601148E 3651222N)

Figure 23 - Outcrop of Oaktasasi granite. Note its massive character and distinct sphereoidal weathering. (Location: 0601354E 3651265N)

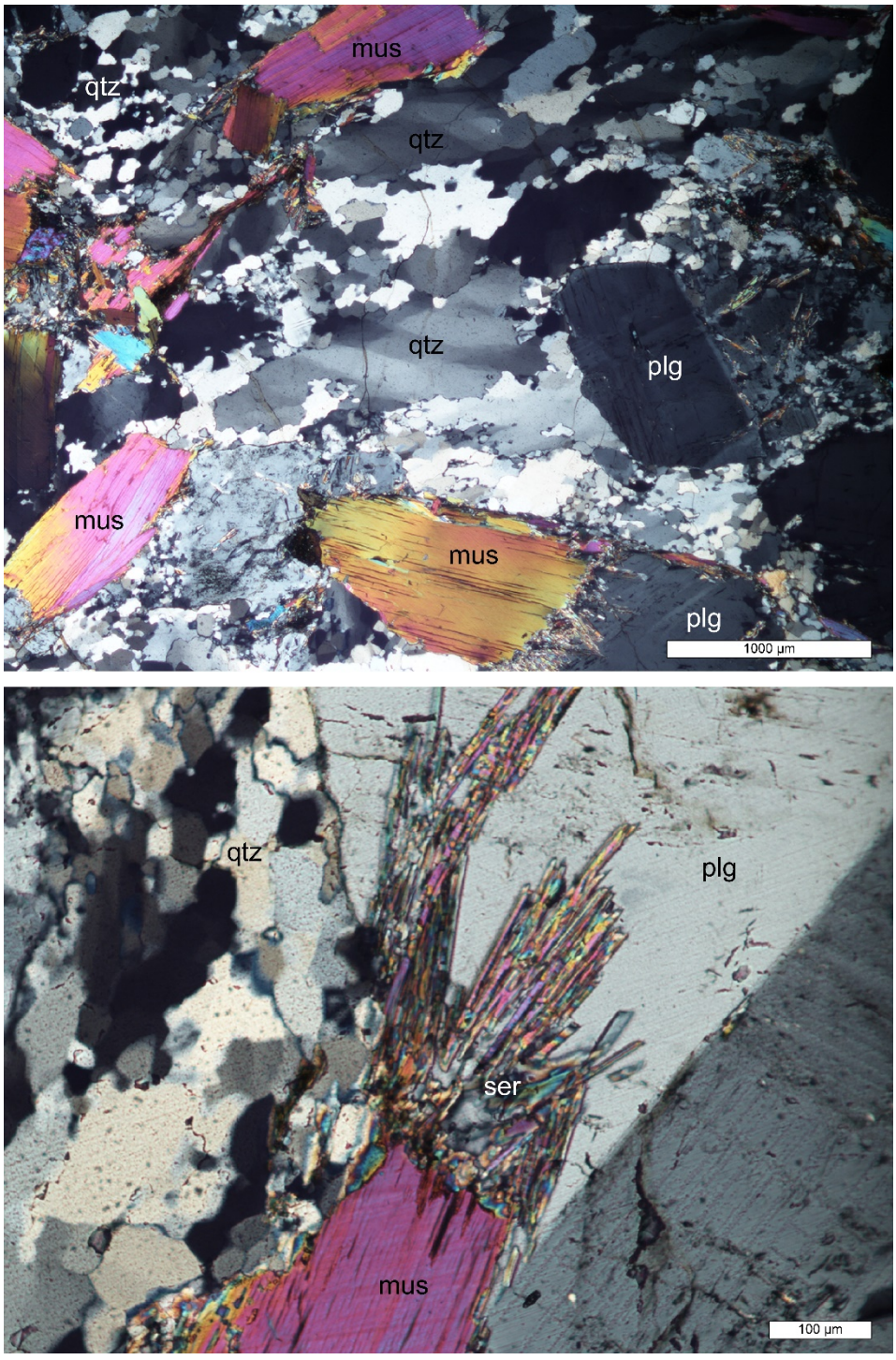

Figure 24 - Photomicrograph of Oaktasasi granite sample 17BRW207. **Top**: Deformation bands can be seen in the longer quartz grains in the center, and lobate boundaries with new grains are the rule in recrystallized areas. Sericite intergrowth into plagioclase in the bottom center. **Bottom:** Zoomed in view of a muscovite-plagioclase grain boundary with sericite growing into the plagioclase grain.

STRUCTURE

Structural observations in the Alexander City quadrangle indicate that rocks underlying the area have been multiply deformed and retain evidence of at least four deformational events, D_1 through D_4 (Table 1; all structural measurements are embedded as data files in the ArcGIS® map). The dominant regional foliation, S_1, formed during or close to peak metamorphic conditions during M_1 and is defined by the parallel alignment of phyllosilicates and other inequant minerals. This is compatible with observations of the Emuckfaw Group within the study area which contains prograde M_1 mineral assemblages comprising muscovite ± biotite ± garnet ± quartz. Petrographic study of thin sections showed no aluminosilicate minerals in rocks of the Wedowee or Emuckfaw suggesting either metamorphic grade never surpassed that of garnet grade, or the bulk composition had insufficient aluminum for the growth of aluminosilicate minerals. It was also noted that some M_1 porphyroblasts (Fig. 12) contain an earlier foliation, S_0 (see also, Hawkins, 2013 in the Our Town Quadrangle directly to the south, and Poole, 2015 in the Jacksons Gap Quadrangle directly east of the Alexander City Quadrangle). The associated mineral lineation and mineral stretching lineation, L_1, generally plunges shallowly to the northeast or southwest (Fig. 25) and is defined by a grain shape preferred orientation of inequant grains, elongated tecto- and phyllo-silicates, and quartz rods. Compositional layering (S_0; bedding?) was deformed into mesoscopic- to microscopic-scale intrafolial tight to isoclinal folds, F_1, in which the hinge surfaces are coplanar with S_1, resulting in a composite S_0/S_1 foliation. F_1 fold hinges are

presumed to be collinear with L_1, although no physical measurements of F_1 folds were made to confirm this relationship.

Table 1 - Summary of deformational events in the Alexander City Quadrangle.

Deformational Phases	Structural Elements	Description
D_1	M_1	Regional prograde amphibolite-facies dynamothermal metamorphism of the eastern Blue Ridge
	S_1	Regional foliation (schistosity and gneissosity); early movement along the Brevard fault zone and Alexander City fault occurred during the late stages of S_1 development
	L_1	Mineral lineation; nematoblastic, and within mylonitized units elongation lineation
D_2	M_2	Retrogressive reactivation and mylonitic shearing related to movement under late-to-post peak M_1 lower amphibolite facies conditions along the Alexander City shear zone
	F_2	Isoclinal, intrafolial folding of the S_0/S_1; late-F_2 folding of the Tallassee synform
	S_2	Local transposition of S_1 into parallelism with S_2
D_3	M_3	Upper greenshist-facies reactivation of the Alexander City fault
	F_3	Rootless asymmetric folds associated with movement along the Alexander City shear zone; reverse-slip crenulations; weak crossfolding
	S_3	Composite S-C mylonitic fabric and reverse-slip crenulation cleavage indicating oblique dextral-normal movement along the Alexander City shear zone
D_4		Brittle reactivation along the Alexander City shear zone resulting in cataclasites and silicified, veined breccias, and high-angle normal faults

A second deformational event, D_2, at lower amphibolite-facies conditions, deformed earlier-formed middle amphibolite facies, M_1, mineral assemblages and D_1 fabrics and structures, producing a new foliation, S_2. S_2 is consistently subparallel to and likely transposes the S_1 foliation. The composite S_1/S_2 foliation measured within the quadrangle strikes on average N35°E with an average dip of 63° to the southeast (Fig. 25). The associated mineral lineation, L_2, is coaxial with L_1 and is defined by a grain shape preferred orientation of inequant and stretched grains (Fig. 25). L_2 lineations generally trend N40°E with shallow plunges of 12°. D_2 structures of the current study are correlated with the late-peak metamorphic shear structures found elsewhere in association with the Alexander City and Brevard shear zones (Steltenpohl et al., 2013b).

F_2 folds are characterized by microscopic to mesoscopic, tight to open folds that are collinear with L_1/L_2. Additionally, late-stage mesoscale open folds and coincident broad, 10 km half-wavelength, 3 km amplitude macroscale antiforms and synforms are a later phase of the D_2 event (Steltenpohl et al., 1990; VanDervoort et al., 2017; Whitmore and Steltenpohl, 2017). Folding during D_2 produced the gently northeast-plunging Tallassee synform (Figs. 1 and 2), in which the Dadeville Complex defines the core, and the rocks of the Jacksons Gap Group and adjacent eastern Blue Ridge define the west limb for most of its extent.

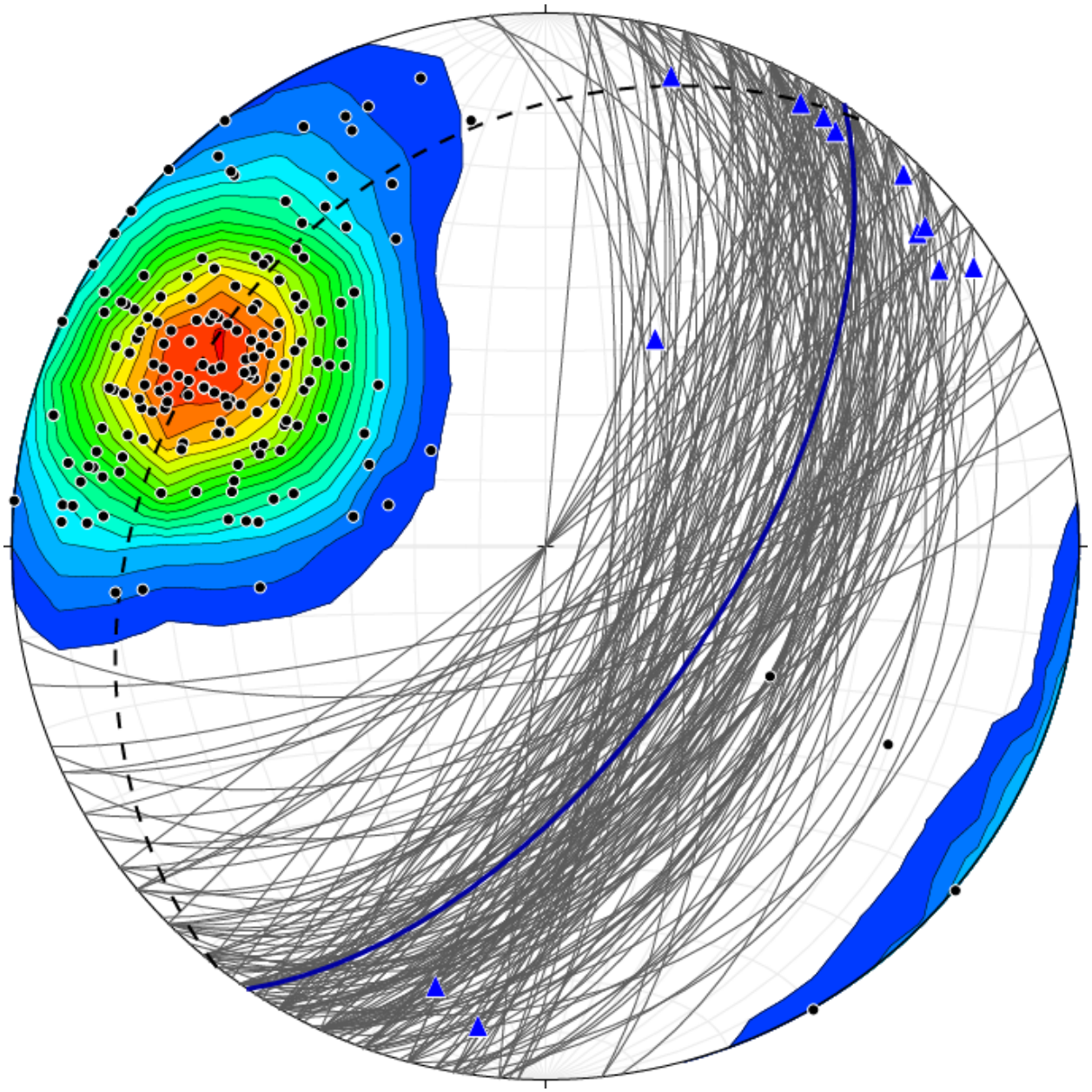

Figure 25 - Lower hemisphere equal-area stereoplot of composite S_1 and S_2 (n = 180) and L_1/L_2 lineation measurements (n = 12) in the Alexander City quadrangle. S_1/S_2 planes shown as gray lines and poles as black dots, and L_1/L_2 lineations as blue triangles. Thick blue line represents the average S_1/S_2 strike and dip of N34°E, 62° SE. Dashed black line is the great circle fit through the contoured partial girdle spread at approximately N38°E, 28° NW, which may suggest a shallow SE-plunging warping event. Differentiation between D_2 and D_3 fabric elements is difficult in the field and vestiges of both events are likely represented here.

The third deformational event, D_3, represents a prominent retrograde, greenschist-facies oblique dextral-normal-slip shearing event associated with the Alexander City shear zone. Figure 26 plots S-C fabrics and slip lines measured in phyllonites and mylonites in the Alexander City Quadrangle. Average strikes and dips of S-C fabrics are N31E 66° SE for C-planes and N18E 66° SE for S-planes. Graphically determined slip lines for the S-C fabrics plot mainly parallel to strike at approximately N27°E but are dispersed along a partial great circle spread along the C-plane (Fig. 25). Slip lines were calculated by using a custom-made Python program, sliplineCalc_0.5.py, written by the author. All algorithms were derived from SCslip.xlsm created by Dr. David Allison. Following Berthé et al (1979), slip lines are assumed to be in the C-plane and perpendicular to intersection of the C- and S-planes. The output of the Python program was then plotted using Stereonet 10 (Fig. 26). Results document oblique right-lateral-and-normal-slip motion with the former being predominant.

Rootless F_3 folds are also present in phyllonites of the study area as rootless, asymmetrical z-folds that plunge oblique- and/or down-dip within the phyllonitic cleavage, S_3, in a reverse-slip crenulation geometry (Dennis and Secor, 1987) (Figs. 8, 9, and 10). One F_3 fold in the Perryville Member of the Emuckfaw Group (Fig. 10A) was measured with S_1 long limb N25°E 60° SE, S_1 short limb N61°W 45° NW, axis N32°E 25° SE, and axial surface N20°W 30° SE (Fig. 10C). The geometries, kinematics, and rheologies of the low-angle right-slip shear zones within the Sugar Creek trondhjemite (Figs. 19 and 20) indicate that they too are D_3 structures. In the

study area, the D_3 shear zones, therefore, are interpreted to correspond to the array of Alleghenian dextral strike-slip shear zones that extend throughout the hinterland to as far northwest as the Goodwater-Enitachopco fault and the Goat Rock fault zone to the southeast (Steltenpohl, 1988; Steltenpohl et al., 2013b).

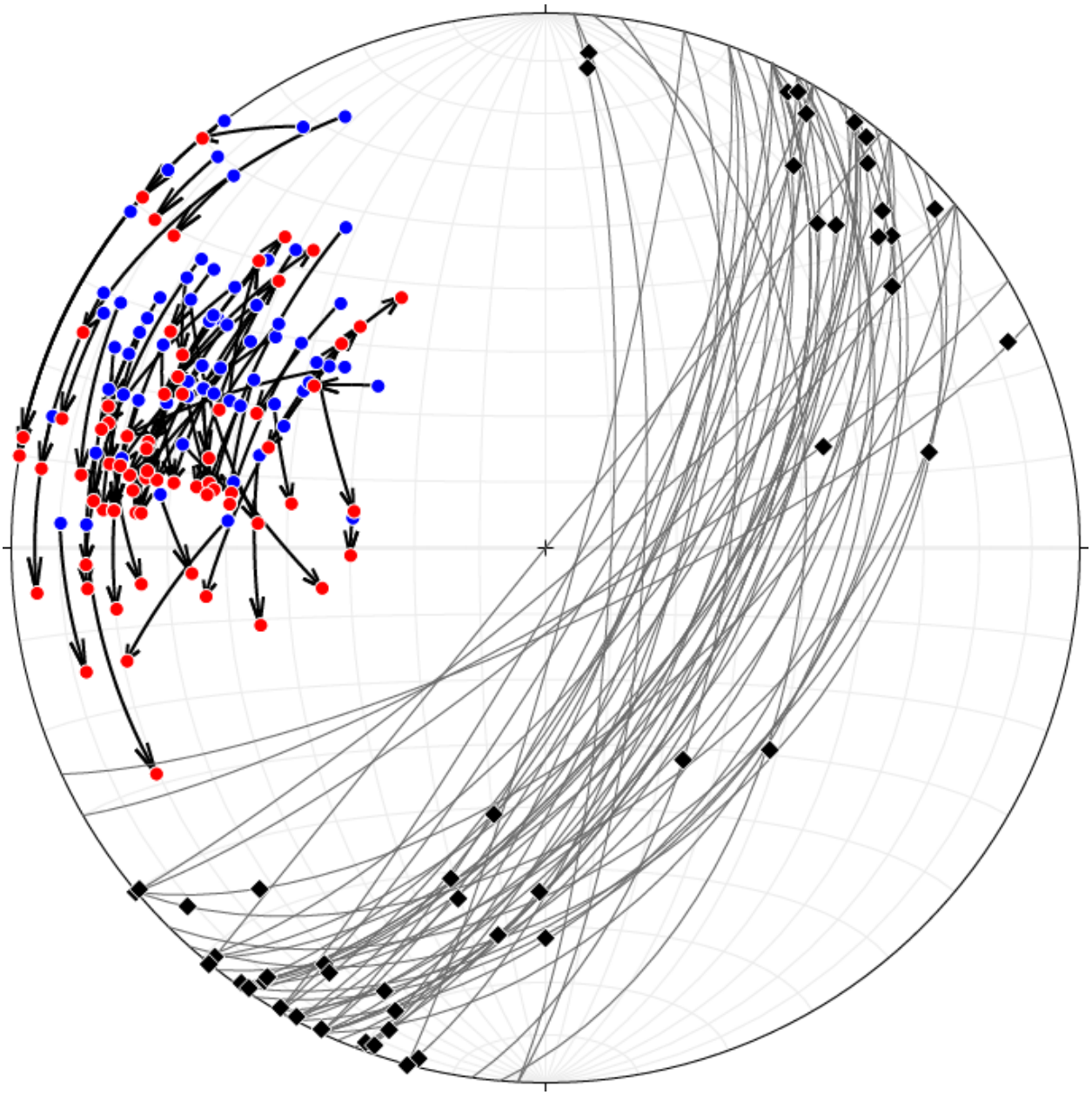

Figure 26 - Lower hemisphere equal-area stereoplot of poles to paired S-C fabrics and sliplines associated within the phyllonites and mylonites of the Alexander City shear zone. Blue dots are poles to C-planes, red dots are poles to S-planes ($N_{c\text{-}pole} = N_{s\text{-}pole} = 74$), black

diamonds are slip lines, gray great circle traces are C-planes ($N_c = N_{slip} = 50$). D_2 and D_3 movements are likely represented in the arcs shown, however it is unlikely that the two can be differentiated with much certainty based on these outcrop observations. Slip lines indicate both strike slip movement (nearest the primitive) as well as oblique-normal movement (down-dip components).

A shallow SE-plunging axis warping event is suggested by the dashed black great circle fit through the N38°E 28° NW trending partial girdle spread of S_1/S_2 measurements in Figure 25. Although this axis of warping was not documented in mesoscopic folds in outcrops, structural analysis indicates that it is similar in orientation and geometry to those reported elsewhere in the Alabama eastern Blue Ridge and the Dadeville and Opelika complexes (see, for example, Steltenpohl et al., 1990, Abrahams, 2014, and VanDervoort et al., 2017), which similarly are not easily inferred from outcrops due to the gentleness of S_1/S_2 warping. Workers have inferred that such cross-folds (i.e., folds formed at a high angle to the overall orogenic trend) reflect either dextral shearing during the main D_3 event that so characterizes the southern Appalachian hinterland (e.g., Steltenpohl, 1988, and Steltenpohl et al., 2013b) or movement along thrust faults propagated across northwest-striking transverse ramps or zones at depth (Thomas, 1977; Tull, 1978).

Two high-angle normal faults were discovered having cut rocks of the study area and these are assigned to a late stage of the D_3 event. High-angle normal faults (Figs. 6) possibly formed through re-activation of prior-formed reverse faults were found within the Elkahatchee Quartz Diorite (0593748E 3647296N). These normal faults are similar in geometry, rheology, and kinematics to those measured

and described by Hawkins et al. (2012), Hawkins (2013) and Steltenpohl et al. (2013b), along the Goodwater-Enitachopco, Alexander City, and Brevard shear zones. Slip along the high-angle faults may have a slight right-slip component but normal slip predominates. Normal faults in this part of the Blue Ridge could have resulted locally where thrust sheets were passively transported across transverse footwall ramps, or more regionally during the Permian-Mesozoic collapse of the Alleghenian orogen or Triassic-Jurassic rifting of Pangaea (Hawkins et al., 2012; Steltenpohl et al., 2013b).

In the northeastern part of the quadrangle, siliceous cataclasites developed along the Alexander City shear zone are assigned to a fourth deformational event, D_4. Zones of similar appearing cataclasites are reported along the northwest side of the Brevard zone (i.e., Abanda fault; Poole, 2015) and in association with the Goodwater-Enitachopco and Alexander City faults (Hawkins, 2013; Steltenpohl et al., 2013b). These cataclasites have overprinted all earlier-formed fabrics and structures and likely represent supra-ductile-brittle transition reactivation (Steltenpohl et al., 2013b). Similar structures are reported to occur throughout the southern Appalachian hinterland (Garihan and Ranson, 1992; Garihan et al., 1993) and have been interpreted as being related to the Mesozoic rifting of the Pangean supercontinent (e.g. the Towaliga Fault, Huebner and Hatcher, 2013).

GEOCHEMISTRY

Whole rock geochemistry was performed for six samples of plutonic igneous rocks from the study area to investigate their petrogenesis and tectonic settings and to compare the results to data sets previously reported for intrusives from throughout the Alabama Blue Ridge. Four samples of Elkahatchee Quartz Diorite were selected (sample locations shown in Fig. 4), three from within the Alexander City quadrangle and one from outside, with one sample being a duplicate for data-quality control. These samples were the same as those that were dated using U-Pb methods, described below. Analyses were done to confirm which sample of Elkahatchee was the most mafic (i.e., lowest SiO_2 content), and to understand the origin and possible mechanism of emplacement of the Elkahatchee. One sample of the Oaktasasi granite and one from the Sugar Creek trondhjemite were also analyzed because no geochemistry is yet reported for these intrusive bodies. Mineralogy and petrography of the Oaktasasi and Sugar Creek clearly do not match with the Elkahatchee Quartz Diorite, so it is useful to compare their geochemistry to that of nearby plutons such as the Rockford and Almond Trondhjemite (e.g. Miller et al., 2006, Ingram, 2012; H. Stowell et al., personal communication, 2018). To better determine the origin of these magmas, major oxides, trace elements, and their ratios (such as Sr, Y, and Yb) were used to construct multiple ternary diagrams, REE and spider diagrams, and Harker plots. Some degree of uncertainty is present in that not all the diagrams agree. The aim is also to evaluate how the current study's granites compare to previous studies on slab melt during

continental collision (e.g. Drummond and Defant, 1990; Moyen, 2009). Analytical results are reported in Appendix A and calculated CIPW mineral norms in Appendix B.

Figure 27 indicates that three of the four samples of Elkahatchee Quartz Diorite plot within the granodiorite field, and one on the line between granodiorite and tonalite on a Barker (1979) An-Ab-Or ternary diagram. All six samples, however, plot as granodiorite using the Strekeisen (1976) QAP triangle. Qualitatively speaking, the Oaktasasi granite looks similar in texture and color to samples of the Rockford Granite, which has been dated at ~377 Ma (Schwartz et al., 2011; Ingram, 2012). Ingram (2012), however, reports that the Rockford Granite plots in the quartz monzonite to quartz monzodiorite fields, whereas, in Figure 28, the Oaktasasi granite plots solidly in the granodiorite field. The Rockford Granite samples had on average ~24% CIPW modal quartz, and the Bluff Springs Granite between 12-22%, whereas the Oaktasasi granite has 35.75% modal quartz. The Oaktasasi granite was compared to Rockford Granite in an array of discriminant plots in an attempt to explore genetic connections between them, but they do not plot similarly, and it appears that they are not likely related.

In both the An-Ab-Or plot (Fig. 27) and the QAP triangle (Fig. 28) the Sugar Creek trondhjemite plots similarly to the Almond Trondhjemite (Ingram, 2012), which suggests that the magmas of each pluton were derived from a similar source. Likewise, the Hog Mountain tonalite samples (Stowell et al., 2015) plot very similarly on the QAP triangle to the Elkahatchee Quartz Diorite, and in hand

sample they both show a resemblance to one another in their mineralogy, grain size, and color. In both Figures 27 and 28, the Oaktasasi granite and Sugar Creek trondhjemite are more similar to the Almond Trondhjemite than they are to the Hog Mountain tonalite. Drummond et al. (1994) reported the Elkahatchee Quartz Diorite as being slightly peraluminous to metaluminous, however, all the samples from the Alexander City Quadrangle plot as (weakly) peraluminous (Fig 29) and samples from Ingram (2012) plot similarly as well.

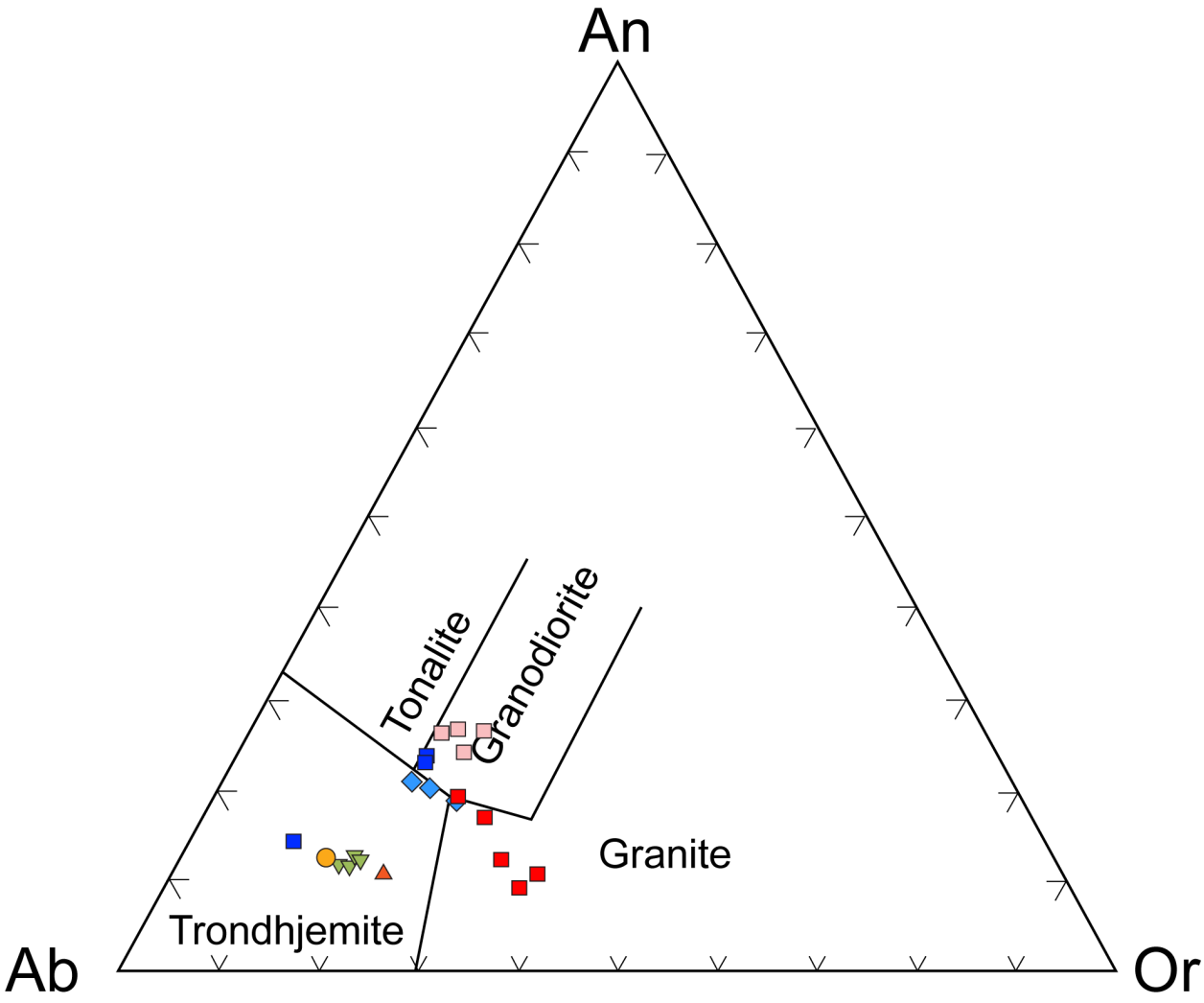

Figure 27 - An-Ab-Or ternary diagram of samples of Elkahatchee Quartz Diorite, Oaktasasi granite, and Sugar Creek trondhjemite including other comparable eastern Blue Ridge granites. Pink squares represent Elkahatchee Quartz Diorite, the dark orange triangle Oaktasasi granite, and the light orange circle Sugar Creek trondhjemite; light blue diamonds are Hog Mountain tonalite (Stowell et al., 2015); and inverted green triangles are Almond Trondhjemite, dark red squares are Rockford Granite, and blue squares are Bluff Springs Granite (Ingram, 2012). Modified from Barker (1979).

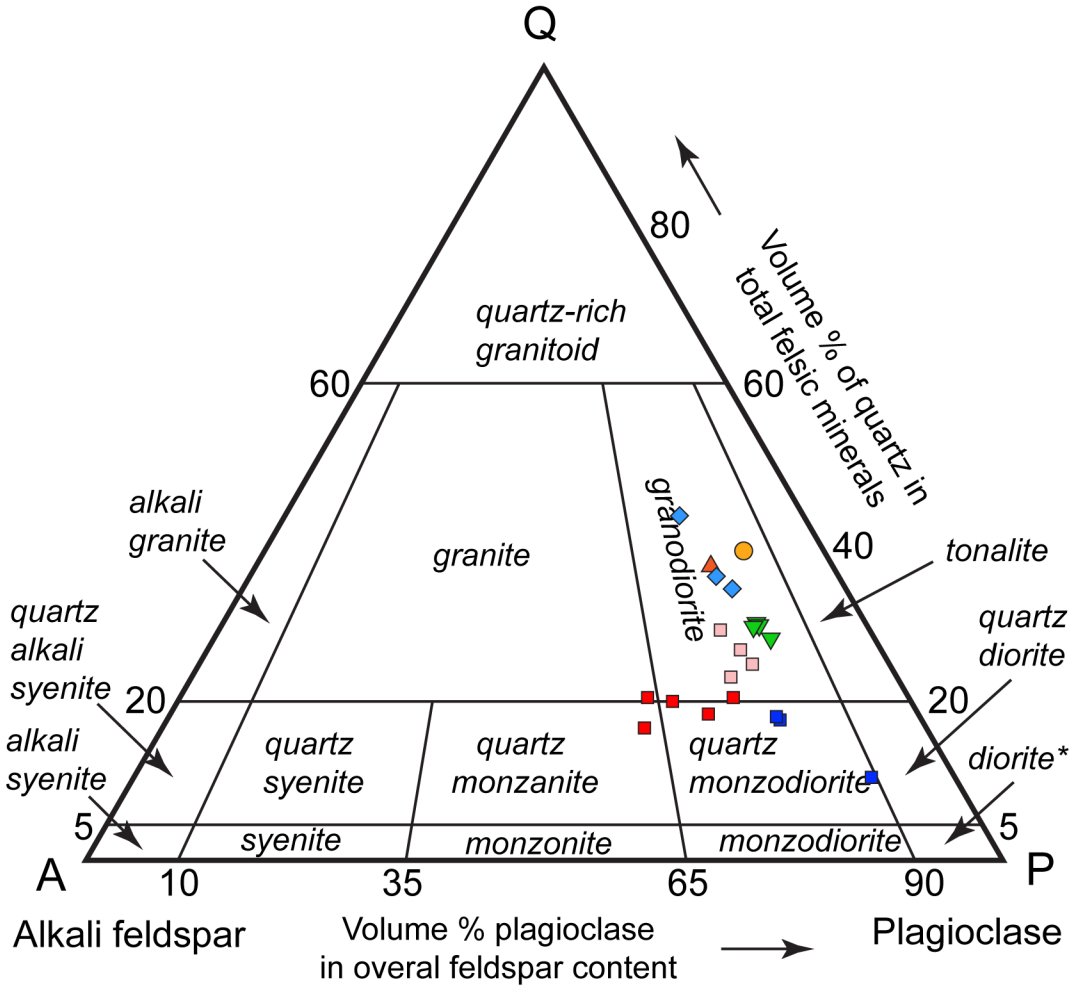

Figure 28 - QAP triangle plotting samples of Elkahatchee Quartz Diorite in pink squares, Oaktasasi granite in the orange triangle, and Sugar Creek trondhjemite in the lighter orange circle. Samples from Ingram (2012) are plotted for comparison; inverted green triangles are Almond Trondhjemite, red squares are Rockford Granite, and blue squares are Bluff Sprigs Granite. Hog Mountain tonalite samples from Stowell et al. (2015) are plotted as blue diamonds. Modified from Streckeisen (1976).

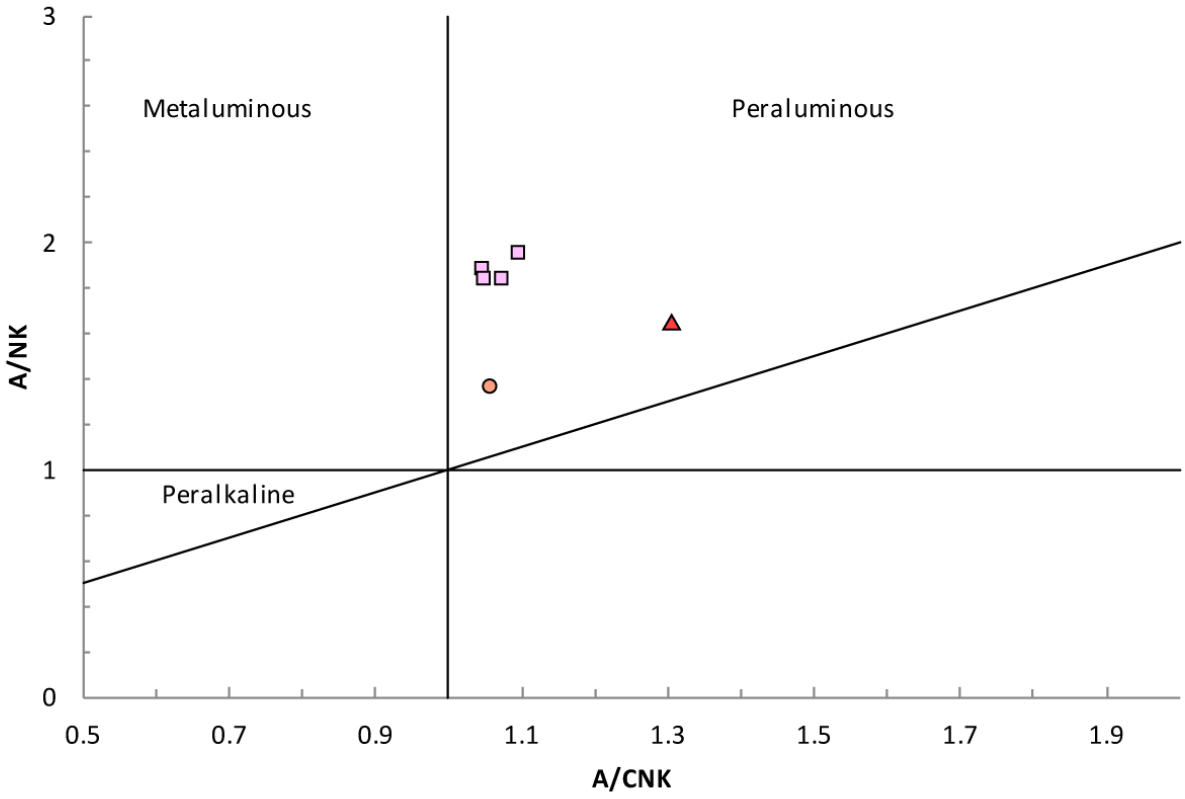

Figure 29 - A/CNK diagram plotting all six samples as weakly peraluminous. Pink squares represent Elkahatchee Quartz Diorite, the red triangle Oaktasasi granite, and the orange circle the Sugar Creek trondhjemite.

Plotting each sample for Rb-(Y+Nb) and Rb-(Y+Ta) in Figure 30 gives insight into the source of the magma for these rocks. Rb-(Y+Nb) plots all the samples within a volcanic arc setting, however, Rb-(Y+Ta) places all of the Elkahatchee samples into the Within-Plate Granite field. Plotting the samples on an Rb-Ta-Hf ternary diagram (Fig. 31) indicates the source of the magma is a volcanic arc setting.

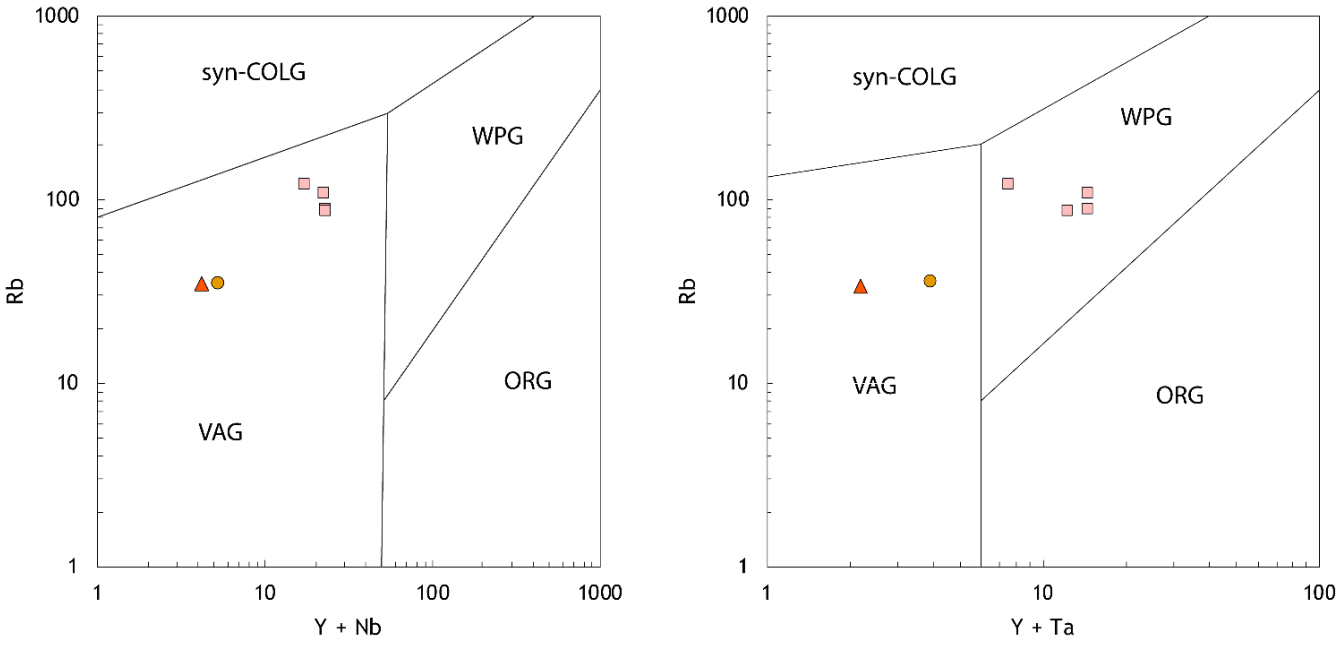

Figure 30 - Rb-(Y+Nb) and Rb-(Y+Ta) tectonic discrimination plots for samples of Elkahatchee Quartz Diorite (pink squares), Oaktasasi granite (orange triangle), and Sugar Creek trondhjemite (orange circle). Modified after Pearce et al. (1984).

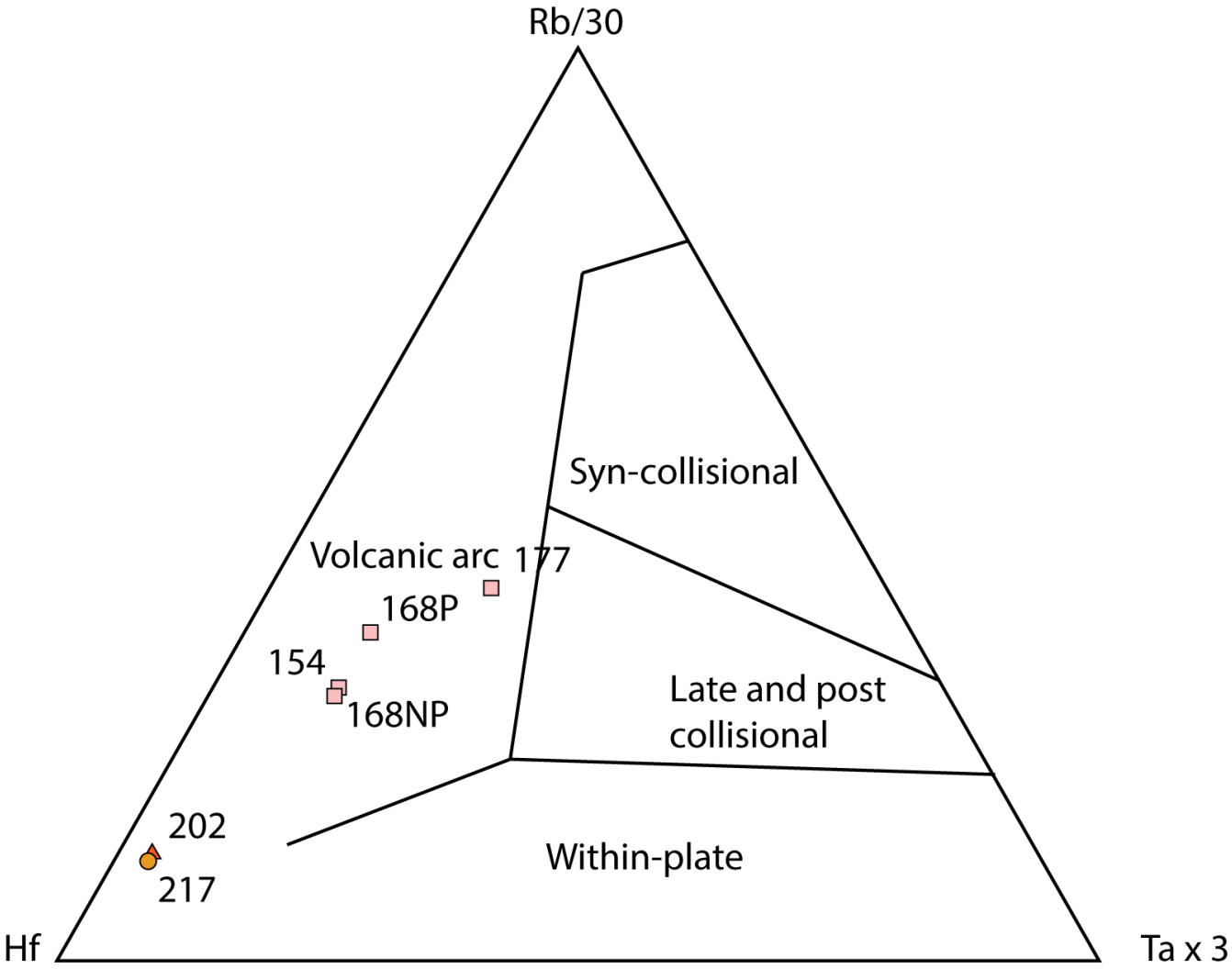

Figure 31 - Rb-Hf-Ta plot for samples of Elkahatchee Quartz Diorite (pink squares), Oaktasasi granite (orange triangle), and Sugar Creek trondhjemite (orange circle). Modified after Harris et al. (1986).

The Elkahatchee Quartz Diorite samples all show enrichment in the light rare earth elements, depletion in the heavy rare earth elements, as well as a lack of a europium anomaly (Fig 32). The Oaktasasi and Sugar Creek samples show a similar trend, with lower values overall compared to those of the Elkahatchee samples. This suggests that the Oaktasasi and Sugar Creek samples are less evolved than the Elkahatchee Quartz Diorite. All of the samples analyzed show relative depletion in Nb and Ta, and relative enrichment in Rb, Ba, Th, U, and Pb (Fig. 32 Bottom). This suggests a suprasubduction zone setting for the formation of the magmas of the Oaktasasi, Sugar Creek, and Elkahatchee Quartz Diorite samples.

Select geochemistry reported in Table 2 shows that all four samples of Elkahatchee Quartz Diorite have high aluminum percentages (>15% wt) as well as moderately high Sr/Y ratios (>= 40 or greater). With exception of sample 17BRW177, the Sr/Y values are all lower than the average value for the seven samples listed by Drummond et al. (1994). All samples show Yb values of 1.1 or lower. Additionally, CIPW normative mineralogy produced normative corundum percentages ranging from 1.45 to 2.16 for the Elkahatchee Quartz Diorite samples. The Elkahatchee rocks also have Sr > 400 ppm, Y < 18 ppm, Yb < 1.9, and MgO < 3 wt. %. $^{87}Sr/^{86}Sr$ was not obtainable for any samples in this study, but Russell (1978) reported a modeled initial $^{87}Sr/^{86}Sr$ value of 0.7036 for the Elkahatchee; the actual measured values ranged from 0.7060 – 0.7111. Results in Table 2 suggest that the samples from the Elkahatchee Quartz Diorite are consistent with adakitic rocks

(Fig. 33) which generally feature SiO_2 > 56 wt %, $Al_2O_3 \geq 15$ wt %, MgO < 3 wt %, Sr > 400 ppm, Y < 18 ppm, Yb < 1.9 ppm, and $^{87}Sr/^{86}Sr$ values < 0.7045 (e.g. Drummond and Defant, 1990). Likewise, the samples from the Oaktasasi granite and Sugar Creek trondhjemite follow a similar pattern (Fig. 33), though perhaps less robustly (Table 2 and Figure 33).

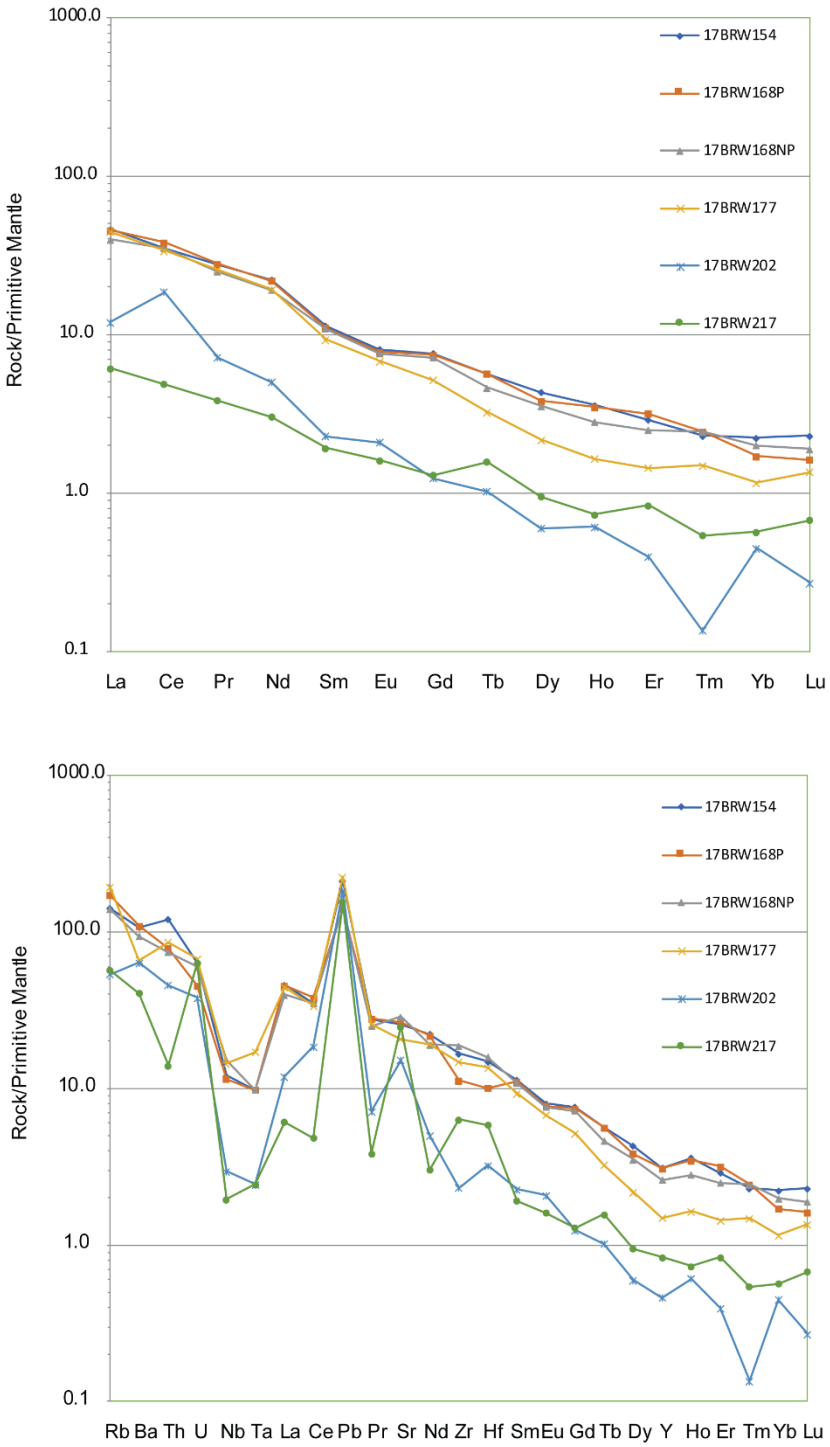

Figure 32 - **Top**: REE diagram of all analyzed intrusive samples. Note the enrichment in LREEs, depletion of HREEs, and a lack of Eu anomalies. Chondrite normalized values taken from Sun and McDonough (1989). **Bottom:** Spider diagram of all analyzed intrusive samples. Note the enrichment in LREEs, depletion of HREEs and a lack of Eu anomalies. Primitive mantle normalized values taken from Sun and McDonough (1989).

Table 2 – Adakitic signature trace elements.

Sample	Sr ppm	Y ppm	Yb ppm	Sr/Y	Al_2O_3% wt	Nomative Corundum
154	545	14.1	1.1	38.65	16.7	2.16
168P	560	14	0.84	40.00	16.3	1.55
168NP	608	11.9	0.98	51.09	16.5	1.45
177	437	6.8	0.57	64.26	15.7	1.77
202	321	2.1	0.22	152.86	15.55	4.09
217	523	3.8	0.28	137.63	13.6	0.92

In summary, the adakitic signature is indicative of each of the magmas having been derived from the partial melting of a subducted slab. Both the geochemistry and the geochronology presented below are consistent with the Elkahatchee Quartz Diorite magmas having formed in a suprasubduction setting during both the Neoacadian and Alleghenian orogenies, which has been suggested by Sagul (2016), Huebner et al (2017), and Tull et al. (2018). The Okatasasi granite and Sugar Creek trondhjemite, however, were more likely derived from a more traditional intrusive arc setting.

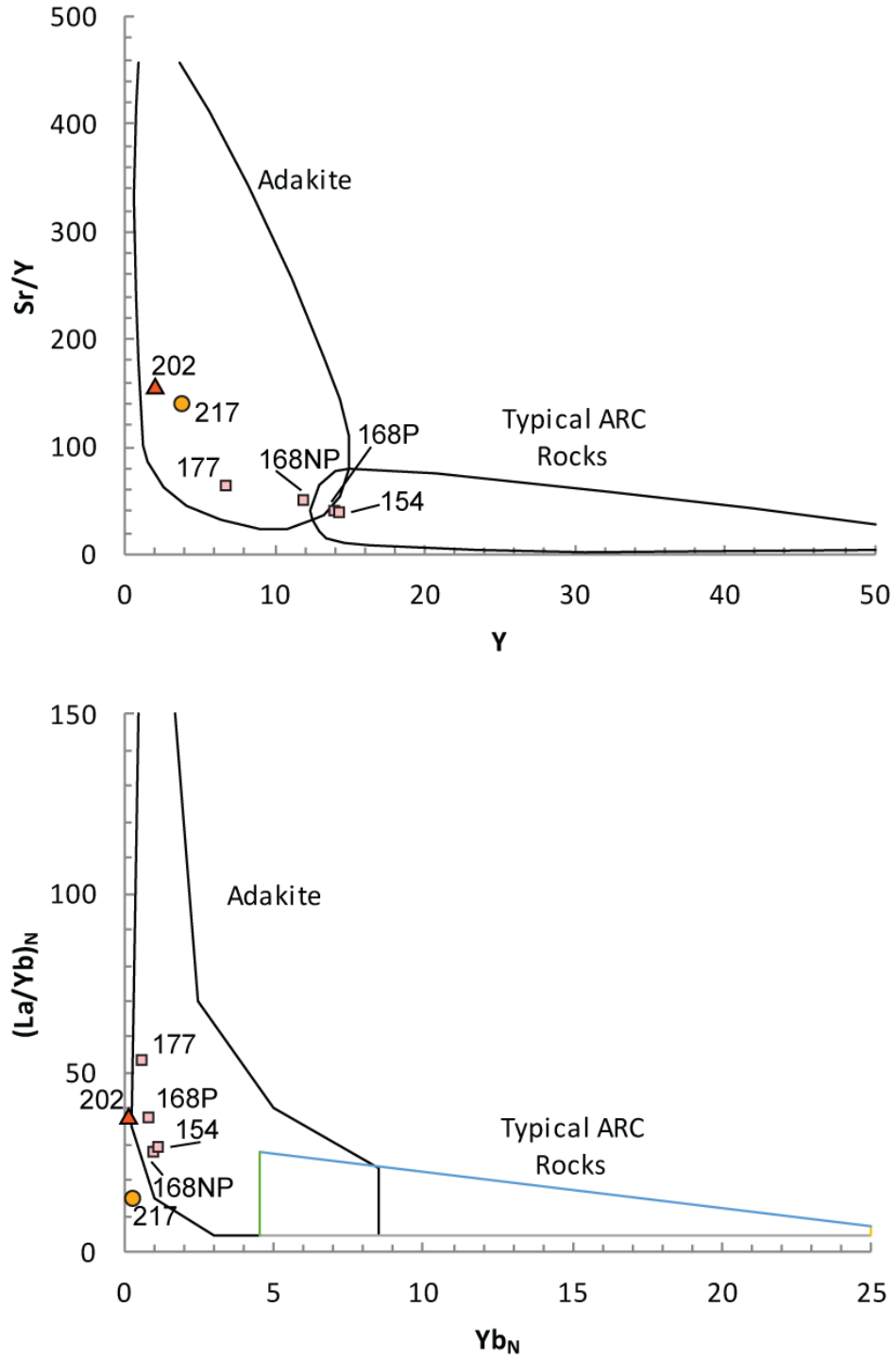

Figure 33 - Adakite plots (Drummond and Defant, 1990) for samples from the current study. Pink squares represent Elkahatchee Quartz Diorite, the red triangle Oaktasasi granite, and the orange circle Sugar Creek trondhjemite. **Top**: Sr/Y-Y plots most of the samples either in or very close to the adakite field. **Bottom**: All four samples of Elkahatchee Quartz Diorite plot within the adakite field, whereas the Okatasasi and Sugar Creek samples do not.

GEOCHRONOLOGY

Three samples of Elkahatchee Quartz Diorite were dated using zircon U-Pb LA-ICP-MS techniques. Care was taken to select samples from rocks that present the best opportunity to explore the age of the oldest intrusive phases of the batholith. Figures 34B, 36B, and 38B show zircon grains with distinct oscillatory zoning, indicating that these are magmatic zircons. Over 100 euhedral grains for each sample were picked with euhedral grains being preferred over broken grains.

Sample 17BRW154 was collected from a large whale-back outcrop of Elkahatchee Quartz Diorite found within the Charles E. Bailey Sportplex in Alexander City (Fig. 4) (0595576N 3642967E). The sample was from an exfoliating slab and the rock was generally massive. This sample was chosen due to its darker color, reflecting relatively abundant biotite and plagioclase, indicating it to be more mafic, especially in comparison to nearby outcrops which were much more leucocratic. Zircons from this sample are mostly euhedral, needle-like grains, 100 – 200 μm in length with length to width ratios around 5, and many of the grains are pale orange in color (Fig 34). Ten out of the twenty-one zircons analyzed yielded concordant $^{238}U/^{206}Pb$ ages of ca. 328.5 ± 5.1 Ma (Fig 35).

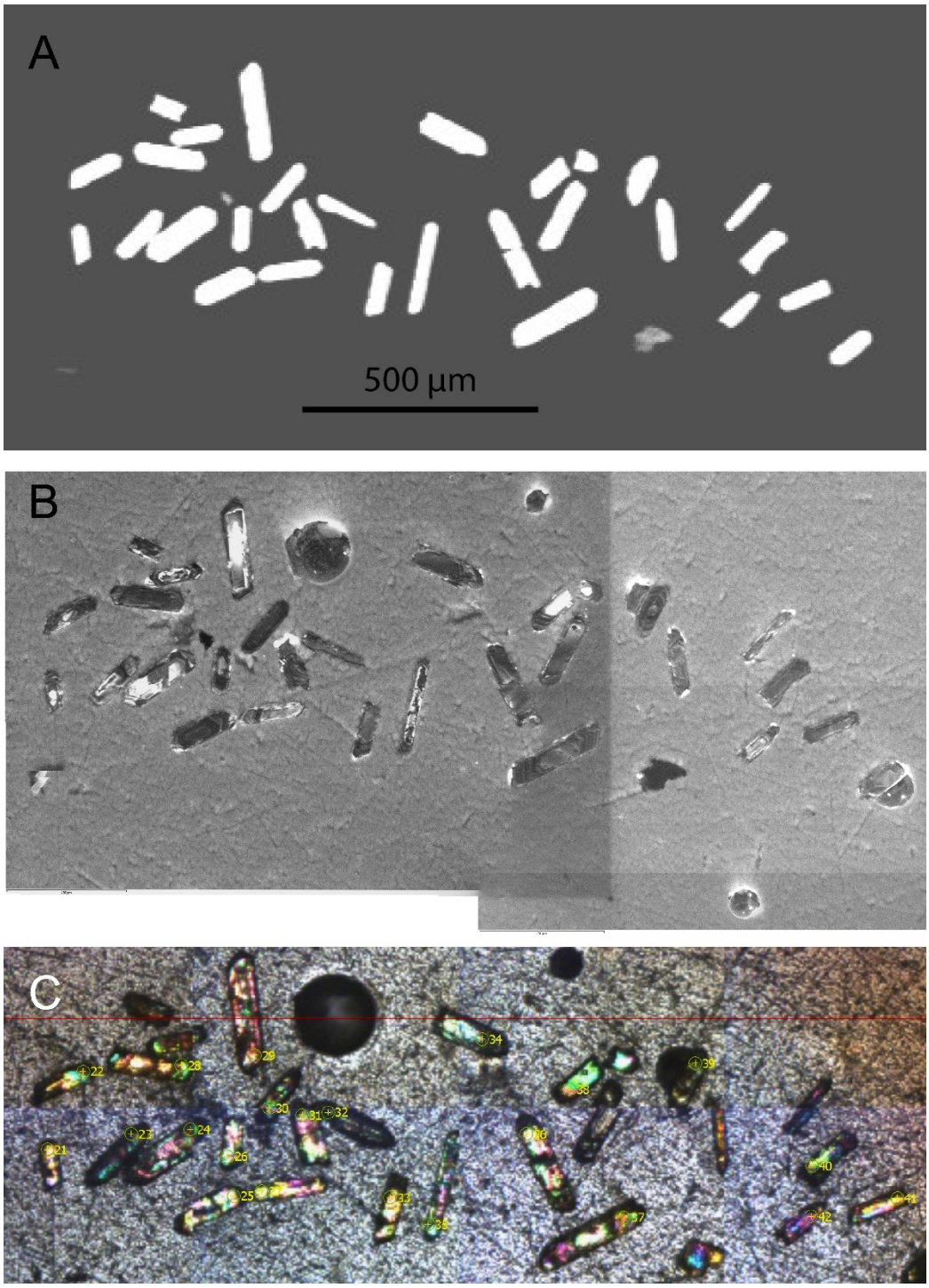

Figure 34 - Magmatic zircons from Elkahatchee Quartz Diorite sample 17BRW154. **A**: Back-scatter electron image of zircons. **B**: Cathodoluminescence image of zircons showing cores and rims. **C**: Reflected light image of zircons showing shot points.

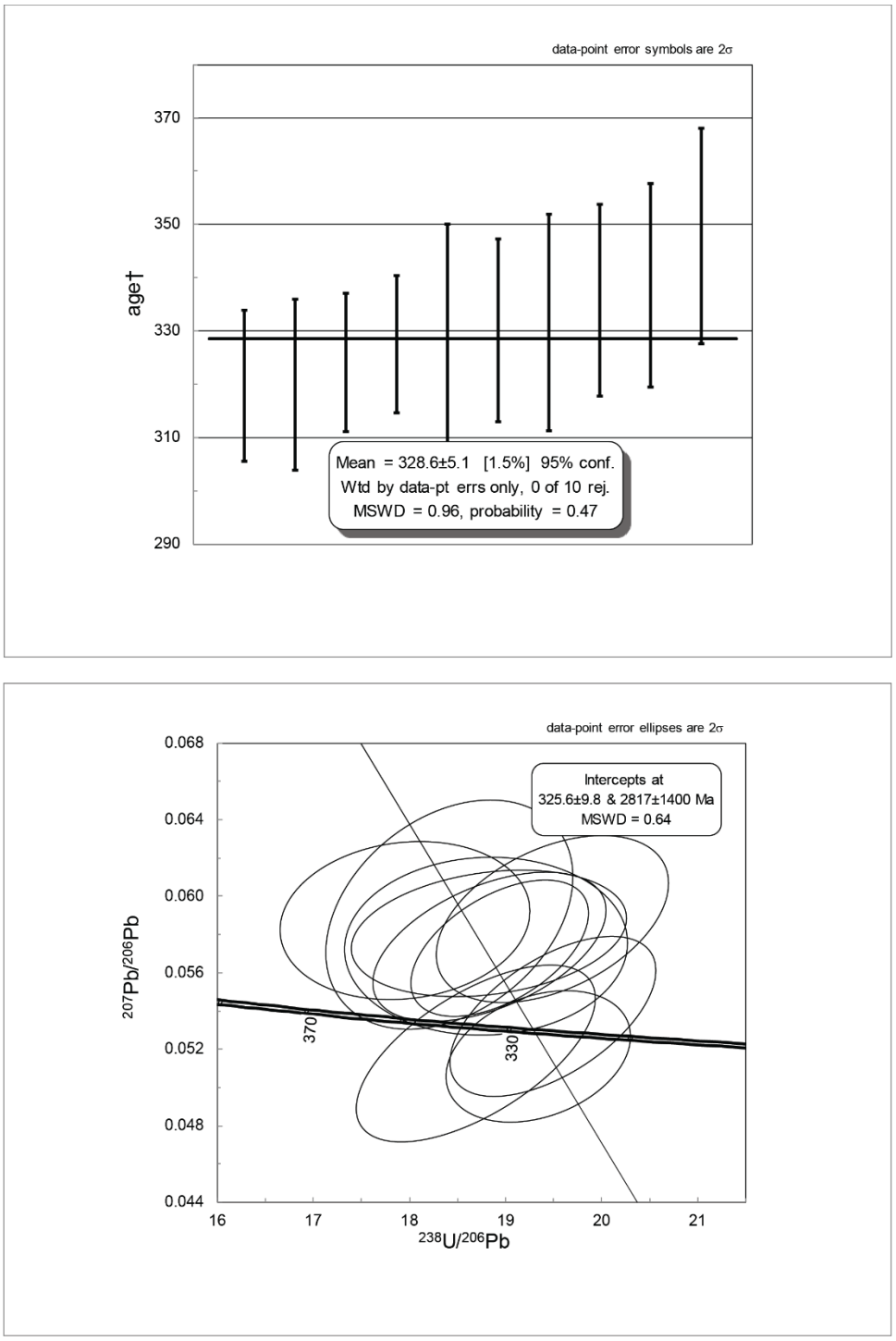

Figure 35 - Zircon dates for Elkahatchee Quartz Diorite sample 17BRW154. **Top**: Average age with 10 concordant $^{238}U/^{206}Pb$ ages showing ages of 328.6 ± 5.1 Ma. **Bottom**: Plots for sample 17BRW154 showing ages of 325.6 ± 9.8 Ma.

Sample 17BRW168 was collected from a large pavement exposure at the bottom of the dam on Elkahatchee Creek where Elkahatchee Road crosses the creek (Fig. 4) (0595485N 3639731E). The sample was chosen due to its darker appearance, suggesting that it also was a more mafic phase as it had an abundance of plagioclase and particularly biotite; this sample also had the lowest SiO_2 content at 62.5% by weight. Zircons from this sample were generally euhedral and colorless with a mixed population of prismatic, needle-shaped grains and stubby ones and range in size from 126 – 320 μm with length to width ratios averaging 3.67 (Fig. 36). Broken grains were generally avoided. Of the thirty-eight mainly prismatic grains analyzed, twenty-six were concordant and gave a $^{238}U/^{206}Pb$ age of 378.5 ± 5.5 Ma (Fig. 37).

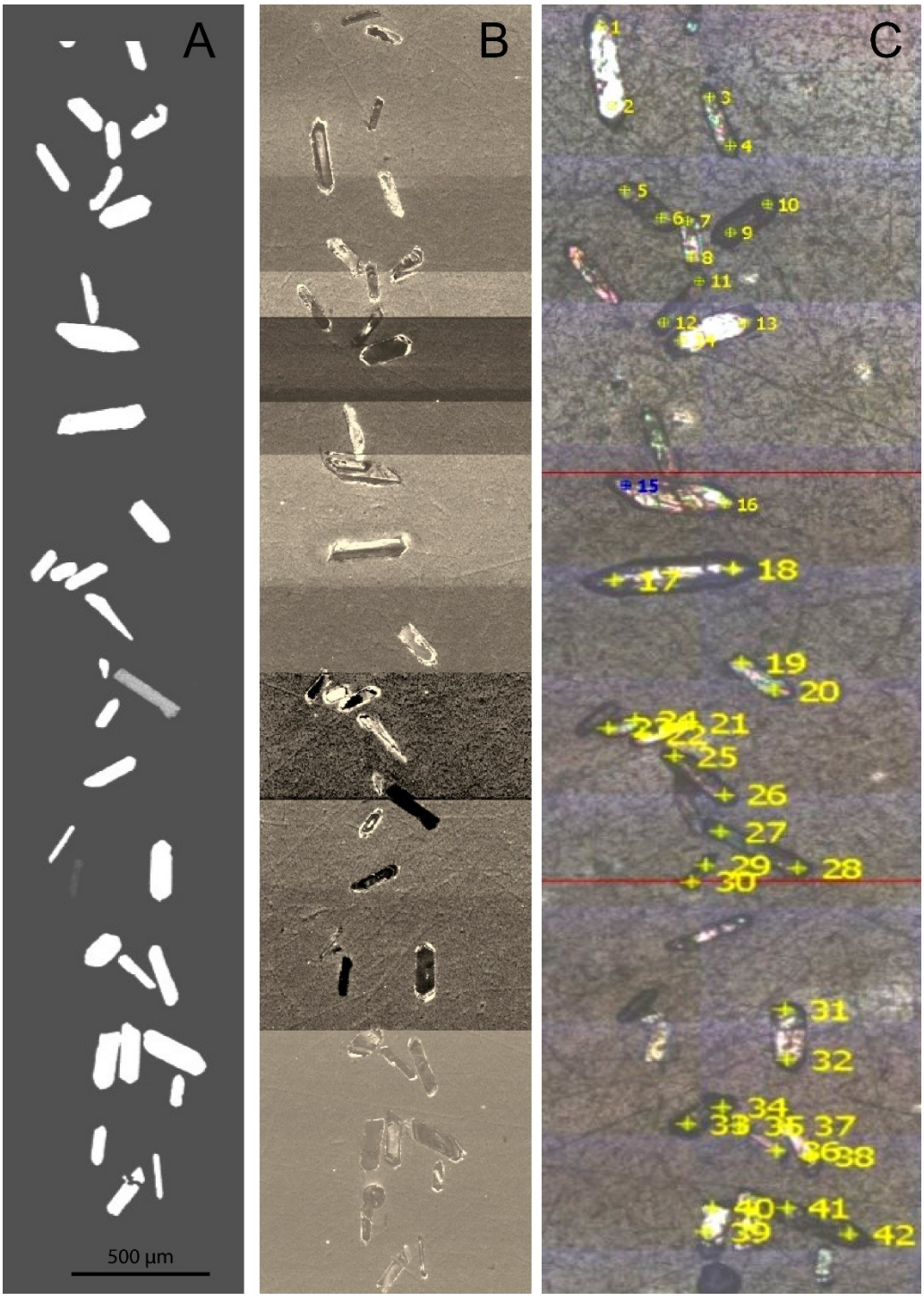

Figure 36 - Magmatic zircons from Elkahatchee Quartz Diorite sample 17BRW168. **A**: Back-scatter electron image of zircons. **B**: Cathodoluminescence image of zircons showing cores and rims. **C**: Reflected light image of zircons showing shot points.

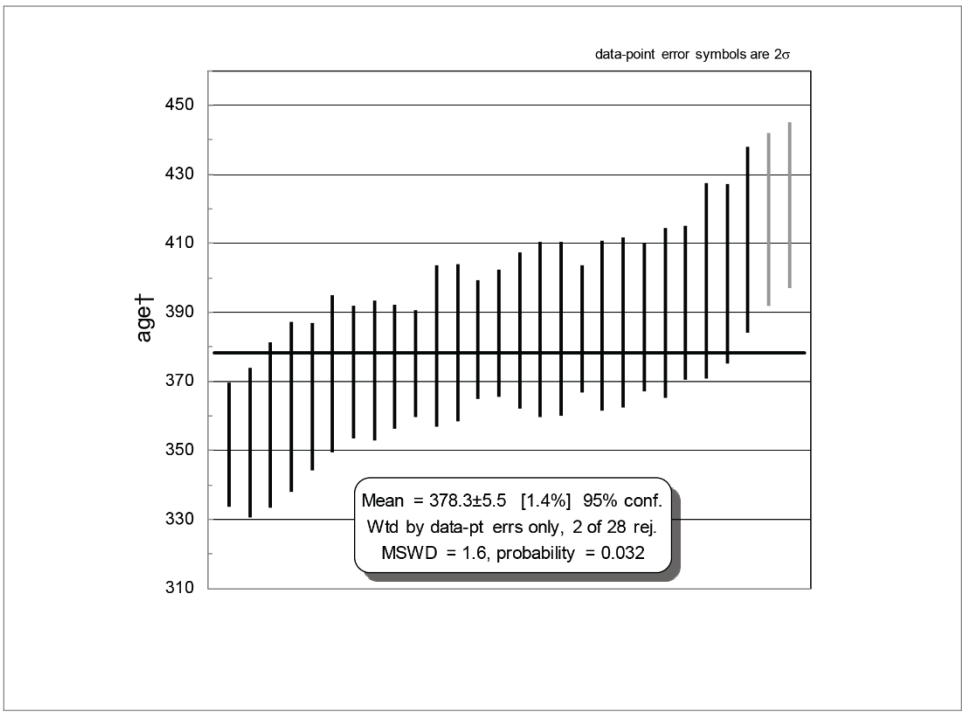

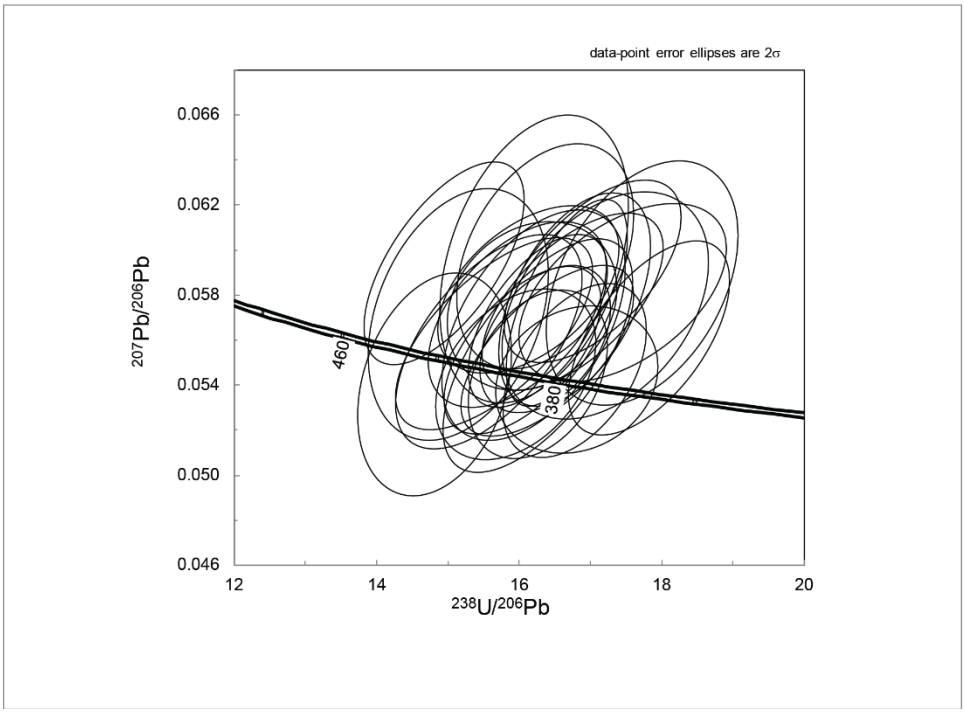

Figure 37 - Zircon dates for sample 17BRW168. **Top**: Average age of 26 concordant $^{238}U/^{206}Pb$ ages showing an average age of zircon crystallization of 378.3 ± 5.5 Ma at a 95% confidence. **Bottom:** Plot for sample 17BRW168.

Sample 17BRW177 was collected at the Alexander City Quarry, located about 3.5 km southwest from the southwest corner of the Alexander City Quadrangle (Fig. 4). This location was chosen because this is the same quarry from which the Cambrian aged sample, FSU 106-110, of Russell (1978) was collected. The sample was taken from freshly quarried granodiorite, avoiding any veins or dikes, which were present within the quarry. The rock here was similar in appearance to that described for 17BRW168. Zircons from this sample also were similar to those of sample 17BRW168, showing a mixed population of colorless and euhedral prismatic, needle grains and fat, stubby grains ranging in size from 110 – 330 μm in length with an average length to width ratio of 2.78 (Fig 38). Nine mainly prismatic grains of the nineteen analyzed were concordant and yielded a $^{238}U/^{206}Pb$ age of 329.3 ± 5.3 Ma (Fig 39).

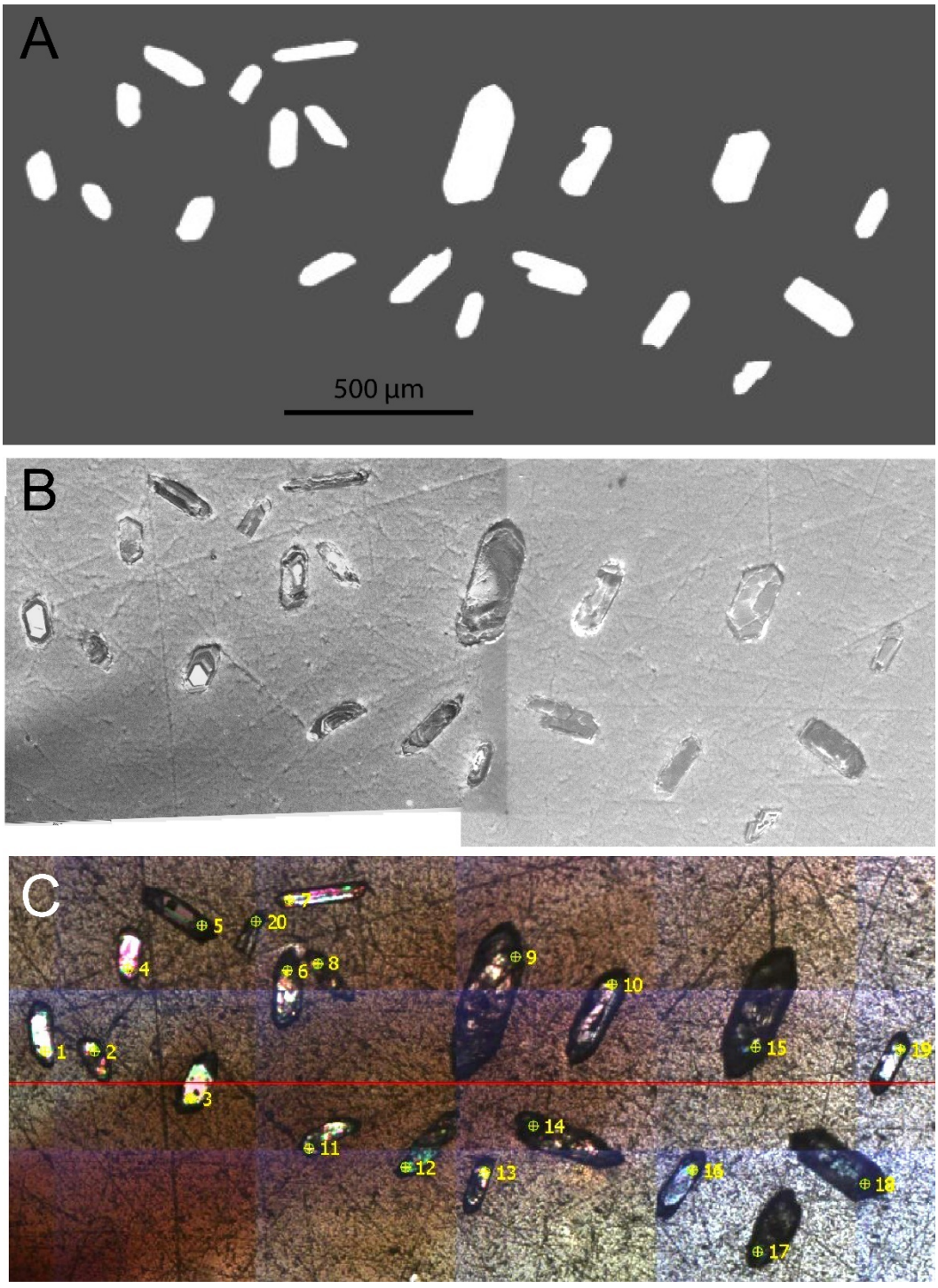

Figure 38 - Magmatic zircons from Elkahatchee Quartz Diorite sample 17BRW177. **A**: Back-scatter electron image of zircons. **B**: Cathodoluminescence image of zircons showing cores and rims. **C**: Reflected light image of zircons showing shot points.

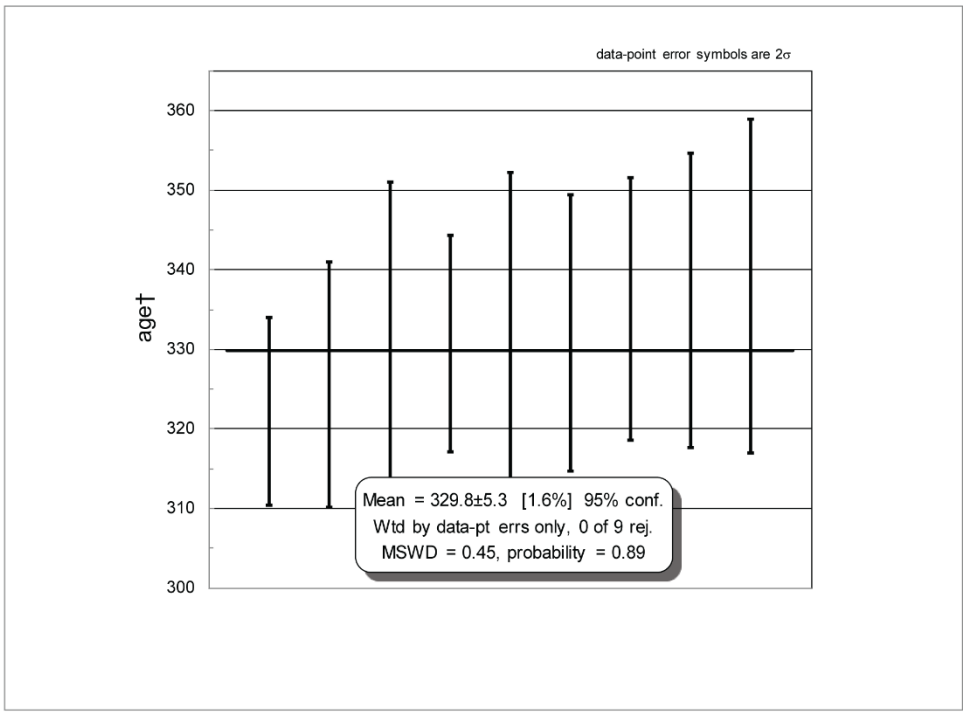

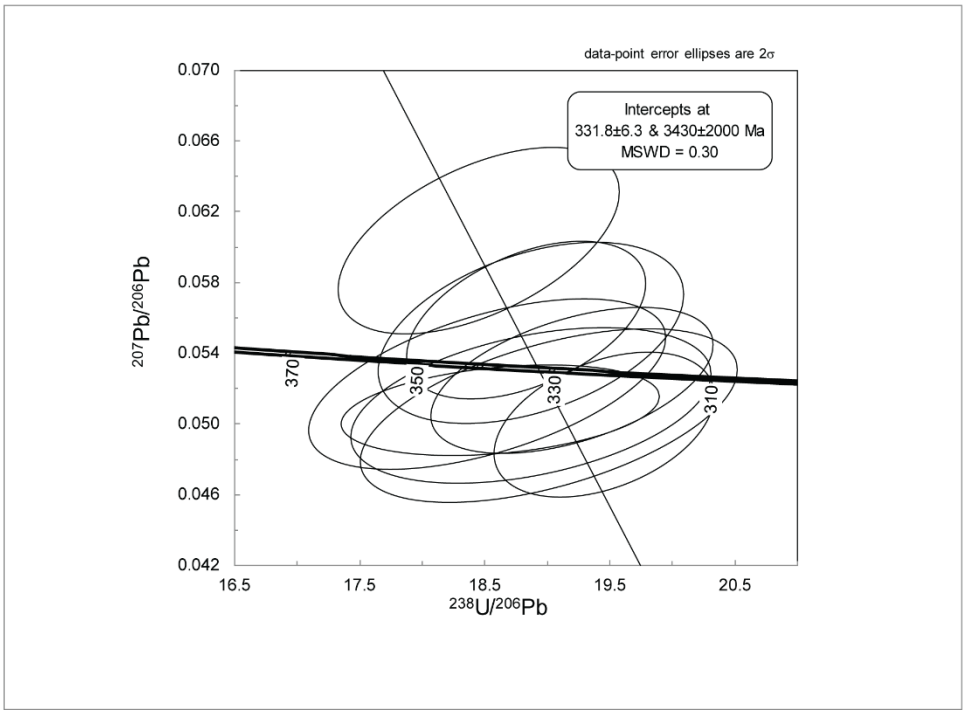

Figure 39 - Zircon dates for Elkahatchee Quartz Diorite sample 17BRW177. **Top**: Average age of 9 concordant ages showing an average $^{238}U/^{206}Pb$ age of 329.8 ± 5.3 Ma. **Bottom**: Plot showing an age of 331.8 ± 6.3 Ma with a 95% confidence.

$^{238}U/^{206}Pb$ radiometric dates on magmatic zircons from the Elkahatchee Quartz Diorite of the study area show two age populations, one at 378.3 ± 5.5 Ma and a second, younger population at 328.6 ± 5.1 to 329.8 ± 5.3 Ma. This result is surprising for two reasons. Firstly, the author had carefully sought out the oldest intrusive phase of the batholith to test for the presence of earlier Paleozoic phases as suggested in Russell's (1978) earlier report. Secondly, a late Mississippian phase of the Elkahatchee was discovered among my samples that also were preferentially collected on field and geochemical grounds to test for the oldest phase in the batholith. Results further demonstrate the multiple-phase nature of the batholith. The 378 Ma date on sample 17BRW168 is consistent with the 370-382 Ma dates reported by Tull et al. (2009) for samples from the same outcrops, implying that much of the fabric development in this phase of the Elkahatchee indeed formed during a short span of time in order to be cut by 369 Ma dikes (Steltenpohl et al., 2013a).

One explanation for the multiphase nature of the batholith, following Drummond et al. (1994), is that the sheared felsic pods are younger, more felsic phases of the Elkahatchee with the older, more mafic phases being less evolved and having crystallized first. In this model, as shown in Figure 3, the magma cooled in convection cells, with the more mafic magma first on the margins, and the more felsic magma towards the center. While the oldest phase of the Elkahatchee, within the study area, is indeed the most mafic phase, it seems unlikely that convection cell cooling would last for 50 Ma. The older pulse of magma likely was derived from

slab melt during the Neoacadian orogeny and the second pulse came from a similar source under similar conditions during the Alleghenian orogeny. The author favors the interpretation that the two age populations are products of different magmatic pulses related to Neoacadian and Alleghenian magmatism, respectively, an interpretation that is consistent with other researchers working in the southern parts of the Appalachian Blue Ridge (e.g. Miller et al., 2006; Tull et al., 2009; Ingram, 2012; H. Stowell et al., personal communication, 2018). One possible exception is a sample of the Kowaliga Gneiss that produced a U-Pb zircon date of 340 ± 4 Ma (Sagul, 2016).

CONCLUSIONS

1. Geologic mapping of the Alexander City Quadrangle confirms that mylonites, ultramylonites, and phyllonites and later-formed cataclasites correspond to the position of the contact between the Wedowee and Emuckfaw groups, which has been argued to be the Alexander City fault. Fault rocks not only characterize this boundary but they are found to variably but widely affect schists and gneisses throughout the study area, particularly in the southeast parts of the quadrangle. For this reason, the author favors the term Alexander City shear zone for referring to these fault rocks that formed during the Carboniferous Alleghenian orogeny through oblique dextral- and normal-slip shear.

2. U-Pb zircon geochronology of this report documents that the Elkahatchee Quartz Diorite is a multi-phase batholith with at least two age populations, one circa 378 Ma and a second, younger one at circa 329 Ma. Distinguishing between rocks of the two different age phases is not simple in the field, as the main differentiator is the degree of foliation development, with the younger phase having a slightly more massive appearance. Future work may reveal additional age-phases within the batholith.

3. The Elkahatchee batholith is mainly composed of tonalite to granodiorite but granitic phases are more common than was previously reported. Lozenge-like pods of granite crop out with similar foliations that parallel the main batholith. This is most likely due to two pulses of magmatism; the first during the Neoacadian orogeny, and the second during Alleghenian orogeny. The adakitic geochemical signature suggests that the magmas were sourced from the melting of a subducted slab.
4. The Oaktasasi granite partly corresponds to areas previously mapped as Hackneyville Schist. Minor, small outcrops of hard, dense paragneiss associated with the Oaktasasi are assigned to the Hackneyville Schist. The Oaktasasi granite is a massive to weakly foliated granite that intrudes the Elkahatchee Quartz Diorite as series of sill-like bodies that parallel the regional northeast strike and southeast dip. The minor amount of strain implies that it is one of the younger intrusive units in the quadrangle and likely associated with later stages of the Alleghenian orogeny. Future geochronology is needed to assess the igneous crystallization age of Oaktasasi granite.
5. Another intrusive body into the Elkahatchee Quartz Diorite is the ~335 Ma Sugar Creek trondhjemite. Geochemistry and discriminant analysis indicate that both the Oaktasasi granite and the Sugar Creek trondhjemite were likely derived from a traditional intrusive arc setting.

6. The ages herein determined for the Elkahatchee Quartz Diorite (Devonian and Mississippian), the previously reported age for the Sugar Creek trondhjemite (Mississippian), and the field and petrographic observations reported herein supporting a Carboniferous age for the Oaktasasi granite further supports that the Wedowee-Emuckfaw boundary, on a regional scale, separates rock bodies intruded by granites of Carboniferous age to the northwest from the Middle Ordovician plutons to the southeast. It is possible that such age-specific plutons could preferentially intrude different structural levels within an intact stratigraphic package or that a fault is responsible for the age disparity. The author favors that a cryptic fault may best explain this relationship. Zones of cataclasite found along and adjacent to the contact between the Wedowee and Emuckfaw units, as well as in multiple locations along the Alexander City shear zone, suggest that it does not everywhere follow the igneous intrusive contact between the Elkahatchee Quartz Diorite and the Wedowee Group as has been suggested (Harstad, 2015). Multiple exposures of supra-ductile-brittle faults, most of which show predominantly normal down-dip movements, are present along this boundary within rocks of the study area.
7. High-angle oblique-dextral/normal faults were discovered in the Alexander City Quadrangle. Composite S-C planar fabrics, sigma porphyroclasts, asymmetric composite phaicoids, and drag folds combine to document oblique dextral/normal motion. Low angle strike-slip

mylonitic shear zones with tops-southwest movement cut the Sugar Creek trondhjemite .

REFERENCES

Abrahams, J.B., 2014, Geology of the Dadeville Quadrangle and the Tallassee synform in characterizing the Dog River window [unpublished M.S. thesis]: Auburn University, Auburn, Alabama, 126 p.

Adams, G.I., 1926, the crystalline rocks in Adams, G.I., Butts, D., Stephenson, L.W., and Cooke, C.W., eds., Geology of Alabama: Alabama Geological Survey Special Report 14, p. 40-223.

Adams, G.I., 1930, Gold deposits of Alabama, and occurrences of copper, pyrite, arsenic and tin: Alabama Geological Survey Bulletin 40, p. 91.

Adams, G.I., 1933, General geology of the crystalline rocks of Alabama: The Journal of Geology, v. 41, p. 159-173.

Allmendinger, R. W., Cardozo, N., and Fisher, D., 2012, Structural geology algorithms: Vectors and tensors in structural geology: Cambridge University

Allison, D., 1992, Structural evolution and metamorphic petrogenesis of a metasediment and metaigneous complex, Coosa County, Alabama [Ph.D. thesis]: Florida State University, Tallahassee, Florida, 377 p.

Barker, F., 1979, Trondhjemite: definition, environment, and hypothesis of origin: Developments in Petrology, v. 6, p. 1-12.

Barineau, C.I., 2009, Superposed fault systems of the southernmost Appalachian Talladega Belt: Implications for Paleozoic orogenesis in the southern Appalachians [Ph.D. thesis]: Florida State University, Tallahassee, Florida, 150 p.

Barineau, C.I., and Tull, J.F., eds., 2012, The Talladega Slate Belt and eastern Blue Ridge: Laurentian Plate Passive Margin to Back-Arc Basin Tectonics in the Southern Appalachian Orogen: Alabama Geological Society, 49th Annual Field Trip Guidebook, 302 p.

Barineau, C.I., Espinosa, S., Harstad, R., and Smenner, R., 2014, Mapping and structural analysis across Emuckfaw Group-Wedowee Group contacts in the eastern Blue Ridge of Alabama: Geological Society of America Abstracts with Programs, v. 46, no. 3, p. 13.

Bentley, R. D. and Neathery, T. L., 1970, Geology of the Brevard Fault Zone and Related Rocks of the Inner Piedmont of Alabama: Alabama Geological Society, 8th Annual Field Trip Guidebook, 119 p.

Berthé, D., Choukroune, P., and Jegouzo, P., 1979, Orthogneiss, mylonite and non coaxial deformation of granites: The example of the South Armorican shear zone: Journal of Structural Geology, v. 1, p. 31-42.

Bobyarchick, Andy R., Steven H. Edelman, and J. W. Horton Jr., 1988, The role of dextral strike-slip in the displacement history of the Brevard zone: Southeastern Geological Excursions: Geological Society of America 1988 Annual Meeting Field Trip Guidebook, p. 53-104.

Bream, B.R., 2002, The southern Appalachian Inner Piedmont: New perspectives based on recent detailed geologic mapping, Nd isotopic evidence, and zircon geochronology, *in* Hatcher, R.D., Jr., and Bream, B.R., eds., Inner Piedmont geology in the South Mountains–Blue Ridge Foothills and the southwestern Brushy Mountains, central-western North Carolina: Annual field trip guidebook: Durham, North Carolina, Carolina Geological Society, p. 45–63.

Bream, B.R., 2003, Tectonic implications of para- and orthogneiss: Geochronology and geochemistry from the southern Appalachian crystalline core [Ph.D. thesis]: Knoxville, University of Tennessee, 296 p.

Bream, B., Hatcher, R., Miller, C., and Fullagar, P., 2004, Detrital zircon ages and Nd isotopic data from the southern Appalachian crystalline core, Georgia, South Carolina, North Carolina, and Tennessee: New provenance constraints for part of the Laurentian margin, *in* Tollo, R.P., McLelland, J., Corriveau, L., and Bartholomew, M.J., eds., Proterozoic Tectonic Evolution of the Grenville Orogen in North America: Geological Society of America Memoir 197, p. 459–475, doi:10.1130/0-8137-1197-5.459.

Cardozo, N., and Allmendinger, R.W., 2013, Spherical projections with OSXStereonet: Computers & Geosciences, v. 51, p. 193 – 205, doi:10.1016/j.cageo.2012.07.021.

Carrigan, C.W., Bream, B., Miller, C.F., and Hatcher, R.D., Jr., 2001, Ion microprobe analyses of zircon rims from the eastern Blue Ridge and Inner Piedmont, CSC-GA: Implications for the timing of Paleozoic metamorphism in the southern Appalachians: Geological Society of America Abstracts with Programs, v. 33, p. 7.

Cook, F.A., Albaugh, D.S., Brown, L.D., Kaufman, S., Oliver, J.E., and Hatcher, R.D., Jr., 1979, Thin-skinned tectonics in the crystalline southern Appalachians: COCORP seismic-reflection profiling of the Blue Ridge and Piedmont: Geology, v. 7, p. 563–568, doi:10.1130/0091-7613(1979)7<563:TTITCS>2.0.CO;2.

Cook F.A., Brown, L.D., Kaufman, S., and Oliver, J.E.,1983, COCORP seimic reflection profiling of the southern Appalachians: American Association of Petroleum Geologists Studies in Geology, no. 14, 61 p.

Cyphers, S.R., and Hatcher, R.D., Jr., 2006, The Chattahoochee-Holland mountain fault: A terrane boundary in the Blue Ridge of western North Carolina: Geological Society of America Abstracts with Programs, v. 38, no. 3, p. 66.

Dean, L.S., 1979, Petrogenetic relationships of trondhjemitic rocks in the northern Alabama Piedmont [M.S. thesis]: Tuscaloosa, University of Alabama, 125 p.

Defant, M.J., 1980, A geochemical and petrogenetic analysis of the Almond and Blakes Ferry plutons, Randolph County, Alabama [M.S. thesis]: University of Alabama, Tuscaloosa, Alabama, 118 p.

Defant, M.J., and Ragland, P.C., 1981, Petrochemistry of the trondhjemitic Almond and Blakes Ferry plutons, Randolph County, Alabama: Geological Society of America Abstracts and Program, v. 13, p. 6.

Defant, M.J., Drummond, M.S., Arthur, J.D., and Ragland, P.C., 1987, The petrogenesis of the Blakes Ferry pluton, Randolph County, Alabama, *in* Drummond, M.S., and Green, N.L., eds., Granites of Alabama: Alabama Geological Survey Bulletin 128, p. 97-116.

Deininger, R.W., 1975, Granitic rocks in the northern Alabama Piedmont, in Neathery, T.L. and Tull, J.F., eds., Geologic Profiles in the Northern Alabama Piedmont: Alabama Geological Society 13th Annual Field Trip Guidebook, p. 49–62.

Deininger, R.W., Neathery, T.L., and Bentley, R.D., 1973, Genetic relationships among granitic rocks in the northern Alabama Piedmont: Alabama Geological Survey, Open-File Report, 18 p.

Dennis, A.J., and Secor, D.T., 1987, A model for the development of crenulations in shear zones with applications from the southern Appalachian Piedmont: Journal of Structural Geology, v. 9, no. 7, p. 809-817.

Dennis, A.J., and Wright, J.E., 1997, Middle and late Paleozoic monazite U-Pb ages, Inner Piedmont, South Carolina: Geological Society of America Abstracts with Programs, v. 29, no. 3, p. 12.

Drummond, M.S., 1986, Igneous, metamorphic, and structural history of the Alabama Tin Belt, Coosa County, Alabama [unpublished Ph.D. thesis]: Florida State University Tallahassee, Florida, 411 p.

Drummond, M.S., and Guthrie, G.M., 1986, Stratigraphy, metamorphism, and deformation of the northern Alabama Piedmont, in Whittington, D., Guthrie, G.M., Defant, M.J., Drummond, M.S., and Allison, D., eds., Mineral resources of the northern Alabama Piedmont: Southeastern Section of the Geological Society of America, Field Trip Guidebook, no. 27, p. 2-25.

Drummond, M.S. and Defant, M.J., 1990, A model for trondhjemite-tonalite-dacite genesis and crustal growth via slab melting: Archean to modern comparisons, Journal of Geophysical Research, v. 95, no. B13, p. 503-521.

Drummond, M.S., Allison, D.T., Wesolowski, D.J., 1994, Igneous petrogenensis and tectonic setting of the Elkahatchee Quartz Diorite, Alabama Appalachians: Implications for Penobscotian magmatism in the eastern Blue Ridge: American Journal of Science, v. 294, p. 173-236.

Drummond, M.S., Neilson, M.J., Allison, D.T., and Tull, J.F., 1997, Igneous petrogenesis and tectonic setting of granitic rocks from the eastern Blue Ridge and Inner Piedmont, Alabama Appalachians, *in* Sinha, A.K., et al., eds., The nature of magmatism in the Appalachian orogen: Geological Society of America Memoir 191, p. 47–164, doi:10.1130/0-8137-1191-6 .147.

Ernst, W. G., 1973, Interpretive synthesis of metamorphism in the Alps: Geological Society of America Bulletin, v. 84, p. 2053-2078.

Gault, H. R., 1945, Petrography, structures, and petrofabrics of the Pinckneyville Quartz Diorite, Alabama: Bulletin of the Geological Society of America, v. 56, p. 181-246.

Garihan, J.M., and Ranson, W.A., 1992, Structure of the Mesozoic Marietta-Tryon graben, South Carolina and adjacent North Carolina, *in* Bartholomew, M.J., et al., eds., Basement tectonics 8: Characterization of ancient and Mesozoic continental margins—Proceedings of the 8th International Conference on Basement Tectonics, Butte, Montana, 1988: Dordrecht, Netherlands, Kluwer Academic Publishers, p. 539–555.

Garihan, J.M., Preddy, M.S., and Ranson, W.A., 1993, Summary of mid-Mesozoic brittle faulting in the Inner Piedmont and nearby Charlotte belt of the Carolinas, *in* Hatcher, R.D., Jr., and Davis, T., eds., Studies of Inner Piedmont geology with a focus on the Columbus Promontory: Carolina Geological Society Field Trip Guidebook, p. 55–66.

Grimes, J.E., 1993, Geology of the Piedmont rocks between the Dadeville Complex and the Pine Mountain Window in parts of Lee, Macon, and Tallapoosa Counties, Alabama [unpublished M.S. thesis]: Auburn University, Auburn, Alabama, 129 p.

Guthrie, G. M., editor, 1995, The Timing and Tectonic mechanism of the Alleghenian orogeny, Alabama Piedmont: Alabama Geological Society 32nd Annual Field Trip Guidebook, Tuscaloosa, Alabama, Geological Survey of Alabama, 98 p.

Guthrie, G. M., and Dean, L.S., 1989, Geology of the New Site 7.5 Minute Quadrangle, Tallapoosa and Clay Counties, Alabama: Alabama Geological Survey Quadrangle Map 9, p. 41.

Hames, W.E., Tull, J.F., Barbeau, D.L., Jr., McDonald, W.M., and Steltenpohl, M.G., 2007, Laser $^{40}Ar/^{39}Ar$ ages of muscovite and evidence for Mississippian (Visean) deformation near the thrust front of the southwestern Blue Ridge province: Geological Society of America Abstracts with Programs, v. 39, no. 2, p. 78.

Harris, N.B.W., Pearce, J.A., and Tindle, A.G., 1986, Geochemical characteristics of collision zone magmatism, *in* Coward, M.P., and Reis, A.C., eds., Collision tectonics: Special Publication Geological Society, v. 19, p. 67-81.

Harstad, R.P., 2015, Kinematic and age constraints on the Alexander City fault, eastern Blue Ridge, Alabama [unpublished undergraduate thesis]: Columbus State University, Columbus, Georgia, 47 p.

Harstad, R.P., 2017, Geology of the Roanoke East Quadrangle and investigations of the Long Island Creek Gneiss, southernmost Appalachians of east Alabama [unpublished M.S. thesis]: Auburn University, Auburn, Alabama, 81 p.

Harstad, R.P., and Barineau, C.I., 2014, Kinematic and age constraints on the Alexander City fault, eastern Blue Ridge, Alabama: Geological Society of America Abstracts with Programs, v. 45, no. 6, p. 504.

Hatcher, R.D., Jr., 1972, Developmental Model for the Southern Appalachians: Geological Society of America Bulletin, v. 83, p. 2735-2760.

Hatcher, R.D., Jr., 1978, Tectonics of the western Piedmont and Blue Ridge, southern Appalachians: Review and speculation: American Journal of Science, v. 278, p. 276–304, doi:10.2475/ajs.278.3.276.

Hatcher, R.D., Jr., 1987, Tectonics of the southern and central Appalachian internides: Annual Review of Earth and Planetary Sciences, v. 15, p. 337-362.

Hatcher, R. D. Jr., 2004, Properties of thrusts and upper bounds for the size of thrust sheets, in K. R. McClay, ed., Thrust tectonics and hydrocarbon systems: AAPG Memoir 82, p. 18–29.

Hatcher, R.D., Jr., 2005, Southern and Central Appalachians: Encyclopedia of Geology, p. 72-81.

Hatcher, R.D., Jr., 2010, The Appalachian orogen: A brief summary, *in* Tollo, R.P., et al., eds., From Rodinia to Pangea: The lithotectonic record of the Appalachian region: Geological Society of America Memoir 206, p. 1–20, doi:10.1130/2010.1206(01).

Hatcher, R.D., Jr., Ziets, I., and Litehiser, J.J., 1987, Crustal subdivisions of the eastern and central United States and a seismic boundary hypothesis for eastern seismicity: Geology, v. 15, no. 6, p. 528-532.

Hatcher, R.D., Jr., Osberg, P.H., Drake, A.A., Jr., Robinson, P., and Thomas, W.A., 1990, Tectonic Map of the U.S. Appalachians: Boulder, Colorado, Geological Society of America, for The Geology of North America, v. F-2, scale 1:250,000.

Hawkins, J.F., 2013, Geology, Petrology, and Geochronology of Rocks in the Our Town, Alabama Quadrangle [M.S. thesis]: Auburn University, Auburn, Alabama, 101 p.

Hawkins, J.F., Steltenpohl, M.G., and Abrahams, J.B., 2012, Exploring the potential tectonic significance of extensional movement documented along the Brevard zone in Alabama: Geological Society of America Abstracts with Programs, v. 44, no. 7, p. 595.

Hibbard, J.P., Stoddard, E.F., Secor, D.T., Jr., and Dennis, A.J., 2002, The Carolina zone: Overview of Neoproterozoic to early Paleozoic peri-Gondwanan terranes along the eastern flank of the southern Appalachians: Earth-Science Reviews, v. 57, p. 299–339, doi:10.1016/S0012-8252(01)00079-4.

Holdaway, M.J., 1971, Stability of andalusite and the aluminosilicate phase diagram: American Journal of Science, v. 271, p. 97-131.

Horton, J. W., Jr., Zeitz, I., and Neathery, T.L., 1984, Truncation of the Appalachian Piedmont beneath the Coastal Plain of Alabama: Evidence from new magnetic data: Geology, v. 12, p. 51-55.

Huebner, M.T., and Hatcher, R.D., Jr., 2013 – Polyphase Reactivation History of the Towaliga Fault, Central Georgia: Implications regarding the Amalgamation and Breakup of Pangea: Journal of Geology, v. 121, p. 75-90, doi: 10.1086/668602.

Huebner, M.T., Hatcher, R.D. and Merschat, A.J., 2017. Confirmation of the southwest continuation of the Cat Square terrane, southern Appalachian Inner Piedmont, with implications for middle Paleozoic collisional orogenesis: American Journal of Science, v. 317, p. 95-176.

Ingram, S.B., 2012, U-Pb zircon and monazite geochronology and hafnium isotopic geochemistry of Neoacadian and early Alleghenian plutonic rocks in the Alabama eastern Blue Ridge, southern Appalachian Mountains [M.S. Thesis]: University of Alabama, Tuscaloosa, Alabama, 80 p.

Ingram, S., Schwartz, J.J., and Johnson, K., 2011, U-Pb zircon and monzonite geochronology and Hf isotope geochemistry of Neoacadian and early Alleghenian plutonic rocks in the Alabama eastern Blue Ridge, southern Appalachian Mountains: Geological Society of America Abstracts with Programs, v. 43, no. 5, p. 88.

Johnson, M.J., 1988, Geology of the gold occurrences near Jacksons Gap, Tallapoosa County, Alabama [unpublished M.S. thesis]: Auburn, Alabama, Auburn University, p. 156.

Keefer, W.D., 1992, Geology of the Tallassee synform hinge zone and its relationship to the Brevard fault zone, Tallapoosa and Elmore Counties, Alabama [unpublished M.S. thesis]: Auburn University, Auburn, Alabama, 195 p.

McClellan, E.A., Steltenpohl, M.G., Thomas, C., and Miller, C., 2007, Isotopic age constraints and metamorphic history of the Talladega belt: New evidence for timing of arc magmatism and terrane emplacement along the southern Laurentian margin: Journal of Geology, v. 115, p. 541-561.

McCullars, J.M., 2001, Geology and trace-element geochemistry of the Brevard zone near Martin Lake, Tallapoosa County, Alabama [unpublished M.S. thesis]: Auburn University, Auburn, Alabama, 74 p.

McDonald, W.M., Hames, W.E., Marzen, L.J., and Steltenpohl, M.G., 2007, A GIS database for 40Ar/39Ar data of the southwestern Blue Ridge province: Geological Society of America Abstracts with Programs, v. 39, no. 2, p. 81.

Merschat, A.J., Hatcher, R.H., Jr., and Davis, T.L., 2005, The northern Inner Piedmont, Southern Appalachians, USA: Kinematics of transpression and SW-directed mid-crustal flow: Journal of Structural Geology, v. 27, p. 1252–1281, doi:10.1016/j.jsg.2004.08.005.

Miller, B.V., Fetter, A.H., and Stewart, K.G., 2006, Plutonism in three orogenic pulses, Eastern Blue Ridge Province, southern Appalachians: Geological Society of America Bulletin, v. 118, no. 1/2, p. 171-184.

Moyen, J.F., 2009, High Sr/Y and La/Yb ratios: The meaning of the "adakitic signature": Lithos, v. 112, p. 556-564.

Muangnoicharoen, N., 1975, The geology and structure of a portion of the northern piedmont, east-central Alabama [M.S. thesis]: University of Alabama, Tuscaloosa, Alabama, 72 p.

Neathery, T.L., 1975, Rock units in the high-rank belt of the northern Alabama Piedmont, Guidebook for the Annual Field Trip of the Alabama Geological Society, v. 13, p. 9-48.

Neathery, T.L., and Reynolds, J.W., 1973, Stratigraphy and metamorphism of the Wedowee Group- a reconnaissance: American Journal of Science, v. 273, p. 723-741.

Neathery, T.L., and Reynolds, J.W., 1975, Geology of the Lineville East, Ofelia, Wadley North and Mellow Valley quadrangles, Alabama: Geological Survey of Alabama Bulletin 109, 120 p.

Osborne, W.E., Szabo, M.W., Neathery, T.L., and Copeland, C.W., Jr., compilers, 1988, Geologic map of Alabama, northeast sheet: Alabama Geological Survey Special Map 220, scale 1:250,000.

Pardee, J.T., and Park, C.F., Jr., 1948, Gold deposits of the southern Piedmont: U.S. Geological Survey Professional Paper 213, p. 156.

Park, C.F., Jr., 1935 Hog mountain gold district, Alabama: American Institute of Mining and Metallurgical Engineers Transactions, Mining Geology, v. 115, p. 209-228.

Pearce, J.A., Harris, N.B.W., and Tindle, A.G., 1984, Trace element discrimination diagrams for the tectonic interpretation of granitic rocks: Journal of Petroleum Geology, v. 25, p. 956-983.

Poole, J.D., 2015, Geology of the Jacksons Gap, Alabama, Quadrangle and structural implications for the Brevard fault zone [M.S. thesis]: Auburn University, Auburn, Alabama, 174 p.

Phillips, W. B., 1892, a preliminary report on a part of the lower gold belt of Alabama in the counties of Chilton, Coosa, and Tallapoosa: Alabama Geological Survey Bulletin 3, p. 97.

Prouty, W.F., 1923, Geology and Mineral Resources of Clay County, Alabama: Alabama Geological Survey, County Rept. 1, 190 p.

Raymond, D.E., Osborne, W.E., Copeland, C.W., and Neathery, T.L., 1988, Alabama stratigraphy: Alabama Geological Survey Circular 140, 97 p.

Reed, A.S., 1994, Geology of the western portion of the Dadeville 7.5' Quadrangle, Tallapoosa County, Alabama: unpublished M.S. thesis: Auburn University, Auburn, Alabama, 108 p.

Russell, G., 1978, U-Pb, Rb-Sr, and K-Ar geochronology of the Alabama Piedmont [Ph.D. thesis]: Florida State University, Tallahassee, Florida, 196 p.

Saunders, J.A., Steltenpohl, M.G., and Cook, R.B., 2013, Gold Exploration and Potential of the Appalachian Piedmont of Eastern Alabama: Society of Economic Geologists Newsletter, July 2013, no. 94, p. 1; 12-17.

Sagul, D.A., 2016, Constraining the age and petrogenesis of the Zana and Kowaliga Gneisses, eastern Blue Ridge, Alabama [M.S. thesis]: University of Florida, Gainesville, Florida, 150 p.

Schwartz, J.J., Johnson, K., Ingram, S., 2011, U-Pb zircon geochronology of Neoacadian and Early Alleghenian plutonic rocks in the Alabama Eastern Blue Ridge, Southern Appalachian Mountains, Geological Society of America Abstracts with Programs, v. 43, No 1., p. 62.

Singleton, R.F., and Steltenpohl, M.G., 2014, Geology of the 1:24,000 Buttston, Alabama, 7.5-Minute Quadrangle, Tallapoosa County, Alabama: Alabama Geological Survey Open-File Report, 30 p.

Sinha, A.K. et al., 1981, Plutonic Map of the U.S. Appalachians: Geological Society of America Abstracts with Programs, v. 13, no. 7, 584 p.

Stahr, D.W., III, Hatcher, R.D., Jr., Miller, C.F., and Wooden, J.L., 2006, Alleghanian deformation in the Georgia and North Carolina eastern Blue Ridge: Insights from pluton ages and fabrics: Geological Society of America Abstracts with Programs, v. 38, no. 3, p. 20.

Steltenpohl, M.G., 1988, Kinematics of the Towaliga, Bartletts Ferry, and Goat Rock fault zones, Alabama: The late Paleozoic dextral shear system in the southernmost Appalachians: Geology, v. 16, p. 852-855.

Steltenpohl, M.G., 2005, An introduction to the terranes of the southernmost Appalachians of Alabama and Georgia, in Steltenpohl, M.G., Southernmost Appalachian terranes, Alabama and Georgia: Southeastern Section of the Geological Society of America Field Trip Guidebook, p. 1-18. Steltenpohl, M.G., and Kunk, M.J., 1993, $^{40}Ar/^{39}Ar$ thermochronology and Alleghanian development of the southernmost Appalachian Piedmont, Alabama and southwest Georgia: Geological Society of America Bulletin, v. 105, p. 819-833.

Steltenpohl, M.G., and Kunk, M.J., 1993, $^{40}Ar/^{39}Ar$ thermochronology and Alleghanian development of the southernmost Appalachian Piedmont, Alabama and southwest Georgia: Geological Society of America Bulletin, v. 105, p. 819-833.

Steltenpohl, M.G., Neilson, M.J., Bittner, E.I., Colberg, M.R., and Cook, R.B., 1990, Geology of the Alabama Inner Piedmont terrane: Geological Survey of Alabama Bulletin 139, 80 p.

Steltenpohl, M.G., Heatherington, A., Mueller, P., and Miller, B.V., 2005, New isotopic dates on crystalline rocks from Alabama and Georgia: Geological Society of America Field trip guidebook, p. 51-69.

Steltenpohl, M.G., Horton, J.W., Jr., Hatcher, R.D., Jr., Zietz, I., Daniels, D.L., and Higgins, M.W., 2013a, Upper crustal structure from regional magnetic and gravity data: using geology to interpret geophysics, and vice versa: Geosphere, v. 9, no. 4, p. 1–21, doi:10.1130/GES00703.1.

Steltenpohl, M.G., Schwartz, J.J., and Miller, B.V., 2013b, Late-to-post Appalachian strain partitioning and extension in the Blue Ridge of Alabama and Georgia: Geosphere, no. 3, p. 1–20, doi:10.1130/GES00738.1.

Sterling, J.W., 2006, Geology of the southernmost exposures of the Brevard Zone in the Red Hill Quadrangle, Alabama [M.S. Thesis]: Auburn University, Auburn, Alabama, 118 p.

Stoddard, P.V., 1983, A petrographic and geochemical analysis of the Zana Granite and Kowaliga Augen Gneiss: Northern Piedmont, Alabama [M.S. thesis]: Memphis, Tennessee, Memphis State University, 74 p.

Stowell, H.H., Lesher, C.M., Gren, N.L., and Sha, P., 1996, Metamorphism and gold mineralization in the Blue Ridge southernmost Appalachians: Economic Geology and the Bulletin of the Society of Economic Geologists, v. 91, p. 1115–1144, doi:10.2113 /gsecongeo.91.6.1115.

Stowell, H.H., Parker, K.O., Madden, J., 2015, Neoacadian and Alleghanian Intrusion, Metamorphism, and Gold Mineralization in the Eastern Blue Ridge: Alabama Geological Society, 52nd Annual Field Trip Guidebook, 60 p.

Streckeisen, A., 1976, To each plutonic rock its proper name: Earth-Science Reviews, v. 12, no. 1, p. 1-33.

Strong, T.R., and Driscoll R.L., 2016, A Process for Reducing Rocks and Concetrating Heavy Minerals, U.S. Geological Survey Open File Report 2016-1022, 24 p.

Sun, S.S., McDonough, W.F., 1989, Chemical and isotopic systematics of oceanic basalts: implications for mantle composition and processes: Geological Society, London, Special Publications, v. 42, no. 1, p. 313-345.

Thomas, W. A, 1977, Evolution of Appalachian-Ouachita salient and recesses from reentrants and promontories in the continental margin: American Journal of Science, v. 277, p. 1233-1278.

Thomas, W.A., Neathery, T.N., and Ferrill, B.A., 1989, Cross-section A-A′, in Hatcher, R.D., Jr., et al., eds., The Appalachian-Ouachita orogen in the United States: Boulder, Colorado, Geological Society of America, Geology of North America, v. F-2.

Tull, J.F., 1978, Structural Development of the Alabama Piedmont Northwest of the Brevard Zone: American Journal of Science, v. 278, p. 442-460.

Tull, J.F., Barineau, C.I., Mueller, P.A., Wooden, J.L., 2007, Volcanic arc emplacement onto the southernmost Appalachian Laurentian shelf: Characteristics and constraints: Geological Society of America Bulletin, v. 119, no. 3-4, p. 261-274, doi:10.1130/B25998.1

Tull, J.F., Mueller, P.A., Barineau, C.I., and Wooden, J.L., 2009, Age and tectonic implications of the Elkahatchee Quartz Diorite, Eastern Blue Ridge Province, southern Appalachians, USA: Geological Society of America Abstracts with Programs, v. 41, no. 7, p. 288.

Tull, J.F., Mueller, P.A., Farris, D.W. and Davis, B.L., 2018. Taconic suprasubduction zone magmatism in southern Laurentia: Evidence from the Dadeville Complex: Geological Society of America Bulletin, v. 130, p. 1339-1354.

Tuomey, M., 1858, Second biennial report on the geology of Alabama: Alabama Geological Survey Biennial report 2, p. 292.

VanDervoort, D.S., 2016, Geology of the Wadley South Quadrangle and geochronology of the Dadeville Complex, southernmost Appalachians of East Alabama [M.S. Thesis]: Auburn University, Auburn, Alabama, 127 p.

VanDervoort, D.S., Harstad, R.P., Whitmore, J.P, Ma, C., and Steltenpohl, M.G., 2017, Update on 1:24,000 geologic mapping of the Brevard zone and related structures in east-central Alabama: Geological Society of America Abstracts with Programs, v. 49, no. 3, doi:10.1130/abs/2017SE-290867.

White, T.W., 2007, Geology of the 1:24,000 Tallassee, Alabama Quadrangle, Tallapoosa and Elmore Counties [M.S. thesis]: Auburn University, Auburn, Alabama, 73 p.

Whitmore, J.P., 2018, Geology of the Milltown Alabama 7.5' Quadrangle and 40Ar/39Ar geochronology of muscovite from select rocks of the east-central Alabama Piedmont [M.S. thesis]: Auburn University, Auburn, Alabama, 84 p.

Whitmore, J.P., and Steltenpohl, M.G., 2017, Geology of the 1:24,000 Milltown, Alabama, U.S.G.S. Topographic Quadrangle: Alabama Geological Survey Open-File Report, 33 p.

Wielchowsky, C.C., 1983, The geology of the Brevard zone and adjacent terranes in Alabama [unpublished Ph.D. thesis]: Rice University, Houston, Texas, 237 p.

APPENDIX

Appendix A – Geochemistry

Appendix B – CIPW Mineral Norms

Appendix C – Geochronology

Appendix D – Sample List

APPENDIX A – Geochemistry

	SAMPLE	DESCRIPTION	17BRW154	17BRW168P	17BRW168NP	17BRW177	17BRW202	17BRW217
ME-ICP06	SiO2	%	65.3	62.5	65.1	67.2	74.6	75.9
ME-ICP06	Al2O3	%	16.7	16.3	16.5	15.7	15.55	13.6
ME-ICP06	Fe2O3	%	4.43	6.84	4.47	3.92	1.02	0.7
ME-ICP06	CaO	%	3.7	3.82	3.81	3.24	1.33	1.58
ME-ICP06	MgO	%	1.85	2.33	1.83	1.54	0.13	0.13
ME-ICP06	Na2O	%	3.72	3.58	3.98	3.67	4.4	5.06
ME-ICP06	K2O	%	2.23	2.56	2.16	2.38	2.07	1.52
ME-ICP06	Cr2O3	%	0.005	0.005	0.004	0.004	<0.002	0.002
ME-ICP06	TiO2	%	0.64	0.78	0.68	0.52	0.07	0.08
ME-ICP06	MnO	%	0.06	0.09	0.06	0.04	0.01	0.01
ME-ICP06	P2O5	%	0.21	0.29	0.26	0.16	0.02	0.03
ME-ICP06	SrO	%	0.06	0.07	0.07	0.05	0.05	0.06
ME-ICP06	BaO	%	0.09	0.09	0.08	0.06	0.07	0.03
OA-GRA05	LOI	%	0.77	0.61	0.7	0.63	1.86	0.6
TOT-ICP06	Total	%	99.77	99.87	99.7	99.11	101.18	99.3
C-IR07	C	%	0.03	0.05	0.02	0.04	0.03	0.04
S-IR08	S	%	<0.01	0.05	<0.01	0.06	<0.01	0.01
ME-MS81	Ba	ppm	749	767	654	462	443	284
ME-MS81	Ce	ppm	62.2	67.5	62.1	60	32.8	8.6
ME-MS81	Cr	ppm	30	40	20	30	<10	20
ME-MS81	Cs	ppm	2.54	4.93	3.25	4.29	0.42	0.8
ME-MS81	Dy	ppm	3.17	2.81	2.6	1.6	0.44	0.7
ME-MS81	Er	ppm	1.39	1.52	1.2	0.69	0.19	0.4
ME-MS81	Eu	ppm	1.35	1.3	1.28	1.14	0.35	0.27
ME-MS81	Ga	ppm	20.7	23	20.9	20.5	15.8	15
ME-MS81	Gd	ppm	4.53	4.43	4.28	3.08	0.74	0.77
ME-MS81	Ge	ppm	<5	<5	<5	<5	<5	<5
ME-MS81	Hf	ppm	4.6	3.1	4.9	4.2	1	1.8

ME-MS81	Ho	ppm	0.59	0.57	0.46	0.27	0.1	0.12
ME-MS81	La	ppm	31.7	31.2	27.3	30.5	8.2	4.2
ME-MS81	Lu	ppm	0.17	0.12	0.14	0.1	0.02	0.05
ME-MS81	Nb	ppm	8.6	8.2	10.8	10.3	2.1	1.4
ME-MS81	Nd	ppm	30	29.5	25.9	26	6.8	4.1
ME-MS81	Pr	ppm	7.65	7.69	6.9	7.11	1.97	1.06
ME-MS81	Rb	ppm	90	108.5	88.3	122.5	34.2	36.1
ME-MS81	Sm	ppm	5.04	4.9	4.8	4.11	1.01	0.85
ME-MS81	Sn	ppm	2	3	3	5	2	1
ME-MS81	Sr	ppm	545	560	608	437	321	523
ME-MS81	Ta	ppm	0.4	0.4	0.4	0.7	<0.1	<0.1
ME-MS81	Tb	ppm	0.61	0.61	0.5	0.35	0.11	0.17
ME-MS81	Th	ppm	10.25	6.67	6.3	7.28	3.89	1.19
ME-MS81	Tm	ppm	0.17	0.18	0.18	0.11	0.01	0.04
ME-MS81	U	ppm	1.33	0.95	1.26	1.42	0.8	1.32
ME-MS81	V	ppm	83	90	82	69	7	11
ME-MS81	W	ppm	<1	<1	1	<1	<1	<1
ME-MS81	Y	ppm	14.1	14	11.9	6.8	2.1	3.8
ME-MS81	Yb	ppm	1.1	0.84	0.98	0.57	0.22	0.28
ME-MS81	Zr	ppm	187	126	210	165	26	71
ME-MS42	As	ppm	0.6	0.8	0.6	0.3	0.1	0.5
ME-MS42	Bi	ppm	0.01	0.01	0.01	0.01	<0.01	0.01
ME-MS42	Hg	ppm	0.008	<0.005	0.006	0.007	<0.005	0.005
ME-MS42	In	ppm	0.011	0.008	0.006	0.016	0.005	<0.005
ME-MS42	Re	ppm	<0.001	<0.001	<0.001	<0.001	<0.001	<0.001
ME-MS42	Sb	ppm	0.11	0.06	0.12	<0.05	<0.05	0.11
ME-MS42	Se	ppm	<0.2	0.3	<0.2	<0.2	<0.2	<0.2
ME-MS42	Te	ppm	0.01	0.01	<0.01	0.01	0.01	<0.01
ME-MS42	Tl	ppm	0.51	0.67	0.54	0.74	0.03	0.06

ME-4ACD81	Ag	ppm	<0.5	<0.5	<0.5	<0.5	<0.5	<0.5
ME-4ACD81	Cd	ppm	<0.5	<0.5	<0.5	<0.5	<0.5	<0.5
ME-4ACD81	Co	ppm	10	12	9	8	1	1
ME-4ACD81	Cu	ppm	8	21	2	7	1	2
ME-4ACD81	Li	ppm	50	70	50	50	30	20
ME-4ACD81	Mo	ppm	1	1	<1	<1	1	<1
ME-4ACD81	Ni	ppm	11	12	7	8	1	<1
ME-4ACD81	Pb	ppm	15	10	10	16	13	11
ME-4ACD81	Sc	ppm	10	11	10	8	8	1
ME-4ACD81	Zn	ppm	85	121	91	75	18	22

APPENDIX B – CIPW Mineral Norms

Oxides	17BRW154	17BRW168P	17BRW168NP	17BRW177	17BRW202	17BRW217
SiO2	65.3	62.5	65.1	67.2	74.6	75.9
Al2O3	16.7	16.3	16.5	15.7	15.55	13.6
Fe2O3	4.43	6.84	4.47	3.92	1.02	0.7
FeO	0.00	0.00	0.00	0.00	0.00	0.00
MgO	1.85	2.33	1.83	1.54	0.13	0.13
CaO	3.7	3.82	3.81	3.24	1.33	1.58
Na2O	3.72	3.58	3.98	3.67	4.4	5.06
K2O	2.23	2.56	2.16	2.38	2.07	1.52
TiO2	0.64	0.78	0.68	0.52	0.07	0.08
P2O5	0.21	0.29	0.26	0.16	0.02	0.03
MnO	0.06	0.09	0.06	0.04	0.01	0.01
LOI	0.77	0.61	0.7	0.63	1.86	0.6
Total	99.61	99.70	99.55	99.00	101.06	99.21
Fe option						
AsIs(1,0)	1	1	1	1	1	1
3+/Total	0.20	0.20	0.20	0.20	0.20	0.20
Norm						

Q	23.66	19.94	22.20	26.60	35.75	34.99
C	2.16	1.55	1.45	1.77	4.09	0.92
Or	13.44	15.47	13.00	14.44	12.39	9.13
Ab	34.09	32.89	36.41	33.84	40.03	46.20
An	17.33	17.45	17.53	15.43	6.55	7.77
Ne	0.00	0.00	0.00	0.00	0.00	0.00
Di	0.00	0.00	0.00	0.00	0.00	0.00
Hy	5.21	6.58	5.15	4.37	0.36	0.36
Ol	0.00	0.00	0.00	0.00	0.00	0.00
Mt	-1.22	-1.45	-1.30	-1.02	-0.12	-0.15
Hm	1.98	2.92	2.02	1.74	0.40	0.30
Il	0.05	0.07	0.05	0.03	0.01	0.01
Ap	0.45	0.62	0.55	0.34	0.04	0.06
Norm sum.	97.16	96.04	97.06	97.55	99.51	99.60
An	26.72	26.52	26.18	24.22	11.11	12.32
Ab	52.55	49.97	54.39	53.11	67.88	73.21
Or	20.73	23.51	19.42	22.66	21.01	14.47
ANOR						

Q'						
% F-spar	64.86	65.81	66.94	63.72	58.97	63.10
Mg#	44.9	39.9	44.4	43.5	20.0	26.6
Rev. Wt%						
SiO2	65.3	62.5	65.1	67.2	74.6	75.9
Al2O3	16.7	16.3	16.5	15.7	15.55	13.6
Fe2O3	4.43	6.84	4.47	3.92	1.02	0.7
FeO	0	0	0	0	0	0
MgO	1.85	2.33	1.83	1.54	0.13	0.13
CaO	3.7	3.82	3.81	3.24	1.33	1.58
Na2O	3.72	3.58	3.98	3.67	4.4	5.06
K2O	2.23	2.56	2.16	2.38	2.07	1.52
TiO2	0.64	0.78	0.68	0.52	0.07	0.08
P2O5	0.21	0.29	0.26	0.16	0.02	0.03
MnO	0.06	0.09	0.06	0.04	0.01	0.01
Total	98.84	99.09	98.85	98.37	99.2	98.61
Cations						
Si	1.087	1.040	1.083	1.118	1.242	1.263
Al	0.328	0.320	0.324	0.308	0.305	0.267
Fe3	0.055	0.086	0.056	0.049	0.013	0.009
Fe2	0.000	0.000	0.000	0.000	0.000	0.000
Mg	0.046	0.058	0.045	0.038	0.003	0.003
Ca	0.066	0.068	0.068	0.058	0.024	0.028
Na	0.120	0.116	0.128	0.118	0.142	0.163
K	0.047	0.054	0.046	0.051	0.044	0.032
Ti	0.008	0.010	0.009	0.007	0.001	0.001
P	0.003	0.004	0.004	0.002	0.000	0.000
Mn	0.001	0.001	0.001	0.001	0.000	0.000
Total	1.76	1.76	1.76	1.75	1.77	1.77
Cation %						
Si	61.72	59.22	61.43	63.92	70.01	71.48
Al	18.60	18.20	18.35	17.60	17.20	15.09
Fe3	3.15	4.88	3.17	2.81	0.72	0.50
Fe2	0.00	0.00	0.00	0.00	0.00	0.00
Mg	2.61	3.29	2.57	2.18	0.18	0.18
Ca	3.75	3.88	3.85	3.30	1.34	1.59
Na	6.82	6.58	7.28	6.77	8.01	9.24
K	2.69	3.09	2.60	2.89	2.48	1.83
Ti	0.45	0.56	0.48	0.37	0.05	0.06

P	0.17	0.23	0.21	0.13	0.02	0.02
Mn	0.05	0.07	0.05	0.03	0.01	0.01
Total	100	100	100	100	100	100
for Norm						

FeO	0.048	0.072	0.048	0.032	0.008	0.008
Ap	0.449	0.621	0.555	0.344	0.042	0.064
CaO	3.466	3.490	3.505	3.087	1.311	1.554
Il	0.048	0.072	0.048	0.032	0.008	0.008
Ti #2	0.431	0.520	0.459	0.356	0.045	0.053
FeO #3	-0.407	-0.484	-0.435	-0.340	-0.041	-0.049
Or	13.444	15.472	13.001	14.440	12.391	9.131
Al #2	15.911	15.105	15.747	14.710	14.718	13.266
Si-budg	53.653	49.939	53.631	55.258	62.573	66.002
Ab-prov	34.085	32.885	36.409	33.842	40.029	46.197
Al #3	9.09	8.53	8.47	7.94	6.71	4.03
Si-budg	33.202	30.208	31.786	34.952	38.556	38.284
C	2.161	1.549	1.455	1.768	4.090	0.918
An	17.332	17.449	17.526	15.435	6.554	7.772
Si-budg	26.269	23.228	24.775	28.778	35.935	35.176
Hm	1.982	2.922	2.022	1.743	0.402	0.297
Mt	-1.221	-1.451	-1.304	-1.019	-0.124	-0.146
FM	2.606	3.291	2.574	2.183	0.182	0.182
Ca-budg	0.000	0.000	0.000	0.000	0.000	0.000
Di	0	0	0	0	0	0
FM-budg	2.606	3.291	2.574	2.183	0.182	0.182
Hy-prov1	5.213	6.582	5.148	4.367	0.364	0.365
Si-budg	23.663	19.937	22.201	26.595	35.753	34.993
Q	23.66	19.94	22.20	26.60	35.75	34.99
Si-def	FALSE	FALSE	FALSE	FALSE	FALSE	FALSE
Ol-prov	0.000	0.000	0.000	0.000	0.000	0.000
Hy-prov2	0.000	0.000	0.000	0.000	0.000	0.000
Hy	5.213	6.582	5.148	4.367	0.364	0.365

Si-budg	23.663	19.937	22.201	26.595	35.753	34.993
Ol	0.000	0.000	0.000	0.000	0.000	0.000
Si-budg	23.663	19.937	22.201	26.595	35.753	34.993
Si-def	0.000	0.000	0.000	0.000	0.000	0.000
Ne	0.000	0.000	0.000	0.000	0.000	0.000
Ab	34.085	32.885	36.409	33.842	40.029	46.197

APPENDIX C – U-Pb Geochronology

Name	U (ppm)	U Th	238U 206Pb	2 sigma % error	207Pb 206Pb	2 sigma % error	206/238 age†	2 sigma abs err	207/206 age	2 sigma abs err	Discordance %
R33_16	370	1.2	15.4799	6.97%	0.0533	9.57%	403.0	28.0	320.0	200.0	-9.5%
R33_2	598	1.1	14.7710	5.91%	0.0517	4.84%	421.0	24.0	270.0	100.0	-8.2%
R33_14	359	1.1	15.2439	7.47%	0.0547	8.04%	409.0	30.0	380.0	170.0	-5.7%
R33_7	123	2.0	15.1286	13.01%	0.0574	9.93%	411.0	52.0	450.0	210.0	-1.7%
R33_8	306	1.0	15.6250	5.47%	0.0544	6.99%	400.0	21.0	340.0	140.0	-1.3%
R33_12	482	1.0	15.1057	6.34%	0.0523	7.27%	413.0	26.0	300.0	150.0	-1.2%
R33_18	356	1.0	15.1057	5.74%	0.0564	9.93%	417.0	24.0	370.0	200.0	-0.5%
R33_10	429	1.0	15.3139	5.97%	0.0559	7.51%	407.0	24.0	450.0	150.0	0.2%
R33_9	468	1.1	15.1286	7.72%	0.0557	8.26%	412.0	31.0	400.0	170.0	0.5%
R33_11	595	0.9	15.0376	5.26%	0.0546	7.69%	414.0	21.0	330.0	160.0	1.9%
R33_6	332	0.9	15.4799	7.89%	0.0525	14.29%	403.0	31.0	340.0	290.0	2.4%
R33_17	387	1.2	14.8368	6.08%	0.0531	6.59%	420.0	25.0	320.0	140.0	2.6%
R33_15	506	0.8	14.8588	5.94%	0.0542	7.01%	419.0	24.0	390.0	150.0	2.6%
R33_4	293	1.1	15.7233	5.35%	0.0569	6.85%	396.4	20.9	430.0	140.0	2.7%
R33_5	290	1.2	14.9925	6.30%	0.0560	6.96%	415.0	25.0	440.0	150.0	3.0%
R33_19	211	1.0	16.0000	8.00%	0.0577	7.97%	389.3	30.6	450.0	170.0	3.5%
R33_1	520	1.0	15.1976	7.75%	0.0601	9.82%	410.0	31.0	530.0	200.0	5.3%
R33_13	661	0.8	15.6986	6.91%	0.0546	6.23%	398.1	27.0	350.0	130.0	5.5%
R33_3	245	1.2	14.8148	10.81%	0.0610	14.59%	420.0	43.0	570.0	310.0	5.6%
X17BRW154_5	2,410	5.3	18.0505	5.05%	0.0516	4.65%	348.4	17.3	270.0	100.0	-12.7%
X17BRW154_3	4,000	3.7	24.5700	4.91%	0.0607	6.75%	254.2	12.4	550.0	140.0	7.2%
X17BRW154_4	1,460	6.7	19.4932	4.48%	0.0600	6.33%	319.7	14.2	550.0	140.0	1.8%
X17BRW154_20	1,422	3.1	19.4932	5.07%	0.0593	6.07%	320.0	16.0	550.0	130.0	8.3%
X17BRW154_16	1,376	5.1	19.3424	4.06%	0.0552	5.43%	324.0	13.0	410.0	110.0	-2.5%
X17BRW154_6	2,420	4.8	18.9394	3.98%	0.0632	5.06%	327.6	12.9	670.0	110.0	6.2%
X17BRW154_7	1,880	6.1	18.7970	6.39%	0.0650	6.62%	329.3	20.8	750.0	130.0	5.4%
X17BRW154_12	2,700	3.7	18.8324	5.27%	0.0615	5.53%	330.1	17.2	600.0	120.0	5.9%
X17BRW154_18	2,080	4.4	18.8324	6.21%	0.0579	4.66%	331.6	20.3	520.0	100.0	6.7%
X17BRW154_17	3,420	8.7	18.6916	5.42%	0.0535	7.29%	335.8	18.0	310.0	150.0	-1.8%
X17BRW154_21	1,680	1.1	18.4162	5.71%	0.0590	8.31%	338.5	19.1	510.0	170.0	7.6%
X17BRW154_19	2,630	3.8	17.9533	5.92%	0.0572	5.77%	347.8	20.3	460.0	130.0	6.7%
X17BRW154_8	3,130	2.7	17.6678	6.36%	0.0614	7.00%	351.5	22.1	620.0	150.0	3.8%
X17BRW154_9	1,330	1.9	17.4520	6.28%	0.0588	5.44%	357.0	22.1	530.0	120.0	-3.5%
X17BRW154_13	1,060	3.8	17.3010	6.23%	0.0595	6.55%	359.7	22.1	520.0	140.0	1.9%
X17BRW154_14	1,480	3.8	16.9779	6.96%	0.0518	6.18%	369.9	25.3	320.0	130.0	-8.2%
X17BRW154_22	1,523	2.9	18.9394	5.68%	0.0600	5.67%	328.9	18.4	620.0	130.0	12.4%
X17BRW154_11	2,540	3.6	27.2480	6.54%	0.0616	7.63%	229.3	14.9	630.0	170.0	12.5%

X17BRW154_2	2,920	6.4	19.5313	5.27%	0.0739	7.04%	313.6	16.4	1000.0	140.0	16.8%
X17BRW154_10	3,200	2.1	21.0084	5.25%	0.0731	6.16%	292.2	15.2	1010.0	140.0	20.5%
X17BRW154_1	3,490	4.9	19.3798	5.04%	0.0764	6.81%	315.0	15.8	1130.0	140.0	20.6%
X17BRW154_15	2,030	1.8	17.0068	5.44%	0.1125	5.87%	342.0	18.7	1850.0	100.0	43.1%
X17BRW168_26	970	6.2	24.3309	5.35%	0.0562	6.41%	258.1	13.7	460.0	120.0	7.8%
X17BRW168_6	1,430	4.5	23.1481	6.48%	0.0562	6.41%	271.1	17.4	430.0	130.0	7.2%
X17BRW168_21	1,910	4.1	19.6850	4.53%	0.0543	5.16%	318.8	14.3	390.0	110.0	7.5%
X17BRW168_25	1,200	4.2	18.3150	6.96%	0.0578	6.57%	340.8	23.4	490.0	130.0	8.1%
X17BRW168_11	1,102	15.6	17.9856	5.94%	0.0570	4.91%	347.3	20.3	470.0	110.0	5.2%
X17BRW168_37	1,650	3.8	17.8253	5.17%	0.0541	6.28%	351.6	17.9	370.0	140.0	3.3%
X17BRW168_38	2,120	4.3	17.7305	6.21%	0.0568	7.57%	352.3	21.6	410.0	150.0	6.4%
X17BRW168_19	1,800	5.0	17.4520	6.81%	0.0577	5.55%	357.4	24.0	490.0	120.0	5.8%
X17BRW168_39	2,000	4.2	17.2117	6.88%	0.0573	7.16%	362.5	24.6	480.0	140.0	4.5%
X17BRW168_3	1,906	3.3	17.0358	5.96%	0.0588	5.61%	365.5	21.5	540.0	120.0	6.8%
X17BRW168_7	1,830	3.0	16.7504	6.20%	0.0574	5.57%	372.3	22.7	490.0	120.0	5.6%
X17BRW168_28	2,120	6.0	16.7785	5.20%	0.0553	6.69%	372.6	19.1	420.0	140.0	5.1%
X17BRW168_15	2,510	2.6	16.8067	5.55%	0.0528	4.92%	373.1	20.4	370.0	100.0	-0.3%
X17BRW168_4	1,459	5.4	16.7785	4.87%	0.0520	5.77%	374.1	17.9	280.0	110.0	0.5%
X17BRW168_17	880	4.2	16.6667	4.17%	0.0550	6.55%	375.2	15.4	380.0	140.0	6.3%
X17BRW168_30	1,560	6.9	16.3666	6.22%	0.0585	6.84%	380.3	23.3	480.0	140.0	6.6%
X17BRW168_20	866	6.7	16.3934	6.07%	0.0554	5.60%	381.2	22.7	390.0	120.0	3.1%
X17BRW168_10	2,100	4.4	16.3666	4.58%	0.0546	4.76%	382.2	17.2	380.0	100.0	2.3%
X17BRW168_2	1,290	4.3	16.2602	4.88%	0.0562	5.52%	383.9	18.4	440.0	120.0	4.0%
X17BRW168_8	2,130	3.0	16.1812	5.99%	0.0584	5.31%	384.7	22.7	500.0	120.0	3.7%
X17BRW168_29	1,852	5.7	16.2602	6.67%	0.0536	7.65%	385.1	25.3	380.0	160.0	1.0%
X17BRW168_32	1,350	2.5	16.2075	6.65%	0.0561	8.73%	385.1	25.2	460.0	180.0	6.8%
X17BRW168_16	930	5.7	16.2602	4.88%	0.0534	5.62%	385.2	18.5	310.0	120.0	0.3%
X17BRW168_31	630	6.7	16.2075	6.48%	0.0542	7.38%	386.0	24.6	370.0	150.0	2.8%
X17BRW168_1	1,830	4.4	16.1290	6.45%	0.0557	5.21%	387.2	24.6	410.0	110.0	5.1%
X17BRW168_13	1,650	5.6	16.0514	5.62%	0.0567	5.47%	388.5	21.5	450.0	120.0	1.5%
X17BRW168_14	830	4.4	15.9744	6.39%	0.0577	5.89%	389.9	24.5	500.0	130.0	4.2%
X17BRW168_5	1,325	4.1	15.9490	5.74%	0.0529	5.67%	392.8	22.2	350.0	120.0	-0.8%
X17BRW168_18	396	1.9	15.6495	7.20%	0.0551	6.17%	399.1	28.2	430.0	130.0	2.9%
X17BRW168_22	840	3.5	15.5763	6.85%	0.0547	6.95%	401.0	26.0	410.0	140.0	1.2%
X17BRW168_34	1,640	3.0	15.1515	6.82%	0.0550	8.00%	411.0	27.0	350.0	160.0	1.9%
X17BRW168_12	1,970	5.1	14.9477	6.13%	0.0585	6.15%	417.0	25.0	490.0	130.0	5.4%
X17BRW168_33	1,270	2.6	14.8148	5.93%	0.0534	7.49%	421.0	24.0	290.0	150.0	-3.2%
X17BRW168_23	433	2.4	14.7059	4.71%	0.0565	6.73%	424.0	20.0	480.0	140.0	3.6%
X17BRW168_27	980	4.7	14.6843	7.64%	0.0574	8.01%	424.0	31.0	450.0	170.0	6.0%
X17BRW168_35	2,670	3.0	17.9533	6.28%	0.0587	7.84%	347.2	21.5	540.0	170.0	10.7%
X17BRW168_36	1,670	4.2	23.4742	5.40%	0.0576	7.12%	267.0	14.3	500.0	150.0	10.9%
X17BRW168_24	315	5.3	15.5039	5.89%	0.0704	8.10%	403.0	23.0	890.0	170.0	18.8%

X17BRW168_9	2,710	5.1	22.1239	5.75%	0.0810	13.58%	274.9	16.1	990.0	220.0	31.8%
X17BRW177_19	2,140	12.8	19.8807	4.97%	0.0511	6.07%	317.0	15.6	240.0	120.0	-11.3%
X17BRW177_16	3,540	17.1	25.2525	7.07%	0.0545	5.32%	249.3	17.4	420.0	120.0	2.3%
X17BRW177_14	2,210	12.7	24.3309	5.60%	0.0585	5.30%	257.4	14.3	520.0	120.0	5.8%
X17BRW177_10	780	16.2	20.2840	6.09%	0.0534	5.62%	309.9	18.6	320.0	110.0	-5.8%
X17BRW177_17	1,530	7.7	19.7239	5.33%	0.0578	5.71%	316.9	16.7	500.0	130.0	0.3%
X17BRW177_20	1,340	11.0	19.4553	3.70%	0.0553	6.69%	322.2	11.8	390.0	140.0	-5.6%
X17BRW177_11	2,260	10.9	19.1939	4.80%	0.0576	6.42%	325.6	15.4	500.0	140.0	-1.2%
X17BRW177_7	1,800	11.0	19.0114	6.46%	0.0543	7.92%	330.0	21.1	350.0	160.0	-2.8%
X17BRW177_9	1,596	15.0	18.8324	4.14%	0.0600	6.50%	330.7	13.6	540.0	140.0	3.7%
X17BRW177_12	1,488	12.0	18.8679	6.23%	0.0557	7.00%	331.9	20.4	390.0	150.0	-4.4%
X17BRW177_2	1,610	9.0	18.8679	5.28%	0.0551	7.62%	332.1	17.3	410.0	170.0	2.3%
X17BRW177_13	1,680	7.6	18.4502	4.98%	0.0658	7.14%	335.1	16.5	740.0	140.0	9.0%
X17BRW177_15	1,540	15.7	18.6220	5.59%	0.0559	4.11%	336.1	18.5	448.0	92.0	-3.7%
X17BRW177_8	1,725	9.5	18.5185	6.30%	0.0559	7.51%	337.9	21.0	480.0	150.0	0.3%
X17BRW177_5	1,620	11.8	18.5529	5.57%	0.0544	7.72%	337.9	18.6	390.0	170.0	0.9%
X17BRW177_4	1,500	12.0	17.9533	6.28%	0.0563	8.88%	348.2	21.6	370.0	180.0	0.9%
X17BRW177_6	2,410	10.9	17.8571	4.82%	0.0541	5.18%	351.0	16.7	370.0	110.0	-2.3%
X17BRW177_3	441	3.7	16.8067	5.88%	0.0549	7.10%	372.2	21.6	370.0	150.0	-1.9%
X17BRW177_1	1,140	5.1	16.1551	7.11%	0.0563	8.17%	386.3	27.0	460.0	150.0	-1.0%
X17BRW177_18	1,300	3.7	14.4300	5.05%	0.0562	6.05%	431.0	21.0	420.0	130.0	-6.9%
Z_Plesovice_1	925	9.4	18.5185	4.26%	0.0523	7.27%	339.4	14.3	280.0	150.0	-0.3%
Z_Plesovice_2	1,326	8.9	19.1205	5.54%	0.0531	7.53%	328.6	18.0	320.0	140.0	-2.5%
Z_Plesovice_3	1,360	8.1	18.7970	5.83%	0.0561	6.06%	332.9	19.1	410.0	130.0	2.1%
Z_Plesovice_4	904	12.4	19.0476	4.95%	0.0547	6.58%	329.2	16.1	400.0	130.0	2.4%
Z_Plesovice_5	785	11.2	19.0476	5.52%	0.0542	7.38%	329.4	18.0	330.0	150.0	1.5%
Z_Plesovice_6	990	9.9	18.7266	5.24%	0.0513	7.21%	336.1	17.4	310.0	150.0	-0.3%
Z_Plesovice_7	1,163	9.3	18.9036	5.67%	0.0543	5.16%	331.8	18.5	400.0	120.0	3.5%
Z_Plesovice_8	1,601	7.5	20.0803	6.02%	0.0547	6.03%	312.5	18.6	370.0	130.0	5.4%
Z_Plesovice_9	889	9.9	19.0476	6.86%	0.0509	7.66%	330.7	22.4	240.0	160.0	1.2%
Z_Plesovice_10	1,419	7.9	18.7970	7.52%	0.0579	8.64%	332.2	24.7	470.0	180.0	5.1%
Z_Plesovice_11	959	10.5	19.8413	4.96%	0.0536	7.09%	316.6	15.5	370.0	140.0	-2.9%
Z_Plesovice_12	1,550	7.7	18.5874	7.43%	0.0543	7.92%	337.4	24.7	320.0	160.0	-4.7%
Z_Plesovice_13	835	10.1	18.9394	7.39%	0.0526	8.37%	331.9	24.2	310.0	180.0	0.3%
Z_Plesovice_14	1,435	7.8	19.0114	5.13%	0.0518	6.76%	331.0	16.8	260.0	140.0	0.9%
Z_Plesovice_15	1,101	8.7	19.8807	5.37%	0.0542	6.64%	315.8	16.7	350.0	140.0	0.9%
Z_Plesovice_16	1,880	8.5	19.9601	4.59%	0.0506	6.52%	315.9	14.3	290.0	140.0	-2.6%
Z_Plesovice_17	700	9.6	18.6567	7.84%	0.0523	8.03%	336.9	26.0	270.0	160.0	-6.0%
Z_Plesovice_18	1,042	8.6	19.6078	6.27%	0.0519	6.74%	321.0	19.9	260.0	140.0	-3.6%
Z_Plesovice_19	1,040	8.3	19.5313	8.20%	0.0477	8.60%	323.9	26.2	130.0	180.0	-10.7%
Z_Plesovice_20	630	9.4	19.1939	12.67%	0.0530	10.38%	327.4	40.9	290.0	210.0	1.5%

Z_Plesovice_21	960	7.8	18.8324	9.98%	0.0552	10.33%	332.7	32.8	400.0	200.0	7.2%
Z_91500_1	77	2.5	5.5556	5.56%	0.0748	5.48%	1065.0	54.0	1030.0	110.0	1.1%
Z_91500_2	84	2.6	5.7143	8.00%	0.0723	9.27%	1038.0	76.0	940.0	200.0	1.4%
Z_91500_3	85	2.7	5.5340	5.37%	0.0722	7.06%	1076.0	52.0	940.0	140.0	-2.5%
Z_91500_4	84	2.6	5.5866	6.15%	0.0748	6.82%	1060.0	59.0	1080.0	130.0	-1.0%
Z_91500_5	77	2.5	5.4348	6.52%	0.0722	6.79%	1084.0	63.0	980.0	150.0	-2.2%
Z_91500_6	82	2.6	5.6117	4.88%	0.0776	6.96%	1055.0	47.0	1080.0	140.0	2.3%
Z_91500_7	77	2.7	5.6497	5.65%	0.0746	5.90%	1050.0	55.0	1090.0	110.0	0.9%
Z_91500_8	82	2.7	5.5991	3.86%	0.0755	5.70%	1058.0	38.0	1050.0	110.0	0.6%
Z_91500_9	78	2.6	5.5866	6.15%	0.0753	5.58%	1058.0	58.0	1040.0	110.0	-0.5%
Z_91500_10	79	2.7	5.6180	6.74%	0.0752	7.05%	1050.0	67.0	1020.0	140.0	0.7%
Z_91500_11	80	2.7	5.5866	6.15%	0.0782	5.37%	1057.0	59.0	1150.0	100.0	1.7%
Z_91500_12	81	2.7	5.5402	5.37%	0.0745	6.17%	1067.0	53.0	1030.0	130.0	-0.6%
Z_91500_13	80	2.7	5.4615	5.08%	0.0760	6.45%	1081.0	50.0	1090.0	130.0	-0.5%
Z_91500_14	81	2.7	5.6148	4.38%	0.0744	6.05%	1055.0	43.0	1070.0	120.0	0.7%
Z_91500_15	84	2.8	5.6497	5.65%	0.0729	7.27%	1057.0	54.0	1010.0	150.0	-1.9%
Z_91500_16	83	2.8	5.5866	6.15%	0.0782	7.03%	1055.0	61.0	1090.0	140.0	0.7%
Z_91500_17	81	2.6	5.5866	6.15%	0.0766	8.22%	1057.0	59.0	1060.0	170.0	2.8%
Z_91500_18	78	2.7	5.5679	4.45%	0.0732	7.65%	1063.0	44.0	940.0	160.0	-3.0%
Z_91500_19	107	2.8	5.5866	6.70%	0.0722	7.62%	1056.0	63.0	980.0	160.0	-0.4%
Z_91500_20	66	3.7	5.5710	5.40%	0.0763	8.39%	1062.0	53.0	1050.0	180.0	2.0%
Z_91500_21	85	2.9	5.6180	6.18%	0.0713	7.01%	1062.0	55.0	960.0	140.0	-0.4%
Z_91500_22	77	2.8	5.5249	7.73%	0.0741	7.29%	1067.0	76.0	1020.0	150.0	0.4%
Z_91500_23	76	2.5	5.5249	7.18%	0.0764	8.77%	1050.0	59.0	1000.0	180.0	0.5%
Z_91500_24	72	2.5	5.5556	9.44%	0.0763	11.53%	1062.0	95.0	1090.0	240.0	0.9%
Z_91500_25	83	2.7	5.6180	6.18%	0.0756	8.99%	1066.0	56.0	1080.0	190.0	0.5%
Z_91500_26	84	2.7	5.6180	6.18%	0.0756	5.95%	1059.0	57.0	1080.0	120.0	-1.1%
Z_91500_27	86	2.8	5.5249	7.18%	0.0762	6.96%	1069.0	72.0	1090.0	130.0	0.7%
Z_91500_28	80	2.6	5.4945	5.49%	0.0729	7.27%	1075.0	56.0	960.0	150.0	-2.5%
Z_91500_29	81	2.5	5.6180	5.62%	0.0765	6.67%	1053.0	55.0	1090.0	140.0	1.4%
Z_91500_30	99	2.9	5.6180	5.28%	0.0747	6.56%	1053.0	51.0	1080.0	130.0	-0.5%
Z_91500_31	64	3.3	5.5866	5.59%	0.0783	6.77%	1057.0	57.0	1140.0	140.0	1.0%
Z_91500_32	88	2.6	5.5556	7.22%	0.0718	11.00%	1066.0	69.0	920.0	230.0	0.1%
Z_91500_33	86	2.8	5.5866	6.70%	0.0732	8.06%	1058.0	64.0	1030.0	150.0	0.2%
Z_91500_34	84	2.7	5.6818	5.68%	0.0760	5.92%	1042.0	55.0	1040.0	130.0	-0.5%
Z_91500_35	81	2.4	5.5127	5.18%	0.0741	4.59%	1072.0	51.0	1120.0	100.0	0.1%
Z_91500_36	68	2.7	5.4945	6.59%	0.0845	8.76%	1074.0	65.0	1260.0	140.0	1.3%
Z_91500_37	88	2.8	5.5556	8.89%	0.0760	8.82%	1062.0	87.0	1090.0	160.0	3.9%
Z_91500_38	78	2.7	5.6180	5.62%	0.0680	8.24%	1065.0	53.0	830.0	170.0	-2.5%

APPENDIX D – Sample List

Sample Name	Location (UTM Zone 16 North)	Zircon source	Sample Description
17BRW154	0595576E 3642967N	Magmatic zircon	Elkahatchee Quartz Diorite: medium grained muscovite-biotite-quartz-plagioclase granodiorite gneiss
17BRW168	0595485E 3639731N	Magmatic zircon	Elkahatchee Quartz Diorite: medium grained, foliated chlorite-muscovite-biotite-quartz-plagioclase granodiorite gneiss
17BRW177	0589749E 3636891N	Magmatic zircon	Elkahatchee Quart Diorite: medium grained, foliated biotite-muscovite-quartz-plagioclase granodiorite gneiss
17BRW202	0601448E 3651222N	N/A	Oaktasai granite: medium to coarse grained biotite-muscovite-quartz-plagioclase trondjemite
17BRW217	0598028E 3642394N	N/A	Sugar Creek trondhjemite: medium to coarse grained, foliated muscovite-biotite-quartz-plagioclase trondhjemite

PLATE 1 – Geologic Map of the Alexander City Quadrangle

Geologic Map of the Alexander City Quadrangle, Alabama